ADVANCED FUNCTIONAL MATERIALS
www.afm-journal.de

Stable and Dendrite-Free Zinc Metal Anodes Via Interface Nanoarchitectonics for Aqueous Zinc-Ion Batteries

Pragati A. Shinde, Nilesh R. Chodankar,* Lok Kumar Shrestha, Amal Al Ghaferi, Ebrahim Alhajri, and Katsuhiko Ariga**

Aqueous rechargeable zinc-ion batteries (ZIBs) are emerging as promising candidates for next-generation electrochemical energy storage systems due to their low cost, abundant resources, superior safety, and high theoretical storage capacity. However, their energy-storing capacity and cycling stability performance are often hindered by issues related to the zinc (Zn) anode, such as dendrite formation, hydrogen evolution reaction (HER), corrosion, and passivation. To improve the overall electrochemical performance of ZIBs, it's crucial to identify the causes of these Zn anode side reactions and explore strategies to mitigate them. The purpose of this review is twofold: first, to explore the challenges linked to the Zn anode, including the underlying causes and mechanisms of reactions, and second, to discuss various strategies for alleviating dendrite growth and side reactions. Additionally, the different strategies to optimize the Zn anode and electrolyte interface by modifying both components are summarized in detail. The modifications made to the separator also influence the interfacial properties between the Zn anode and the electrolyte. As a result, this review also covers the various engineering approaches used to modify the separator. Finally, potential material design approaches and strategies are outlined to enhance the Zn anode, electrolyte, and separator, which could drive the future development of aqueous ZIBs.

1. Introduction

The modern economic society and industrial development have led to a dramatic surge in the demand for electrical energy, with projections indicating that this demand could double by 2050.[1] The primary goal is to secure cost-effective and reliable electricity from renewable and clean sources. Achieving this goal requires the development of functional materials,[2] nanostructure control,[3] and device fabrication.[4] One crucial requirement is the production of robust electrochemical energy storage (EES) systems, essential for providing a dependable solution to enhance grid stability.[5] EES plays a pivotal role in achieving this objective, offering a reliable solution to enhance grid stability given the fundamentally intermittent and widely distributed nature of renewable energy sources such as wind, photovoltaic, ocean, and earth heat energy.[6] Among the various ESSs available, rechargeable batteries play a pivotal role and are essential for powering handheld gadgets, technology tools, electric vehicles (EVs), and large-scale power grids.[7]

Lithium-ion batteries (LIBs) have prevailed in the energy storage emporium since their introduction in the early 1990s. Their high energy density and elongated cycle life are celebrated as milestones in EES technologies.[7a,8] Over time, LIBs have found widespread application and significantly influenced modern lifestyles.[9] However, despite their success in large-scale production, commercial LIBs face challenges such as high costs driven by limited Li resources and the expense of Li itself.[10] Given these

L. K. Shrestha
Department of Materials Science
Institute of Pure and Applied Sciences
University of Tsukuba
1-1-1, Tennodai, Tsukuba, Ibaraki 305-8573, Japan

The ORCID identification number(s) for the author(s) of this article can be found under https://doi.org/10.1002/adfm.202424242

DOI: 10.1002/adfm.202424242

P. A. Shinde, L. K. Shrestha, K. Ariga
Research Center for Materials Nanoarchitectonics
National Institute for Materials Science (NIMS)
1-1 Namiki, Tsukuba 305-0044, Japan
E-mail: shinde.pragatiankush@nims.go.jp; ariga.katsuhiko@nims.go.jp

N. R. Chodankar, E. Alhajri
Mechanical Engineering Department
Khalifa University of Science and Technology
Abu Dhabi 127788, UAE
E-mail: nilesh.chodankar@ku.ac.ae

A. Al Ghaferi
Rabdan Academy
P.O. Box 127788, Abu Dhabi 114646, UAE

K. Ariga
Graduate School of Frontier Sciences
The University of Tokyo
5-1-5 Kashiwanoha, Kashiwa, Chiba 277-8561, Japan

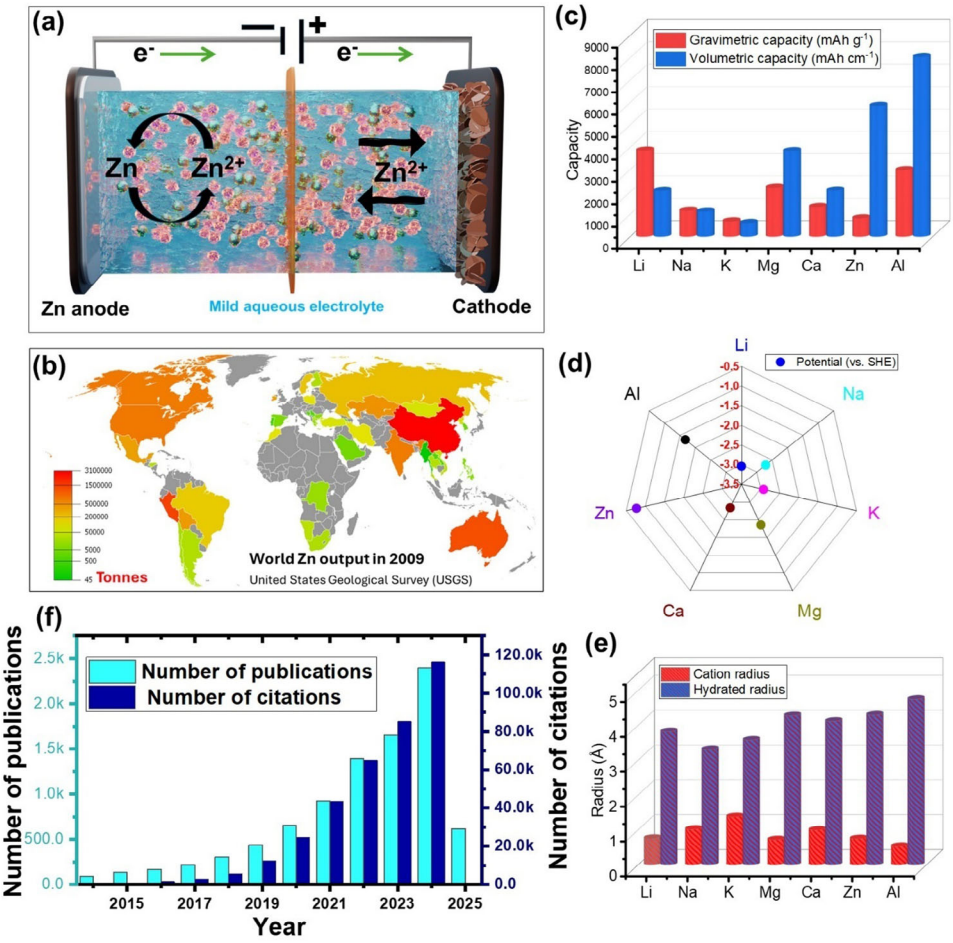

Figure 1. a) Schematic of the ZIBs, b) Worlds Zn production in 2009 through the world, according to the United States Geological Survey (USGS), c) theoretical capacity, d) standard Potential, and e) ionic radius for the different typical monovalent/multivalent metal ion charge carriers. Reproduced with permission.[25] Copyright 2018, American Chemical Society. f) Number of publications and corresponding citations for the last ten years on ZIBs, searched from "Web of Science" with the keyword Zn ion battery.

limitations, urgent action must be taken to substitute EESs with analogous energy and power densities, improve cost-efficiency, and enhance safety.[11] This has driven researchers to explore batteries based on monovalent and multivalent ions.[12] The attractiveness of rechargeable multivalent metal-ion (Mg^{2+}, Ca^{2+}, Zn^{2+}, Al^{3+}) batteries lies in their utilization of earth-abundant multivalent cations and the corresponding multielectron transfer reactions.[13] Among the different multivalent battery chemistries, Zinc-ion batteries (ZIBs) are gaining attention as a cost-effective and safe EES generation.[14] Unlike traditional LIBs, which rely on Li ions, ZIBs use a zinc-ion (Zn^{2+}) storage cathode paired with a zinc metal anode. Here, the energy storage and release occur through the reversible processes of Zn stripping/plating at the anode, alongside the insertion/desertion of Zn^{2+} at the cathode (**Figure 1a**).[15] One key difference between ZIBs is their use of aqueous electrolytes rather than organic ones, which offers improved safety due to their reduced flammability and superior environmental compatibility.[16] This enhances the safety and sustainability of ZIBs, making them a more eco-friendly choice for energy storage.

Aqueous ZIBs offer several unique and intrinsic advantages. The foremost and most compelling reason for the development of ZIBs is the abundant availability of Zn across the globe. Zn is the 24th most abundant element in the Earth's crust, with substantial reserves found in countries such as China, Australia, India, Peru, and the United States (Figure 1b). Unlike Li, which is concentrated in a few regions and is subject to supply chain constraints, Zn is widely distributed, ensuring a more stable and sustainable supply. Furthermore, zinc is predominantly extracted as a byproduct of lead and copper mining, making its production more cost-effective. According to the United States Geological Survey (USGS), the total Zn output worldwide is 12 000 000 tones in a single 2023 year, significantly higher than the production of the Li. In addition to this, the ZIBs are based on conventional aqueous electrolytes, which provide significantly higher ionic conductivity than organic electrolytes.[17] The redox reaction of a single Zn includes two electrons, leading to a high volumetric capacity of up to 5849 mAh cm^{-3}, which is ideal for volume-limited applications.[18] This high volumetric capacity, combined with the superior gravimetric capacity of Zn metal anodes (820 mAh g^{-1}), allows ZIBs to attain a high energy density

(Figure 1c). Furthermore, the equilibrium potential of Zn^{2+}/Zn (−0.76 V vs the standard hydrogen electrode (SHE) helps prevent aggressive reactions between Zn metal and water, making the use of aqueous electrolytes in ZIBs more practical (Figure 1d).[19] Additionally, Zn is preferred over other multivalent metal cations like Al and Mg for aqueous electrolytes due to its smaller hydrated radius, which aids easy ion intercalation in layered cathode materials (Figure 1e).[20] It also forms a less dense surface passivation layer, which minimizes the internal battery resistance. These advantages have led to a surge in research on efficient Zn metal anodes for ZIBs. Considering these advantages, the past decade has witnessed a growing global interest in ZIBs. This surge is reflected in the significant rise in publications and citations over time, as illustrated in Figure 1f.

Nevertheless, the widespread use of ZIBs is limited by several factors, including the low capacity of the cathode, a restricted electrochemical stability window for water-based electrolytes, and the various issues of the Zn anodes.[21] Zn anodes are highly prone to irreversible plating/stripping, which is primarily caused by the formation of dendrites, along with side reactions like HER, corrosion, and passivation.[22] These challenges negatively affect the ZIBs' capacity, lifespan, and rate performance. Dendrite formation reduces Coulombic efficiency (CE) and can cause a short circuit, while detached dendrites create dead zinc, further reducing the anode capacity.[23] Additionally, HER consumes the water content from the electrolyte and causes corrosion of the anode, leading to battery inflammation and electrolyte leakage.[24] These problems together hamper the performance of ZIBs.

Recently, researchers have proposed different strategies to optimize Zn anodes. These strategies include adjusting the interface dynamics of the Zn anode-electrolyte system, electrolyte modification, and separator engineering.[26] These approaches effectively suppress issues related to dendrite and HER and significantly boost the stability of ZIBs. Furthermore, to fully leverage these advancements, it is crucial to systematically understand these Zn anode stabilization strategies and comprehensively discuss the relationship between Zn anode composition, structure, and performance. This insight offers a comprehensive summary of recent advancements in this research field and a guide for future materials design and optimization improvements. This comprehensive perspective can guide researchers in developing advanced materials and techniques, thereby driving further innovation and improvement in ZIB technology. Considering these factors, we provide an in-depth review of the stabilization strategies for Zn metal anodes in ZIBs. The review begins with a discussion on the causes of dendrite formation, HER, and corrosion, including insights into their underlying mechanisms. Following this, strategies to suppress dendrite growth and HER are discussed in detail. We then probe into the specific roles of various approaches, such as Zn anode surface, electrolyte modification, and separator engineering. Furthermore, acknowledging that the development of Zn metal anodes remains in its early stages, we explore the challenges encountered and provide constructive insights to advance academic research, industrial applications, and the commercialization of Zn anodes and ZIBs. This review will enhance understanding, refine optimization strategies, and accelerate the practical application of ZIB technology.

2. Challenges With the Zn Anode

Zinc metal is widely used as an anode material in ZIBs due to its several advantages, including a high theoretical capacity, low cost, and easy availability. The Zn anode acts as a reservoir for metal ions, enabling the reversible intercalation and deintercalation of Zn^{2+} ions during charge and discharge cycles without losing its functionality in the process.[27] Nonetheless, despite the attractive features of ZIBs, numerous challenges have hindered their large-scale adoption. These challenges mainly pertain to the performance and stability of the Zn anode.[28] Considerable research, both experimental and theoretical—has focused on uncovering the limitations of Zn metal anodes and their impact on the overall efficacy of ZIBs. Key issues facing the Zn anode include dendrite formation, the hydrogen evolution reaction (HER), corrosion, and passivation.[29] Dendrite growth can lead to short circuits, posing risks to the battery's safety and lifespan. Meanwhile, the HER diminishes the efficiency of the charge–discharge process and contributes to anode degradation. Additionally, corrosion and passivation further accelerate capacity fading, ultimately shortening the lifespan of ZIBs.[20] In the upcoming sections, we will take a closer look at these challenges, examining the underlying mechanisms and discussing potential strategies to mitigate their negative effects on Zn anodes.

2.1. Root Causes of Dendrite Formation in Zinc Anode

Metallic Zn is a widely used anode material in ZIBs, particularly in aqueous electrolyte systems. In the charging process, Zn^{2+} ions travel from the cathode to the anode, where the zinc metal endures stripping and plating.[30] However, Zn^{2+} ions are accompanied by 5–6 water molecules, forming a hydrated structure with an ionic radius of ≈0.74 to 0.83 nm, which introduces complexity into the electrochemical deposition process (**Figure 2a**).[31] During the charging process, Zn^{2+} ions are released from the cathode and deposited onto the anode. Initially, the hydrated Zn^{2+} ions, which are associated with water molecules, cross the separator due to the applied electric field before reaching the anode. Upon reaching the anode side, these Zn^{2+} ions travel via an electric double layer and undergo dehydration within the Helmholtz layer, driven by direct diffusion. Following desolvation, the newly dehydrated Zn^{2+} ions adsorb onto the surface of the zinc anode. At this point, the ions accept electrons from the external circuit, reducing them to zinc metal.[32] The initial nucleation occurs as Zn^{2+} ions receive electrons from the current collector, with freshly reduced Zn preferentially growing at the nucleation sites. The quality of nucleation and subsequent growth is crucial for ensuring a reversible and efficient plating process.[33] The electroreduction of Zn^{2+} ions at the anode includes reversible plating and stripping. The reactions vary based on electrolyte pH as follows:[34]

In neutral or acidic electrolytes:

$$Zn \leftrightarrow Zn^{2+} + 2e^{-} \quad (1)$$

In alkaline electrolytes:

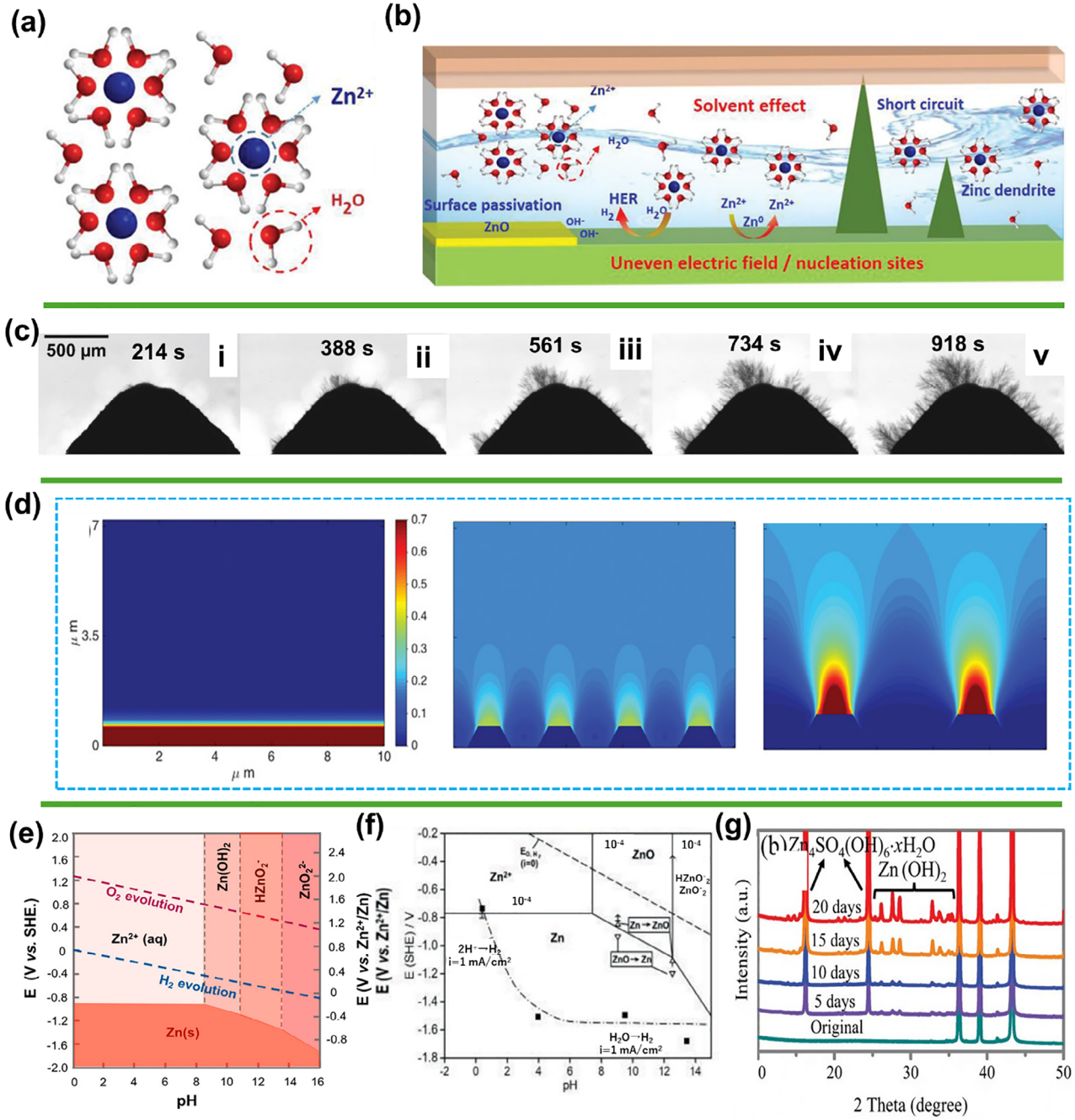

Figure 2. a) The Zn^{2+} surrounded by water molecules and b) Representation of Zn anode in aqueous environment. Reproduced with permission.[31] Copyright 2020, Wiley-VCH GmbH. c) Operando Study of Zinc Dendrite Growth. Reproduced with permission.[36] Copyright 2019, Elsevier. d) The electric field gathered around the Zn curvatures. Reproduced with permission.[38] Copyright 2019, Wiley-VCH GmbH. e) Pourbaix diagram for 10^{-6} mol L^{-1} Zn^{2+}. Reproduced with permission.[41] Copyright 2020, American Chemical Society. f) Pourbaix diagram for 10^{-4} mol L^{-1} Zn^{2+}. Reproduced with permission.[42] Copyright 1991, Elsevier. g) The in-situ XRD Zn immersed in 2 M $ZnSO_4$ electrolyte, showing the presence of $Zn_4SO_4(OH)_6{\cdot}xH_2O$ and $Zn(OH)_2$. Reproduced with permission.[43] Copyright 2021, Wiley-VCH GmbH.

$$Zn\,(s) + 4OH^- \leftrightarrow Zn\,(OH)_4^{2-} + 2e^- \quad (2)$$

$$Zn\,(OH)_4^{2-} \leftrightarrow ZnO\,(s) + H_2O + 2OH^- \quad (3)$$

During nucleation, Zn^{2+} ions must overcome the nucleation overpotential, representing the energy barrier associated with zinc deposition. A higher nucleation overpotential complicates the process, while aspects like the irregular surface of the zinc anode, unstable Zn^{2+} concentrations, and the occurrence of water

molecules close to the anode post-desolvation contribute to a complex deposition environment. As a result, zinc reduction rarely produces a uniform surface. Instead, newly deposited zinc tends to grow preferentially in specific directions, leading to irregular nucleation and a non-uniform distribution of ion flux (Figure 2b). This self-reinforcing irregular growth ultimately results in the development of dendrites, similar to those seen in LIBs, which continue to grow during battery operation and present substantial challenges.[13b,35] Yufit et al.[36] performed operando visualization of Zn dendrite formation. In this system, zinc dendrites were deposited on a cone-shaped zinc anode by applying a constant negative current of 10 mA (≈30 mA cm^{-2}) between the zinc anode and a carbon air cathode, separated by ≈3 mm of aqueous electrolyte. Dendrite growth begins once a critical overpotential is reached. Figure 2c-i shows small dendrites (<≈30 µm) on the cone tip after 214 s of deposition. Growth is accompanied by hydrogen evolution (white semicircles) from water electroreduction. Dendrites form at various locations on the cone tip and surroundings (Figure 2c-ii,iii), likely due to non-uniform current density from surface irregularities. Prolonged deposition leads to secondary dendrites on primary trunks (Figure 2c-iv), restricting primary thickening. The morphology remains consistent, with trunks and blade-like branches influenced by local crystallography and current. Tertiary dendrites later emerge from secondary trunks (Figure 2c-v).

Furthermore, dendrite formation in ZIBs, driven by uneven ion diffusion and zinc deposition on the anode, has long hindered the system's safety and performance stability. Ideally, the Zn anode should maintain a flat surface to ensure high CE and high stability.[37] However, due to the uneven electric field delivery near the Zn anode-electrolyte, maintaining a uniform Zn^{2+} distribution is difficult, which promotes dendrite growth (Figure 2d).[38] The vertical growth of dendrites from the substrate leads to a slack and porous structure, contributing to anode volume expansion and providing more sites for corrosion and side reactions.[39] These side reactions consume electrolyte and active zinc material, compromising battery performance. Additionally, sharp, needle-like zinc dendrites cause the hazard of separator penetration, potentially leading to internal short circuits. Zinc dendrites that have slack contact with the substrate can isolate and form inactive, or "dead," zinc, further depleting the available active material.[40] Side reactions, electrolyte consumption, and dead zinc formation reduce the battery capacity and CE. Even minimal dendrite formation can significantly impact ZIB's performance, making a thorough understanding of dendrite growth mechanisms critical to justifying their development.

Zinc deposition during electroplating at the Zn anode/electrolyte interface occurs in four stages: diffusion of Zn^{2+} ions, reduction of Zn^{2+}, nucleation of Zn, and subsequent crystal growth.[44] The process of zinc nucleation and subsequent crystal growth involves overcoming an energy barrier that is significantly influenced by factors such as the surface morphology of the substrate, the distribution of the electric field at the interface, and the substrate's affinity for zinc. Achieving uniform and dendrite-free zinc deposition requires maintaining this energy barrier at a consistently low and stable level throughout the electroplating process. The overall electrochemical kinetics, particularly the polarization of the Zn anode, perform a critical part in the Zn deposition rate. As the surface polarization of the Zn anode increases, the overpotential increases.[45] Given the thin electric double layer, even a minor increase in overpotential can significantly strengthen the local electric field. This leads to electron/ion accumulation at the liquid interface, hindering uniform and rapid deposition of zinc. Thus, minimizing concentration and electrochemical polarization at the Zn anode is critical for controlling the deposition process.

Concentration polarization occurs when the electrochemical potential of a cell shifts away from its equilibrium value due to variations in ion concentration amid the electrode surface and in the bulk electrolyte.[46] This factor is a main factor in the establishment of dendrites, adversely affecting the stability and overall performance of the device. In particular, concentration polarization commonly occurs in nonaqueous electrolytes and during metal deposition due to insufficient ionic transport within the electrolyte.[46] By utilizing supporting electrolyte additives that boost ionic conductivity without engaging in the electrochemical reaction and ensure a stable potential window, Zn electrodeposition can be regulated as a diffusion-controlled process.[47] In this scenario, the movement of Zn^{2+} ions is fundamental to the Zn deposition process. The associated mass transport flux (J) can be expressed using the following equation.

$$J = \frac{zecD}{kT}\frac{dV}{dx} - D\left(\frac{dc}{dx}\right) + cv_x \tag{4}$$

Here, z, the charge number, e, the elementary charge; c, the ion concentration; D, the diffusion coefficient; V_x, the convective velocity; k, the Boltzmann constant; T, the absolute temperature; V, the electric potential; and x, the distance measured from the cathode. A high value of J is desirable to reduce polarization, which can be achieved by increasing both c and Vx, as indicated by the Equation (4). Thus, adjusting electrolyte concentration and enhancing convection through stirring are employed to suppress dendrite formation.[48] However, concentration polarization and ion diffusion models fall short of fully explaining Zn deposition behavior in ZIBs, particularly in aqueous systems, where the concentration and diffusion rate of Zn^{2+} ions are comparatively higher.

In practical terms, Zn deposition occurs during charging due to various forms of polarization, which is consistent with experimental observations. From a kinetic perspective, the increased Zn^{2+} ion diffusion rate and reduced polarization facilitate more uniform Zn deposition. Considering these factors, significant research efforts have focused on modifying the substrate surface, which is crucial in alleviating the Zn anode. Specifically, increasing the substrate affinity for Zn lowers the energy barrier for Zn nucleation, promoting consistent Zn deposition. The performance of the zinc anode is closely linked to the areal current density, as it directly influences the Zn deposition rate and significantly impacts the polarization in the charging process of ZIBs. The polarization of the Zn anode tends to rise as the areal current density increases. Consequently, maintaining a lower areal current density is essential to mitigate dendrite formation. To address this, structural substrate designs are frequently utilized as they enhance the specific surface area and lower the areal current density, effectively reducing anode polarization in ZIBs. Moreover, electrolyte modifications have been explored to suppress Zn dendrite formation.[31]

2.2. H_2 Evolution at Zn Anode Surface

HER on the Zn anode surface occurs together with metal corrosion, which is one of the significant challenges in developing ZIBs. The HER occurs because zinc, with a lower electronegativity than hydrogen, tends to react with water, leading to HER in slightly acidic or neutral electrolytes.[49] This reaction leads to hydrogen evolution and corrodes the Zn anode surface, compromising battery performance and increasing safety risks.[50] Moreover, the development of hydrogen bubbles on the irregular Zn metal further accelerates degradation, resulting in reduced battery efficiency. Besides, due to the ingesting H^+ from the water, the concentration of OH^- ions close to the Zn anode-electrolyte boundary increases along with the Zn^{2+} ions and other electrolyte byproducts forming, which hinders the uniform Zn plating.[30,51] These byproducts with poor ionic conductivity and slack structure impede Zn plating/stripping and confine straight exchange between the Zn anode and electrolyte. As a result, HER will continue consuming active Zn species and electrolytes, thereby decreasing CE. HER also results in a narrow potential window of ZIBs, which confines the practical energy density of the battery.[52]

Figure 2e represents the Pourbaix illustration of Zn metal in aqueous electrolytes, illustrating that the equilibrium potential of Zn^{2+}/Zn redox couple consistently remains lower than that of the H_2O/H_2 couple across the entire pH spectrum.[41] Thus, representing the spontaneous existence of HER and corrosion on the Zn anode surface. As pH increases, the stable potential range of the Zn anode no longer aligns with the electrochemical stability window of water. This misalignment indicates that the coexistence of Zn and water becomes thermodynamically unfavorable, leading to continuous water reduction and subsequent hydrogen gas production. Nevertheless, the kinetics of HER must be considered when assessing HER suppression in practical ZIBs.[53] In general, the HER process involves two steps. H_2O molecules generate H_3O^+ ions, which diffuse and migrate toward the Zn anode surface.[54]

Step 1 (Volmer reaction): Initially, H_3O^+ ions are reduced, resulting in the generation of hydrogen atoms on the surface of the electrode accordingly.

$$H_3O^+ + e^- \leftrightarrow H + H_2O \quad (5)$$

Step 2 (Heyrovsky reaction): H_3O^+ interacts with H atoms previously adsorbed on the Zn anode surface to form H_2

$$H_3O^+ + H + e^- \leftrightarrow H_2 + H_2O \quad (6)$$

Simultaneously, H atoms adsorbed on the Zn anode are transformed to

Tafel reaction

$$2H_{ad} \leftrightarrow H_2 \quad (7)$$

Finally, H_2 detaches from the electrode, moves into the electrolyte, forms a bubble, and is released. In the case of the HER on the zinc anode, the rate is primarily governed by the Volmer step. The elevated Tafel slope (0.12 V) and intercept (1.24 V) lead to a significant overpotential, which lowers the effective HER potential beneath the equilibrium potential of Zn^{2+}/Zn.[55] Thus, HER and corrosion are self-limiting at high rates (Figure 2f).[42] In practice, HER is more complex than theoretical predictions suggest due to the high overpotential of zinc in aqueous electrolytes. However, HER becomes more prominent in neutral and mildly acidic electrolytes, which are typically employed in ZIBs, leading to significant challenges in the stability of the zinc anode.[56] A competitive interaction occurs between the hydrogen evolution reaction (HER) and zinc plating/stripping. As the potential is reduced, solvated Zn^{2+} and H_3O^+ ions, which participate in both the plating and HER processes, move toward the anode surface. During this process, factors such as pH, electrolyte concentration, and conductivity play a crucial role in determining the concentration overpotential, which in turn influences the rate of ion diffusion. Additionally, the formation of an electric double layer on the anode surface affects the local organization of ions and water molecules, thereby restricting the diffusion of charge carriers like Zn^{2+} and H_3O^+.[57] Following this, charge carriers are adsorbed onto the surface of the anode, where they compete for electrochemically active sites. These sites are significantly affected by the surface's morphology, its hydrophilic and hydrophobic properties, and any absorbed additives. At the same time, the charge carriers also compete for electrons, which impacts the reversibility of the Zn plating/stripping processes. In summary, the hydrogen evolution reaction (HER) plays a pivotal role in influencing the performance of zinc-ion batteries (ZIBs), presenting a challenge to their long-term stability.

2.3. Corrosion and Passivation of Zn Anode

During prolonged charge/discharge cycles, the Zn anode undergoes irreversible degradation through three primary mechanisms. First, "dead Zn" forms as detached Zn dendrites accumulate, reducing active material and weakening redox activity. Second, electrochemical corrosion in the electrolyte causes material loss and moderate performance. Third, electrolyte anions complex with Zn^{2+} near the anode, driving degradation. Passivation involves the establishment of an insulating layer on the electrode surface in alkaline solutions, which decreases overall conductivity and hampers the movement of discharge products or OH^- ions, thereby hindering again discharge.[58] Corrosion and passivation occur differently in alkaline and mild electrolytes.[23] In alkaline systems, dual chemical and electrochemical processes drive Zn dissolution, forming soluble $Zn(OH)_4^{2-}$ and inert ZnO, which eventually leads to electrode passivation:

$$Zn + 4OH^- \rightarrow Zn(OH)_4^{2-} + 2e^- \rightarrow ZnO + 2OH^- + H_2O \quad (8)$$

In neutral or acidic electrolytes, processes of corrosion and passivation are primarily associated with hydrogen evolution.[32b] Water decomposition and H^+ depletion increase OH^- near the zinc anode, forming insoluble by-products $Zn_4SO_4(OH)_6{\cdot}xH_2O$ (Figure 2f) that deactivate the anode.[59] The side reactions occurring can be described as follows:

$$Zn^{2+} + 6OH^- + SO_4^{2-} + xH_2O = Zn_4\ SO_4(OH)_6 \cdot xH_2O \quad (9)$$

Thus, the formation of Zn dendrites roughens the anode surface, increases the active area, and creates additional HER sites,

which promote H_2 gas evolution. The HER process increases the local pH around the anode, forming inert by-products. These by-products worsen surface non-uniformity, irregular electric field distribution, and quicken dendrite growth. Together, these interconnected degradation mechanisms hinder the efficiency, stability, and scalability of ZIBs. In conclusion, addressing hydrogen evolution, dendrite formation, and passivation is essential for improving ZIB performance and extending their cycle life. Strategies to optimize these factors for stabilization of the Zn anode are discussed in detail in the following section.

3. Surface Modifications of the Zn Anode

Surface modification of the Zn anode has become an important approach for enhancing the stability and performance of ZIBs, particularly in terms of long-term cycling. This approach addresses several limitations associated with the inherent instability of the Zn anode in charge-discharge processes, such as dendrite creation, side reactions, and non-even Zn deposition.[60] The goal of surface modification is to isolate the Zn anode from the aqueous electrolyte to mitigate side reactions and promote uniform Zn^{2+} deposition, thereby enhancing the anode's overall performance and cycling stability. The surface-modified Zn anode serves as a protective layer, preventing detrimental side reactions and facilitating the uniform deposition of Zn during plating and stripping. This is essential for maintaining the structural integrity and efficiency of the anode throughout many cycles of operation. Several materials and techniques have been explored to modify the surface of Zn anodes, with the most commonly used materials being carbon-based, metals, polymers, and 2D materials like MXene.[61] The modification processes are diverse, including doctor-blade coating, pre-reaction treatments, physical vapor deposition (PVD), and chemical vapor deposition (CVD). For a surface modification to be effective, it must satisfy several critical criteria. First and foremost, the material used must exhibit high Zn^{2+} conductivity, which is crucial for facilitating fast ion diffusion during the charge/discharge cycles. This ensures that the anode can deliver high efficiency and performance over extended periods. Second, the modified surface should exhibit good mechanical stability, particularly under repeated Zn plating and stripping stress. This is necessary to prevent structural degradation, cracking, or delamination of the protective layer, which could compromise the performance of the Zn anode.[62] Additionally, the material must be highly compatible with the Zn anode surface to ensure strong interfacial bonding, contributing to the modification's longevity and reliability. The thickness of the modified layer should be minimal to avoid excessive energy loss and to maintain high energy and power densities. A lightweight coating is also preferred to avoid adding significant weight to the system, which would otherwise negatively affect the overall efficiency of the battery. Cost-effectiveness and scalability are crucial factors in selecting surface modification materials and techniques. Ideally, the chosen materials should be abundant, inexpensive, and easily scalable for large-scale manufacturing, ensuring that the modifications can be applied to commercial ZIBs without driving up production costs.[63] In this section, we have concise recent advancements in surface modification methods for Zn anodes, focusing on the materials used, their functional properties, and their effectiveness in stabilizing the Zn anode for long-term cycling. Researchers have made notable progress in enhancing the stability, performance, and longevity of Zn anodes by investigating various materials, such as conductive polymers, carbon, and 2D materials like MXene. These innovations offer considerable potential for the advancement of more efficient, long-lasting, and economical zinc-based energy storage technologies.

3.1. Stable Zn Anodes Via Carbon Coatings

Surface modifications of Zn anodes, especially for use in ZIBs, aim to improve the overall performance by enhancing cycling stability, reducing dendrite formation, and improving the efficiency of charge and discharge cycles. Carbon-based materials are commonly used in these modifications owing to their favorable assets, including high electrical conductivity, structural stability, and ability to prevent side reactions.[64] To do this, a range of carbon-based materials, such as activated carbon, carbon nanofibers, and 2D graphene, have been decorated on the Zn anode surface. For instance, Yin et al.[65] developed the Zn ion capacitor (ZIC) using the porous carbon (PC) derived from the pyromellitic acid tetra-potassium salt as a cathode material and protecting material for the Zn anode. Interestingly, the cell developed with the Zn/PC anode demonstrates excellent cycling stability over 30 000 cycles. At the same time, the cell with the pristine Zn anode fails to demonstrate good cycling stability, and it shorts after 4092 charge-discharge cycles. Due to the uneven deposition and dissolution of Zn during the charging and discharging cycles, sharp Zn dendrites gradually formed and eventually pierced the separator of the Zn//PC ZIC by the 4092nd cycle. For the Zn/PC anode, the modified surface provides multiple active sites for homogeneous Zn deposition and, as a result, consistently disperses carrot-shaped zinc particles other than zinc dendrites on the surface. Furthermore, Du et al.[66] developed stable ZIBs by decorating the carbon fiber micron film (CFMF) onto the Zn anode as a protective layer and to assist the even plating/stripping of the Zn anode in aqueous electrolytes. The commercially available CFMF was blended homogeneously with acetylene black and polyvinylidene fluoride (PVDF), using a few drops of N-methyl-2-pyrrolidone (NMP) solvent to prepare the slurry. This mixture was then applied onto the surface of Zn foil through spraying and subsequently vacuum-dried at 80 °C for 6 h. **Figure 3**a,b shows the SEM images of the Zn anode before and after CFMF decorating. The uniform CFMF decoration on the Zn anode surface is seen in Figure 3b, which will advance Zn electrodeposition kinetics and regulate the electrical field. As a result, the assembled symmetric cell with the CFMF/Zn anode demonstrates outstanding plating/stripping ability over 2500 h at a current density of 1 mA cm^{-2} and negligible voltage hysteresis of 59.5 mV at the 1st cycle. Meanwhile, the symmetric cell with the Zn anode cannot run under the same conditions for over 500 h (Figure 3c). In addition, the symmetric cell with the CFMF/Zn anode can stably cycle for 1500 h at a much higher current density of 5 mA cm^{-2} with a stripping/plating capacity of 5 mAh cm^{-2}. Later, they developed the full-cell battery using the conventional MnO_2 as a cathode and CFMF/Zn anode in Zn-based electrolyte (mixture of 2 M $ZnSO_4$ and 0.1 M $MnSO_4$ in deionized water) and performed electrochemical testing. As seen in Figure 3d, the resultant

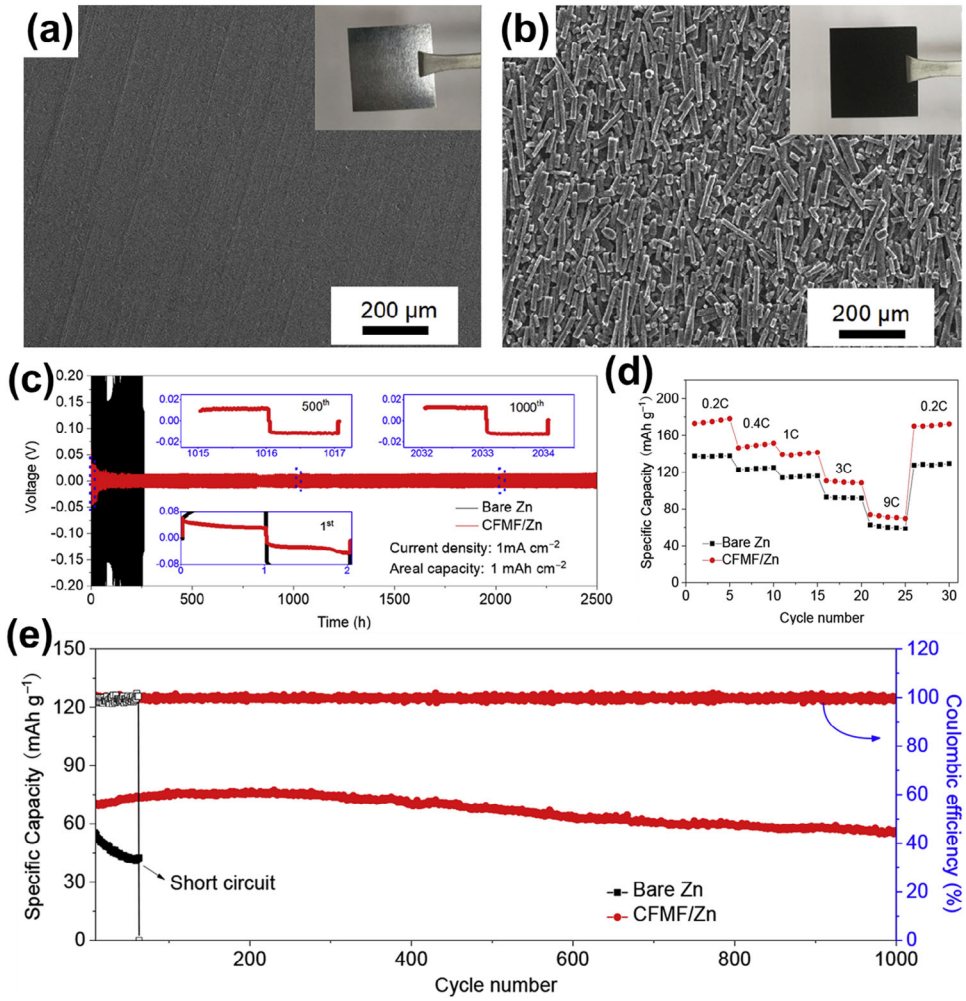

Figure 3. SEM image for the a) bare Zn anode, b) CFMF/Zn, c) Stripping/plating stability for the symmetric cells with bare Zn metal and CFMF/Zn composite electrodes at the current density of 1 mA cm^{-2}/1 mAh cm^{-2}. Insets show the enlarged plating and stripping voltage profiles at different times, d) Specific capacity at different cycles and different C rates for the Zn–MnO_2 full cell and CFMF/Zn–MnO_2 full cell e) stability test for the Zn–MnO_2 full cell and CFMF/Zn–MnO_2 full cell. Reproduced with permission.[66]

specific capacity for the CFMF/Zn anode-based battery is higher than that assembled with a Zn anode without CFMF. At a 0.2 C rate, the discharge capacities (calculated based on the MnO_2 mass) of the Zn–MnO_2 and the CFMF/Zn–MnO_2 full cell are 137.4 and 171.6 mAh g^{-1}, respectively. Notably, the Zn–MnO_2 full cell undergoes short-circuiting at higher current rates (such as 9 C) after only 63 cycles. In contrast, the CFMF/Zn–MnO_2 full cell can cycle stably for 1000 cycles, demonstrating high-capacity retention of 80.1%. This indicates that CFMF effectively suppresses Zn dendrite formation and contributes to the stabilization of the full cell (Figure 3e).

Li et al.[67] developed a simple yet scalable pencil drawing approach to engineer the Zn anode surface to protect it from severe degradation during electrochemical cycling. Pencil drawing on the Zn anode causes the formation of a shielding graphite layer on the Zn anode. Graphite is typically made up of layers of carbon atoms organized in a hexagonal pattern. Each layer contains carbon atoms attached in a flat structure, with weak van der Waals forces keeping the layers together, allowing them to slide over each other easily. Additionally, graphite has excellent electrical conductivity because the carbon atoms within the layers have free electrons that can move around.[68] This property is advantageous for various electrochemical applications. In the case of the Zn anode, the coating of the graphite on the surface of the Zn anode can turn into an ion buffer and assist in uniform nucleation of Zn^{2+} in graphite voids to avoid the dendrite formation on the Zn anode. As presented in **Figure** 4a, the color of the Zn anode changed to black after the pencil drawing. Furthermore, the author performed the stability test in the 2 M $ZnSO_4$ electrolytes. The pristine Zn surface experienced significant oxidation, resulting in a noticeable color change from silver to gray. In contrast, the Zn–G electrode maintained a stable surface without any apparent byproducts even 15 days later (Figure 4a). This observation highlights the effectiveness of the straightforward strategy employed to create a durable zinc anode. Figure 4b,c depicts the SEM image of the Zn anode before and after graphite coating. Before graphite coating, the surface of the Zn anode was rough, with abundant uneven defects, which may

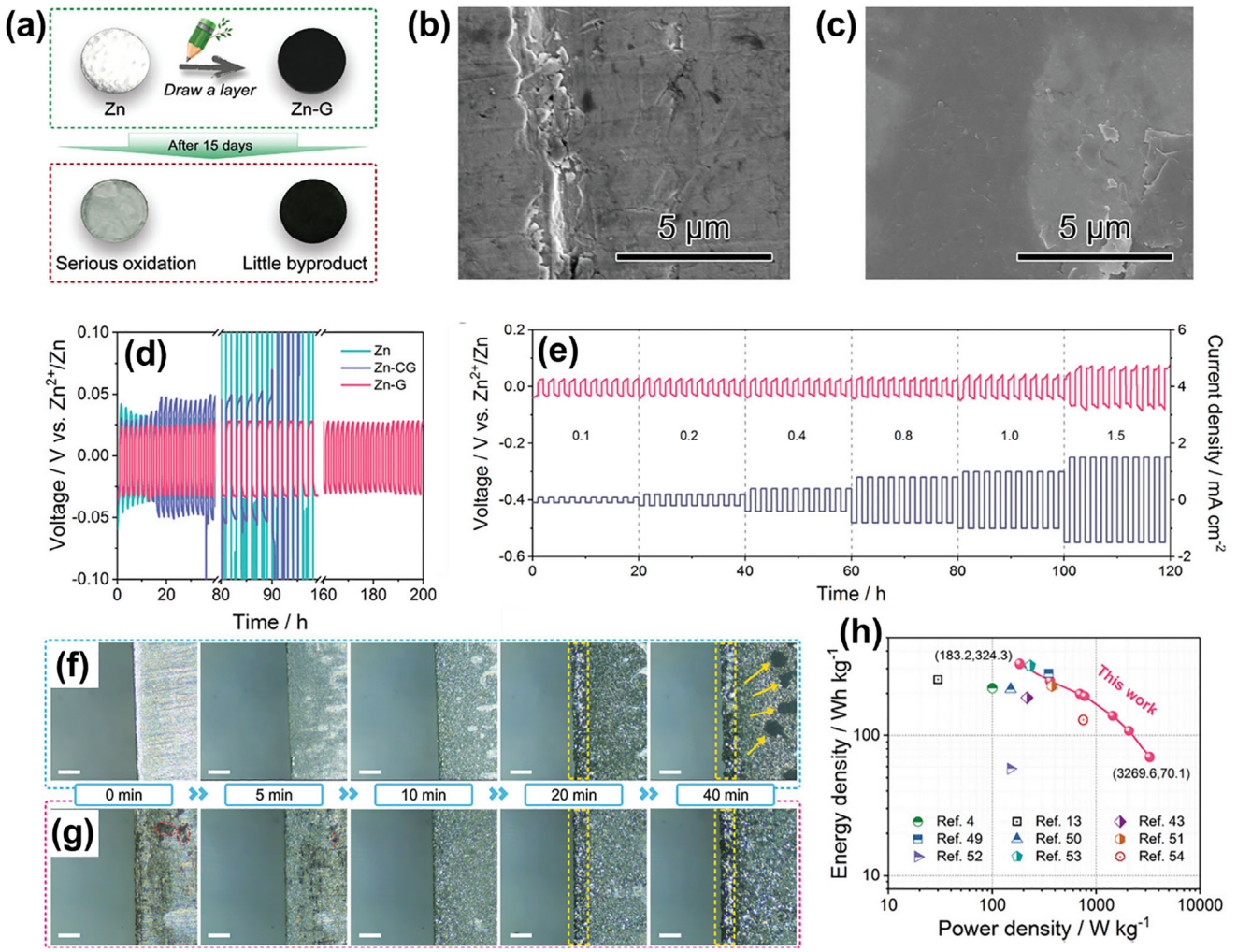

Figure 4. a) Illustrates the modification process and the stability in 2 M $ZnSO_4$ electrolyte of Zn and Zn–G anodes for 15 days. SEM images for the b) Pristine Zn anode and c) Zn-G anode d) Plating/stripping stability tests for the Zn//Zn, Zn-G//Zn-G, Zn-CG//Zn-CG symmetric cells, e) Rate performance for the Zn-G//Zn-G symmetric cell at different applied current densities. The optical images for the transparent cell were assembled by using the f) pristine Zn anode and g) Zn-G anode-based symmetric cell. h) Comparative Ragone plot for the Zn–G//$V_2O_5{\cdot}xH_2O$ with the previous reports on the ZIBs. Reproduced with permission.[67]

have been due to the manufacturing procedure. After graphite coating, the uneven Zn surface becomes smooth, providing a uniform electric field. The electrochemical stability of Zn and Zn–G anodes was assessed further in 2 M $ZnSO_4$ through repeated galvanostatic tests in symmetric cells. Figure 4d demonstrates that the Zn–G/Zn–G cell retains a steady voltage profile with a minimal voltage hysteresis of ≈28 mV over 200 h at a current density of 0.1 mA cm^{-2}. In comparison, the Zn/Zn and Zn-CG/Zn-CG (commercial graphite-modified) cells experience quick deterioration, with a noticeable increase in voltage after about 70 and 90 h of plating/stripping, respectively. This failure is likely due to dendrite formation, which leads to internal short circuits. In addition, they found 100% energy efficiency over 100 cycles, indicating the Zn-G anode's high stability in a Zn-based electrolyte system. In the case of the pristine Zn anode-based symmetrical cell, the energy efficiency drops below 75% after 35 cycles, further highlighting the advantages of the Zn–G anode. The rate performance test (Figure 4e) Zn-G/Zn-G cell exhibits an exceptionally low voltage hysteresis (27.3 to ≈72.9 mV) across a current density range of 0.1 to 1.5 mA cm^{-2}, significantly lower than the voltage hysteresis observed in the Zn/Zn symmetrical cell, which spans 40.9 to ≈757.2 mV under identical conditions. A transparent symmetric cell was designed for real-time monitoring using an optical microscope linked to an electrochemical workstation to observe the formation and growth of Zn dendrites during the electrochemical process. When a relatively high current density of 1 mA cm^{-2} was applied, the irregular surface of pure Zn facilitated the formation of non-uniform nuclei (Figure 4f). After 20 min of plating, multiple nuclei were observed at the edges and surface. At the 40-min mark, partial corrosion appeared at the Zn edges, and large dendrites (highlighted by yellow arrows) began to form and grow, which notably affected the stability and durability of the ZIBs. In contrast, the Zn–G electrode maintained a smooth surface with a well-structured graphite layer (red circle

in Figure 4g). Over the course of further plating, the Zn–G maintained even nucleation, with no noticeable dendrites or corrosion even for 40 min (Figure 4h). Notably, the absence of graphite sheets throughout the plating process is mostly due to the alloying of Zn nuclei within the internal space of the coated graphite. This distinctive characteristic helps prevent dendrite formation, enhancing the reversibility and durability of Zn-based devices. In addition, to further test the performance of the Zn-G anode for the actual battery application, the ZIB was developed by using the $V_2O_5{\cdot}xH_2O$ as a cathode electrode. Surprisingly, the assembled Zn–G//$V_2O_5{\cdot}xH_2O$ ZIB delivers a high energy density of 324.3 Wh kg^{-1} at a power density of 183.2 W kg^{-1}, considering the mass of the cathode material. Developed ZIB can deliver the high-power density of 3269.8 W kg^{-1} at an energy density of 70.1 Wh kg^{-1}. Moreover, the assembled battery delivers excellent cycling stability over 1500 cycles at a current density of 5 A g^{-1}.

Graphene, a 2D carbon-based material, has been utilized in various applications, from biomedical to energy sectors. This is mainly due to its exceptional properties, including high electrical conductivity, a 2D sheet-like structure, and a high specific surface area, all at a lower cost than inorganic materials.[69] While 2D graphene has been utilized as a cathode material to enhance the stability of conventional inorganic materials, it is also employed as a protective layer on the Zn anode side. Zhou et al.[70] prepared nitrogen (N)-doped graphene oxide (NGO) interface film using a one-step Langmuir–Blodgett technique, resulting in a uniform and ultrathin modification layer (≈120 nm) on the surface of Zn foil. **Figure 5a** shows the schematic for the synthesis procedure NGO on the Zn anode. The NGO sample was initially synthesized by pyrolyzing graphene oxide in ammonia (NH_3) gas at 600 °C. This treatment introduces nitrogen-containing functional groups while preserving some hydrophilic oxygen anions. The resulting NGO nanosheets were then evenly dispersed in ethanol, and the Zn anode was immersed in this dispersion. Given the redox potential of Zn/Zn^{2+} (−0.76 V vs. SHE) and NGO (−0.4 V vs. SHE), the gradual lifting of the Zn foil leads to the reduction of negatively charged oxygen-containing groups, which enhances the adhesion of NGO nanosheets to the Zn foil.[71] Figure 5b presents an actual photo of the Zn foil after it has been coated with NGO, showing a uniform black region across the Zn foil that indicates the deposition of NGO. The top view of the Zn foil after NGO coating is depicted in the SEM images (Figure 5c). The wrinkles in the graphene are visible, confirming the application of parallel NGO on the Zn foil. Moreover, the XPS analysis confirmed the occurrence of the nitrogen- and oxygen-based functional groups in the NGO. The atomic content of the O and N in the NGO is 19.04 and 1.58 wt.%, respectively. The narrow scan XPS spectra for the N 1s are shown in Figure 5d, which displays the three significant contributions from the pyridinic (Npd), pyrrolic (Npr), and quaternary (Nq) N, with binding energies of 398.1, 400.1, and 402.5 eV, respectively. The functional group on the graphene helps enhance the wettability of the electrolyte, and it has been established that the functional groups on the graphene are promising for Li metal deposition because of the presence of the free electrons.[71] Considering the necessity of the Zn anode's plating/stripping stability, the plating/stripping measurements were performed at low and high current densities. Interestingly, the NGO@Zn anode works excellently in symmetric design at low and high applied current density over a longer period. At 1 mA cm^{-2} (Figure 5e), the Zn/Zn battery initially exhibited a 31 mV overpotential in the early cycles, which slowly increased in voltage hysteresis after about 100 h, ultimately failing abruptly after just 190 h. In contrast, the NGO@Zn/NGO@Zn symmetric cell demonstrated exceptional durability, maintaining stable cycling for over 1200 h (600 cycles) with a minimal overpotential of just 17 mV at 1 mA cm^{-2} (Figure 5e), and exhibited robust stability even at 3 mA cm^{-2}. When tested at 5 mA cm^{-2} and a plating/stripping capacity of 5 mAh cm^{-2} (Figure 5f), the bare Zn electrode showed severe voltage variations and nearly no stable cycling, starting with a significantly higher overpotential of 142 mV. Additional insights were gathered using an in-situ optical microscope. As shown in Figure 5g, when a small amount of electrolyte was used, the bare Zn electrode exhibited multiple sharp protrusions and an irregular surface texture during Zn metal deposition at 5 mA cm^{-2}. The pronounced height variations in the surface-profilometry image provide further evidence of the formation of disordered Zn dendrites on the bare Zn electrode after 90 min of plating. In divergence, the NGO@Zn electrode maintained a flat surface throughout the plating procedure (Figure 5g), with the corresponding area image revealing a minor height variation (Figure 5h). Further, the full-cell ZIB was developed using the LMO cathode and NGO@Zn anode, and the optical image of the developed cell is presented in Figure 5i. The LMO//NGO@Zn cell demonstrated outstanding cycling stability over 178 cycles at 1 °C, maintaining more than 80% of its initial capacity and a CE greater than 98.5%. The battery exhibited a high energy density of 199.88 Wh kg^{-1} during its first cycle, which remained relatively stable at 163 Wh kg^{-1} after 178 cycles, at 36% depth of discharge (DOD). This impressive performance is primarily ascribed to the minimized side reactions and the uniform deposition, which enhance the electronic kinetics of Zn deposition and help reduce the formation of "dead Zn" during cycling. The carbon coating on the Zn anode is a highly effective solution to address the significant stability challenges of zinc anodes in aqueous electrolytes. It significantly improves conductivity, stability, and efficiency by preventing dendrite formation and undesirable side reactions, including HER and corrosion. This coating enhances the overall performance of the Zn anode, ensuring more reliable and long-lasting operation.

3.2. Zn Anode Stabilization Via Metal Coatings

Beyond carbon, different materials, including metal, have been used to alter the Zn anode surface. The higher conductivity of almost all metals and their affinity toward Zn can be helpful in the creation of nucleation regions and unifying the electric field distribution on the Zn anode. Adding metal coatings on the Zn anode can help to create an additional even electric field across the surface. A uniform electric field is essential for ensuring that the charge distribution during cycling is balanced, which in turn helps improve the cycle life and stability of the anode. Metals with good conductivity can also help to distribute the electric field more evenly, thus preventing localized overheating or excessive strain on specific areas of the Zn anode. In addition, the metals that exhibit good chemical compatibility with zinc, such as nickel (Ni) or silver (Ag), can interact favorably with the

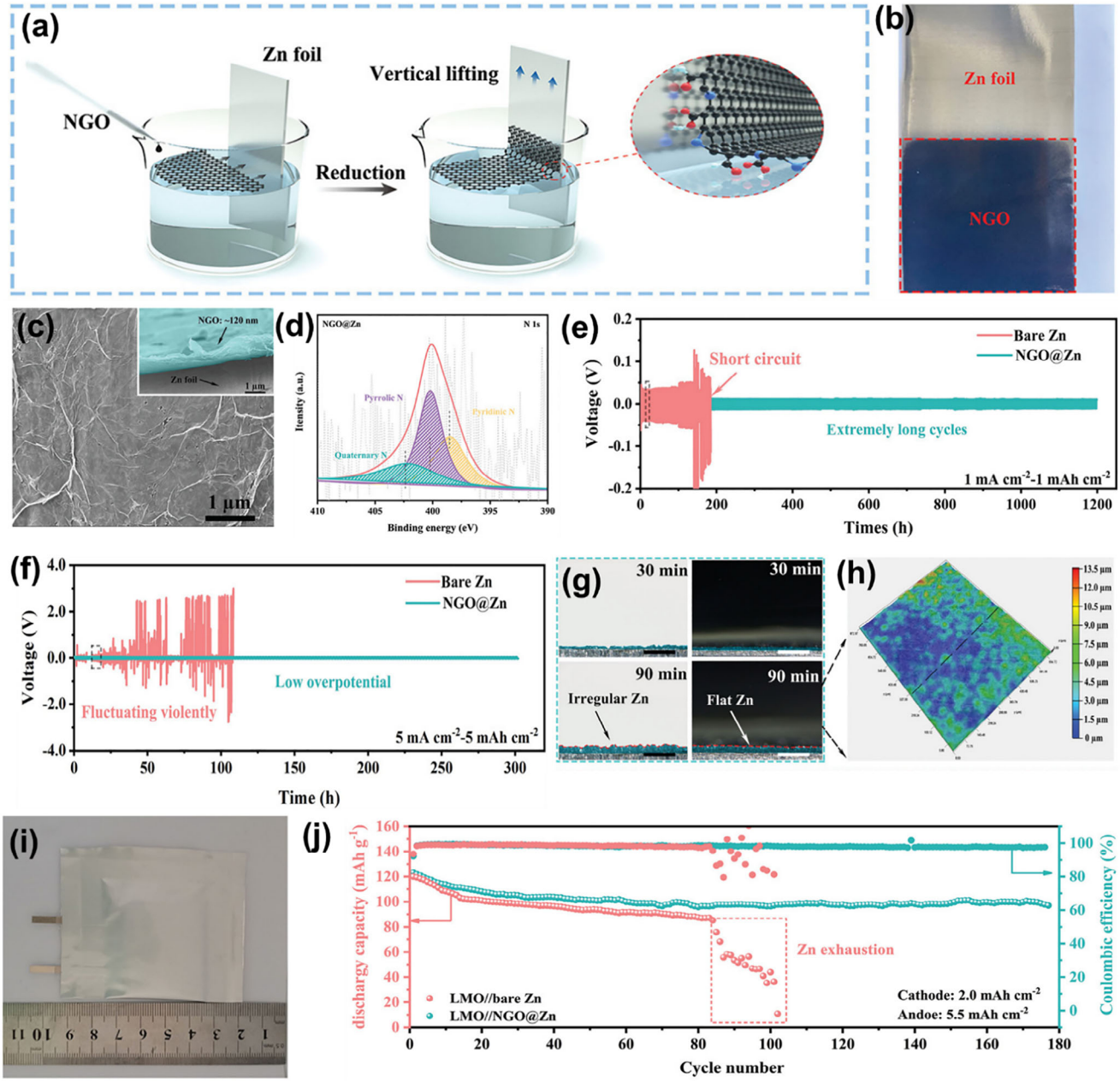

Figure 5. a) Schematic illustration to prepare graphene layer on the Zn anode, b) Optical image of the Zn foil coated with NGO, c) SEM image for the NGO@Zn, d) Narrow scan XPS spectra for the N1 S for NGO@Zn, the plating/stripping stability test for the NGO@Zn//NGO@Zn and Zn//Zn symmetric cell at current density of e) 1 mA cm^{-2} and f) 5 mA cm^{-2}. g) In situ optical microscopy visualization of Zn plating on bare Zn (left) and NGO@Zn electrodes (right). h) Optical surface-profilometry image of the NGO@Zn electrode. i) Optical image for the developed LMO//NGO@Zn ZIB and j) the cycling stability plot for the LMO//NGO@Zn ZIB. Reproduced with permission.[70]

Zn surface. This affinity can help to reduce side reactions, such as the development of undesirable by-products, which could degrade the battery's performance over time. Based on this assumption, Lu et al.[72] reported a diverse seed method to decorate the quasi-isolated nano-Au particles (Au-NPs), enabling an even and steady Zn-plating/stripping process on the anodes. The sputtering route has been employed to directly prepare the Au-NPs on the Zn anode with the size of the nanoparticles of about 100 nm. The Au-NPs on the Zn anode act as heterogeneous seeds, enabling uniform Zn plating/stripping (**Figure 6**a). The uniform decoration of the Au-NPs is seen in the SEM images (Figure 6b,c), which will help to minimize the side reactions and dendrite formation. The symmetric cell test further confirmed the excellent plating/stripping of the Au-NPs decorated Zn anode, showing the lower overpotential (Figure 6d) with enhanced stability up to 2000 h (Figure 6e). While excellent stability has been observed for the sputtered Ag-NPs decorated Zn anode at low current densities, achieving similar stability at higher current densities may

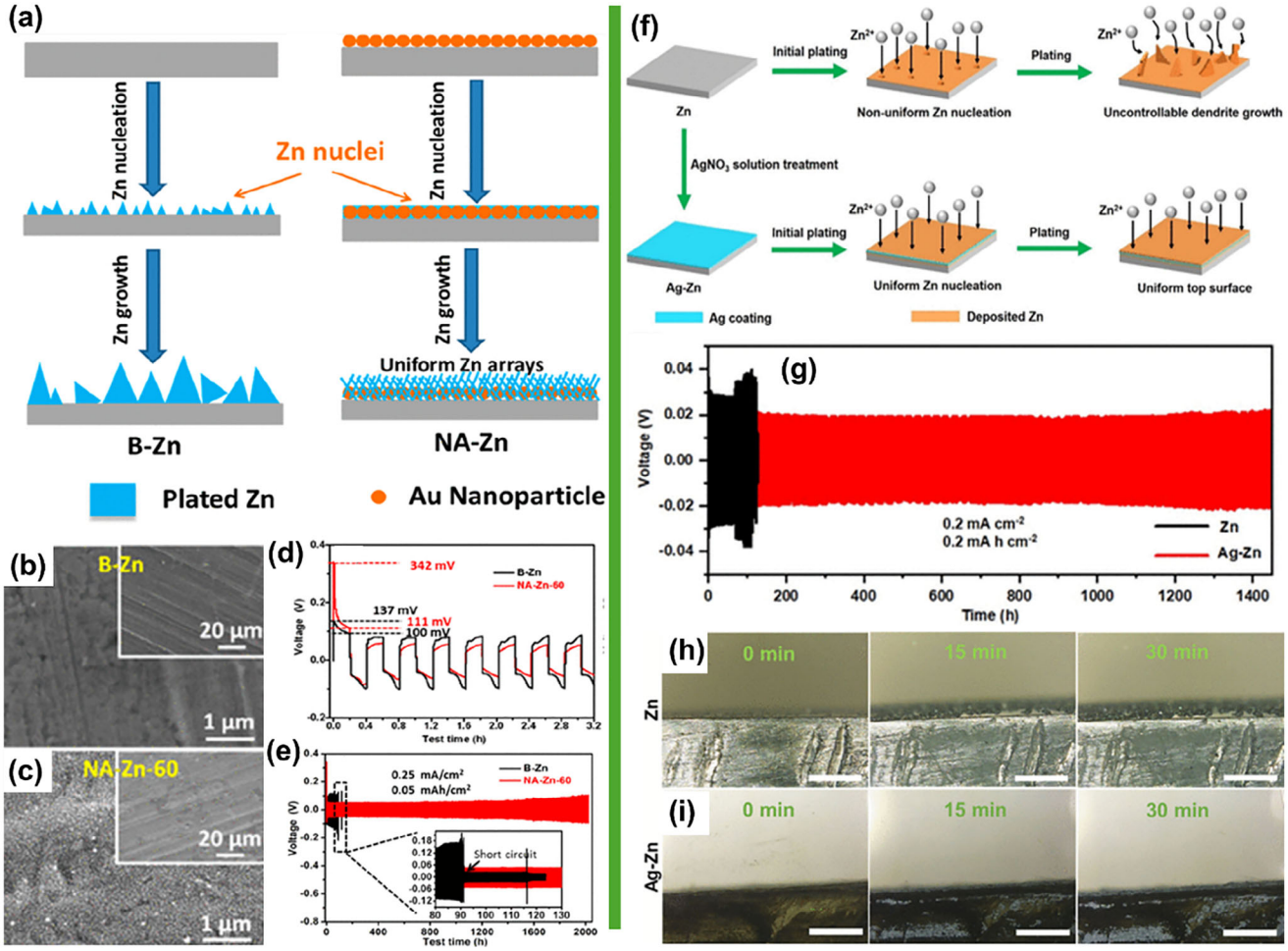

Figure 6. a) Representation showing uniform Zn deposition by Au nanoparticle via sputtering approach SEM for the b) pristine Zn and Zn-Ag NPs anode, d,e) plating/striping stability for the Zn//Zn and Zn-Ag NPs// Zn-Ag NPs symmetric cells. Reproduced with permission.[72] f) Schematic illustration for chemical synthesis of the Ag on the Zn anode g) plating/stripping stability for the Ag-Zn//Ag-Zn symmetric cell over 1450 h, Optical images for the in situ plating/striping at the current density of 10 mA cm^{-2} for the h) Zn//Zn and i) Ag-Zn//Ag-Zn symmetric cell. Reproduced with permission.[73]

prove challenging. This difficulty arises because the coating layers created through a physical preprocessing method often need help with issues such as poor interfacial contact and coating inhomogeneity. To address this issue, Lu et al.[73] developed a chemical route to decorate the Ag-NPs on the Zn anode via a replacement reaction between Zn and $AgNO_3$. Figure 6f shows the schematic to prepare the Ag on the Zn (Ag-Zn) anode, where the $AgNO_3$ solution was simply dropped on the Zn anode for a few minutes, there was an unprompted auxiliary reaction between $AgNO_3$ and Zn owing to the reactive nature of Zn rather than Ag. As an intact decoration of the Ag on the Zn, excellent stability has been seen at different current densities in the Ag-Zn/Ag-Zn symmetric cell. Figure 6g shows the plating/stripping stability for the Ag-Zn/Ag-Zn symmetric cell over 1450 h, deprived of any fluctuation and smaller overpotential. Moreover, cells demonstrate a small overpotential of 23 mV at a high current density of 1 mA cm^{-2} at a prolonged cycle life of 350 h. Even at a further high current density of 2 mA cm^{-2}, the Ag-Zn/Ag-Zn also showed a low overpotential of ≈26 mV, confirming the excellent stability of the chemically deposited Ag on the Zn anode. The in situ optical images further confirm the intact and dendrite-free surface on the Ag-Zn anode (Figure 6i), while in the case of the pristine Zn anode, prominent protrusions/dendrites have been seen even after 15 min, as seen in Figure 6h. While excellent stability has been observed after applying an Ag coating on the Zn anode, the high cost of silver makes it unsuitable for large-scale applications. Additionally, the cost-effectiveness of ZIBs must be maintained, meaning it is essential to identify a more affordable alternative metal that can serve as a protective layer.

Recently, different multimetals have been employed as a zincophilic layer on the Zn anode, including Cu, Sb, In, and their alloys with Zn. For example, Hong et al.[74] developed the Sb protecting layer on the Zn anode, considering the theoretical calculation. According to theoretical calculations, the binding energy of a Zn atom to the Sb (001) surface is higher than that of the Zn (001) surface. The lower binding energy for the Zn (001) surface (−0.63 eV) compared to the Sb (001) surface (−0.71 eV) indicates a stronger interaction between Zn and Sb (001). This suggests that Zn is more likely to preferentially deposit on the Sb (001) surface than on the Zn (001) surface. (**Figure** 7a).

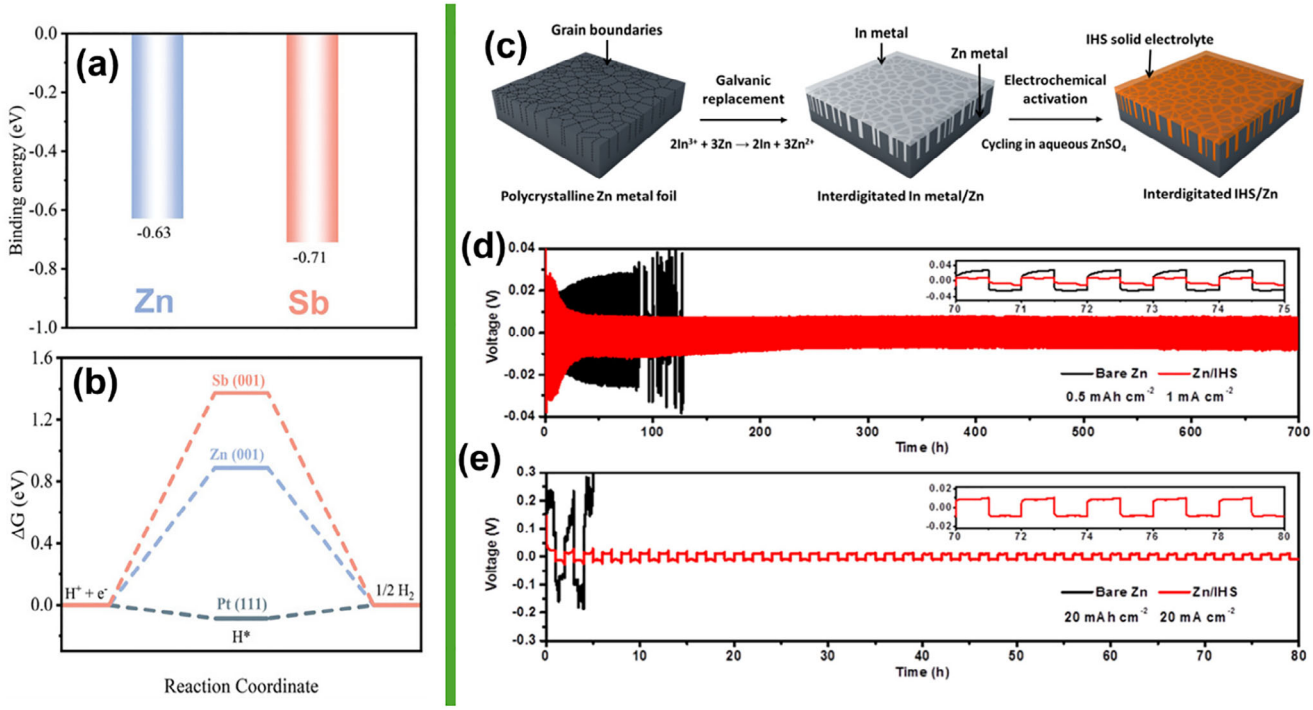

Figure 7. a) The binding energy for the Zn (001) and Sb (001) surface, b) Gibbs free energy plot for the Sb (001), Zn (001), and Pt (111) surface. Reproduced with permission. Reproduced with permission[74] c) Schematic illustration to prepare the IHS@Zn, the platting/striping stability for the IHS@Zn/IHS@Zn symmetric cell at d) 1 mA cm^{-2} and e) 20 mA cm^{-2}. Reproduced with permission. Reproduced with permission.[75]

Additionally, the more considerable Gibbs free energy (ΔG_H) for the Sb surface compared to the Zn surface indicates less favorable conditions for HER (Figure 7b). As seen in Figure 7b, the ΔG_H for Sb (001) is 1.37 eV, which is much higher than the Zn (001, 0.89 eV) and Pt (111, −0.09 eV), representative that Sb could overwhelm the HER, and this feature is essential to suppress the further side reactions. According to theoretical calculations, forming a thin layer of Sb that features numerous Zn-attracting sites and weak hydrogen adsorption capabilities is suggested as an active approach to curb the growth of zinc dendrites and reduce HER. Furthermore, enhanced wettability was seen for the Zn@Sb surface with a contact angle of 58.0°, much smaller than the pristine Zn surface (98.1°). The improved surface energy promotes the uniform distribution of electrolytes on the anode surface. Consequently, the assembled symmetric cell with Zn@Sb demonstrates outstanding plating/stripping stability under low and high current densities for over 1000 h, with minimal overpotential. Furthermore, Cao et al.[75] developed the In passivated Zn anode via galvanic replacement reaction from Zn/In architecture, which further transformed into the Zn/amorphous indium hydroxide sulfate (IHS) during the electrochemical activation cycling in the $ZnSO_4$ electrolytes (Figure 7c). Interestingly, the modified Zn anode with HIS layer demonstrates superior stability at 1 and 20 mA cm^{-2} (Figure 7d,e). Furthermore, metallic Cu was also better for defeating the side reactions and the dendrite formation over the Zn anode.[76] For example, Zhang et al.[77] reported the thin metallic Cu layer on the Zn anode via facile thermal evaporation. Remarkably, a Cu-coated zinc anode achieved an average CE of 99.7% over 3000 plating and stripping cycles at 10 mA cm^{-2} in a symmetric cell. The modified zinc anode demonstrated stable cycling for over 2500 cycles (equivalent to 5000 h) at a current density of 1 mA cm^{-2}. Additionally, a lifespan of 500 cycles was achieved for a full cell paired with a MnO_2 cathode.

3.3. Improving Zn Anodes Stability with Inorganic Materials

Inorganic compounds are widely employed as Zn anode coatings due to their outstanding electrochemical and chemical stability in mild electrolytes. These stable coatings form a protective barrier, preventing side reactions like HER and Zn corrosion, which can degrade performance. Common inorganic coatings contain metal oxides (e.g., ZnO, TiO_2), metal sulfides (e.g., ZnS, CuS), metal nitrides (e.g., TiN, ZrN), and MXenes (e.g., Ti_3C_2Tx).[32a] These materials avoid straight contact between Zn and the electrolyte, reducing dendrite formation and enhancing cycle life. Additionally, they alter the electrochemical environment, lowering HER overpotentials and promoting uniform Zn deposition.[78] Inorganic coatings thus advance the stability, efficiency, and durability of Zn anodes, making them crucial for long-lasting, high-performance energy storage systems. Among various inorganic compounds, metal oxides are preferred for researchers looking to passivate the Zn anode. A wide variety of metal oxides can be used for this purpose, and it's intriguing to note that each metal oxide possesses specific characteristics that help mitigate the conventional side reactions associated with the Zn anode. Metal oxides with a high dielectric constant are excellent candidates for creating manageable nucleation sites for Zn^{2+}. They also ease the rapid transport of Zn^{2+} because of the Maxwell-Wagner

polarization amid the Zn anodes and the surrounding layers (**Figure 8a**). Materials with high dielectric constants, such as ZrO_2[79] and Sc_2O_3,[80] have been explored well for this purpose. Liang et al.[79] prepared the ZrO_2 nanoparticles directly on the Zn anode via sol–the sol-gel method. The passivation of the ZrO_2 nanoparticles on the Zn anode results in excellent stability while plating/stripping at different current densities. At 0.25 mA cm^{-2}, they observed the plating/stripping over 3700 h with a smaller overpotential. Moreover, at the higher 5 mA cm^{-2}, the cell exhibited superior stability over 2100 h. Moreover, they have also studied the consequences of cycling on the morphologies of the Zn anode. Interestingly, the ZrO_2 passivated Zn anode shows intact nanoparticle-like morphology even after cycling for 100 cycles at a high current density of 5 mA cm^{-2}, as seen in Figure 8d–e. In the case of the pristine Zn anode, nonuniform and dented surfaces with severe cracks and obvious pulverization are observed after 100 cycles at 5 mA cm^{-2} (Figure 8b,c). Some metal oxides form the Ohmic contact interface with the Zn anode due to their higher work function than that Zn. Metal oxides such as the TiO_2 (4.4–5.0 eV), WO_3 (4.3–4.8 eV), MoO_3 (6.2–6.7 eV), and CeO_2 (4.3–4.7 eV) have higher work function than the Zn (3.6–3.8 eV)[81] electrons move from the Zn to the metal oxide through an interface characterized by Ohmic contact (Figure 8f).[82] To verify the contact type at the Zn-metal oxide interfaces, current-voltage (*I–V*) measurements were conducted. Figure 8g illustrates that all Zn anodes modified with metal oxides such as CeO_2, TiO_2, WO_3, and MoO_3 display a linear behavior, indicating a non-rectifying Ohmic contact. It is important to note that the interface accumulates negative charges, creating an electron-rich region referred to as the "anti-blocking layer." When the system is immersed in the electrolyte, the negative charges in this layer facilitate the attraction of cations and the repulsion of anions due to electrostatic interactions. This process helps control the flow of cations, promoting even Zn deposition (Figure 8h,i). Furthermore, the Al-doped ZnO (AZO) has also been tested as a protective layer on the Zn anode to avoid side reactions. Jin et al.[83] prepared the AZO on the Zn anode via magnetron sputtering, which has strong adsorption energy to Zn^{2+} because of the doped Al. The DFT calculation demonstrates higher adsorption energy for the AZO surface than the Zn anode surface (Figure 8j). The Al doping in ZnO can increase the charge concentration, facilitating a quicker desolvation process and enhancing deposition kinetics.

Generally, the lower adsorption energy is more likely to promote dendrite formation. At the same time, the strong attraction to Zn^{2+} enables the desolvation of hydrated Zn^{2+} and efficiently controls the Zn^{2+} flux over the coating layer and, hence, even deposition on the Zn anode (Figure 8k). As a result of AZO coating on the Zn anode, not only the AZO/AZO cell but also the developed full battery V_2O_5/AZO@Zn works excellently over long-term cycling with high-capacity retention, as seen in Figure 8l. In addition, the low Zn affinity layer has also been proposed to be best for avoiding the side reactions of the Zn anode. Zhang et al.[84] developed the faceted titanium dioxide (F-TiO_2) layer on the Zn anode with the (001) facet exposed to the Zn^{2+} ions. Interestingly, the (001) facet of the F-TiO_2 successively suppressed the side reactions of the Zn anode to stabilize the symmetric cell over 460 h. Theoretical calculations suggest that the (001) facet of the TiO_2 has higher binding energy for the Zn^{2+} ion than the other facet and the Zn anode surface (Figure 8m). Figure 8m shows that the binding energy between the Zn atom and the TiO_2 (100) surface is calculated to be −0.95 eV. This value is greater than the binding energies observed between the Zn atom and Zn surfaces, which are −0.68 and −0.86 eV, respectively. This suggests that zinc has a stronger affinity for the TiO_2 (100) surface compared to the Zn surfaces, favoring deposition on the former. Furthermore, the interaction between the Zn and different facets of the TiO_2 presented in Figure 8n again suggests that the (001) facet of the TiO_2 has a stronger tendency for the Zn.

Beyond metal oxides, several other metal compounds, including metal sulfides, nitrides, fluorides, and phosphides, have also been developed as protective coatings for zinc anodes. These compounds contain elements like sulfur (S), phosphorus (P), selenium (Se), and nitrogen (N), which exhibit a strong tendency to interact with Zn.[39,43,85,87] Han et al.[85] employed an easy technique to fabricate an artificial ZnF_2 layer where they controlled the thickness over 1 µm. This artificial solid electrolyte interphase (SEI) is selectively formed on only one side of the Zn foil through a straightforward chemical reaction conducted in a tube furnace at a relatively low temperature of 210 °C (**Figure 9a**), and the possible corresponding chemical reaction to form the ZnF_2 on the Zn anode is discussed in Figure 9b. Compared with the conventional SEI formation methods, the proposed method enhances the CE.[43] It effectively suppresses dendrite growth by allowing Zn plating/stripping underneath the SEI layer. The Zn anode with the artificial SEI layer demonstrates remarkable long-term cycling stability, with more than 700 h of operation in Zn/Zn symmetric cells at an areal capacity of 0.5 mAh cm^{-2}. Besides, when incorporated into Zn-ZnF_2//MnO_2 full cells, the system retains 89% of its capacity after 3000 cycles at 600 mA g^{-1}, illustrating its excellent cycling performance. In addition, DFT calculations were conducted, providing strong support for the interstitial diffusion mechanism of Zn-ion conduction. Similarly, the in situ ZnSe protecting layer on the Zn anode was developed by Yang et al.[86] using chemical vapor deposition (CVD). Figure 9c illustrates the chemical vapor deposition (CVD) process used to form ZnSe on the Zn anode, along with an enlarged optical image of the prepared ZnSe@Zn anode. During the selenization process, disordered Zn protuberances are converted into ZnSe nanoparticles, resulting in an ultrathin ZnSe layer that uniformly adheres to the Zn metal and forms a ZnSe@Zn heterostructure. This interface modification effectively lowers the Zn nucleation overpotential and enhances the local electric field distribution. The ZnSe overlayer, being zincophilic, promotes efficient Zn ion transport while blocking the movement of solvated species. Consequently, H_2 evolution and the formation of unwanted by-products are greatly reduced. Unlike traditional non-conductive coatings, the unique function of ZnSe is to encourage the preferential growth of the Zn (002) plane during the early stages of extended plating/stripping cycles, helping to prevent the formation of Zn dendrites. The electric field distribution mainly decides the nucleation and deposition of Zn. As depicted in Figure 9d, the bare Zn anode exhibits a uniform electric field distribution. However, micro-protrusions enhance the surrounding field intensity, which may lead to irregular deposition of Zn and contribute to dendrite formation, as illustrated in Figure 9e. Interestingly, the selenation of the Zn anode surface sharply decreases the electric field from 2.2×10^5 to 1.6×104 V m^{-1} with the aid of the ZnSe overlayer (Figure 9). A textured ZnSe coating helps

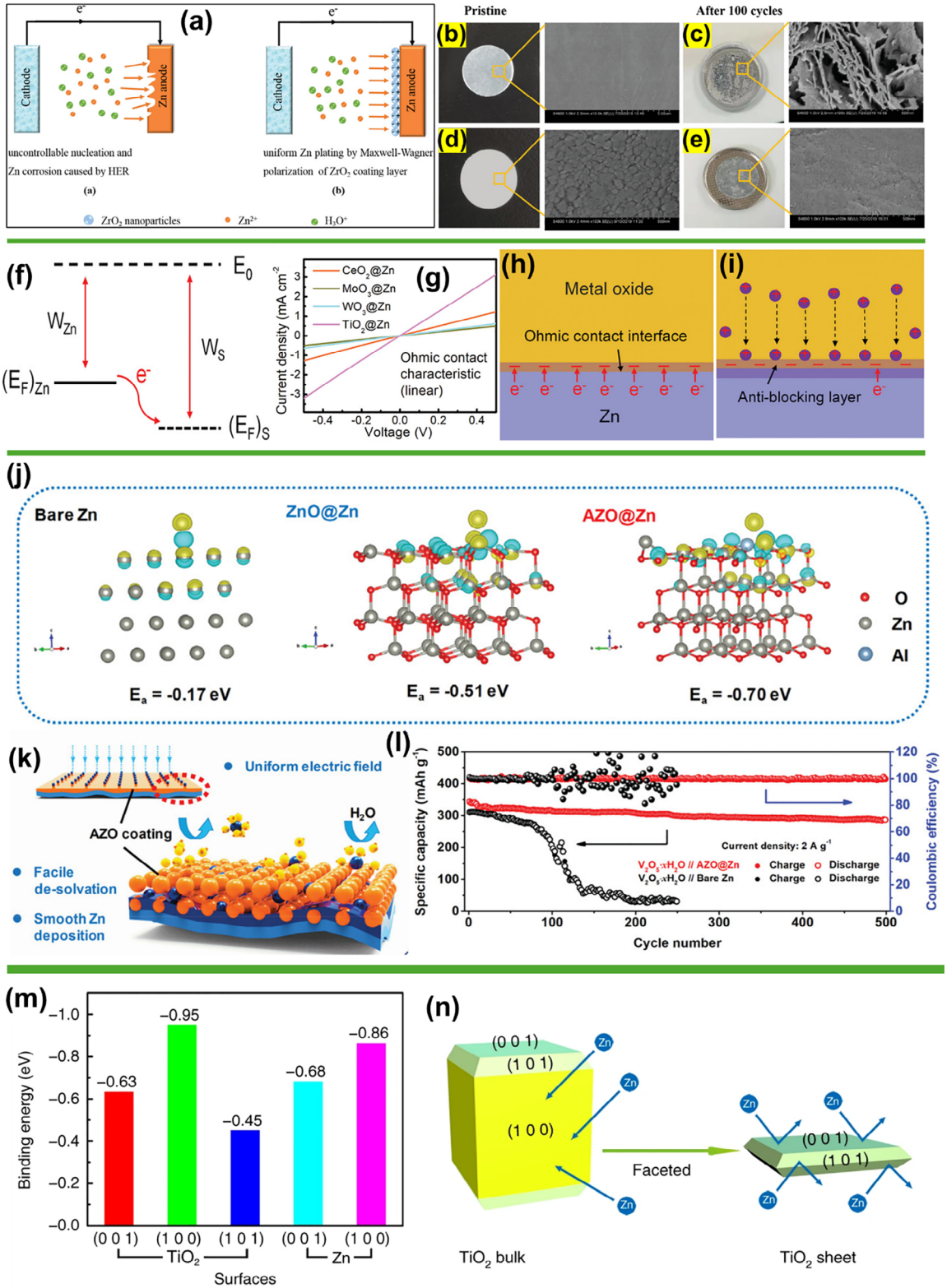

Figure 8. a) Schematic illustrating the stripping/plating processes at the pristine Zn anode and ZrO_2-coated Zn anode. The effect of plating/stripping before and after 100 cycles at a current density of 5 mA cm^{-2} is illustrated in the optical images and corresponding SEM images: b,c) pristine Zn anode and d,e) ZrO_2 coated Zn anode. Reproduced with permission.[80a] f) Electron flow path from the metallic Zn anode to the metal oxide g) Current-voltage curves of the Zn anodes modified by CeO_2, TiO_2, WO_3, and MoO_3 layers and h) the formation of the Ohmic contact interface between Zn and metal oxides and i) corresponding anti-blocking layer upon cycling. Reproduced with permission.[82] j) the Zn^{2+} adsorption energy for the pristine Zn anode,

homogenize the Zn surface's electric field, leading to a uniform charge flux. Moreover, the DFT calculation shows that the adsorption energy of Zn^{2+} on the ZnSe surface is more prominent than on the Zn surface (Figure 9g). Further, the effect of the ZnSe coating on the Zn anode is schematically illustrated in Figure 9h,i. As a result of the ZnSe passivation, the symmetric cell constructed with the ZnSe@Zn anode exhibits superior stability for the plating/stripping at a higher current density of 30 mA cm^{-2} over 172 h. In addition, layered double hydroxides have also been used as a passivation layer on the Zn anode, considering their large interspace, which will serve that Zn^{2+} channel to lower the Zn^{2+} migration barriers.[88] Furthermore, 2D MXene has been considered an effective passivation material to overcome the side reactions of the Zn anode. MXene with different functional groups, such as —OH, —O, and —F, which have high hydrophilicity and superb electronic conductivity, can help induce a uniform electric field distribution on the surface of the Zn anode. With the same consideration, Zhang et al.[89] reported MXene integrated onto the Zn anode using an in situ spontaneous reduction/assembly approach, effectively mitigating the Zn nucleation energy barrier and ensuring a uniform electric field distribution. Consequently, the symmetric cell constructed with the MXene-modified Zn anode exhibits outstanding plating/stripping stability for over 800 h at a current density of 0.2 mA cm^{-2}.

3.4. Organic Compounds Modified Zn Anode

Organic compounds, particularly polymers, are superior to rigid inorganic oxides due to their exceptional flexibility. This flexibility allows them to accommodate significant volume changes during cycling effectively. Moreover, organic compounds boast diverse functional groups, facilitating precise tuning of their properties. The most effective organic materials for modifying Zn anodes include polymers and metal-organic frameworks (MOFs). For instance, Zhao et al.[90] prepared the polyamide (PA) coating layer onto the Zn anode to increase the nucleation barrier and limit the 2D diffusion of Zn^{2+}. **Figure 10**a,b illustrates the effects of the PA coating on the zinc (Zn) anode. Related to the pristine Zn anode surface, the PA-passivated Zn anode surface features an exclusive hydrogen-bonding system and a strong capability to synchronize with metal ions. This allows it to role as a solid-state brightener that promotes uniform nucleation, regulates Zn^{2+} migration, and acts as an inhibitor of water and oxygen. Initially, they tested the stability of the PA-coated Zn anode in water over seven days. As seen in Figure 10c–f, the surface of the Zn anode coated with the PA displays a smooth surface morphology without any dendrite growth. Further, to visualize the effect of the PA coating, they perform gas evolution and corrosion tests. As seen in Figure 10g,h, the pristine Zn anode-based symmetric cell shows the gas evolution on the Zn surface, while in the case of the PA-coated Zn anode, we cannot see any gas evolution. This test was performed while the plating/stripping was at a current density of 0.5 mA cm^{-2}. Similar results have been found in the corrosion test (Figure 10i). The corrosion potential of Zn anode coated with a protective layer increased from −0.9738 V to −0.9627 V compared to uncoated zinc. This coating also led to a reduction in the corrosion current by 312.1 μA cm^{-2}. A more positive corrosion potential typically suggests a lower likelihood of corrosion-related reactions, such as H_2, and passivation caused by dissolved O_2. Furthermore, a decreased corrosion current indicates a slower rate of corrosion. The stability test for the PA-coated Zn anode was done in the symmetric cell, which shows excellent plating/stripping stability over 8000 h at a current density of 0.5 mA cm^{-2}. Wang et al.[91] proposed selectively polarized ferroelectric polymers as a shielding layer for the Zn anode. The proposed solution uses a polarized ferroelectric polymer (P(VDF-TrFE)) as a protective layer on Zn anodes. This layer helps concentrate Zn ions locally, promoting the horizontal growth of Zn plates and preventing dendrite formation. The result is enhanced cycling performance, with symmetrical cells achieving 2000 h of operation at 0.2 mA cm^{-2} and high-rate performance up to 15 mA cm^{-2}. The approach is also demonstrated in a full Zn–MnO_2 battery and ZIC, offering a new method for protecting Zn metal anodes in batteries. In addition to polymers, the MOF has also been investigated as a processing material for the Zn anode. The MOFs' non-conducting and highly hydrophilic nature, with their adjustable pore size distribution, can significantly alter the Zn^{2+} transport. For example, the poor wetting of the Zn anode is the major obstacle to stable SEI, and to overcome this, Liu et al.[92] proposed the nano-level wetting effect by using the non-conducting UIO-66 (Universitetet I Oslo-66) MOFs with an average particle size of 100 nm as a passivation layer on the Zn anode. The passivation of the UIO-66 on the Zn anode improves the wettability and regulates the electrolyte flux on the Zn anode. As a result of the excellent surface energy of the UIO-66 on the Zn anode, the charge-transfer resistance has been suppressed significantly. Interestingly, the contact angle of the aqueous electrolytes (3 M $ZnSO_4$ + 0.1 M $MnSO_4$) on the Zn anode drastically suppressed from 88.3 to 53.4° after coating of the UIO-66. As a result, the performance of Zn^{2+} plating and stripping remains stable and free from dendrite formation for more than 500 cycles. Furthermore, especially at high C-rates, the coating layer significantly reduces the overpotentials in a Zn/MnO_2 aqueous battery during cycling. Furthermore, He et al.[93] engineered the ZIF-11 layer on the Zn anode to block active water molecules at the interface, selectively enhancing cation transport. This effectively prevents parasitic reactions and suppresses dendrite formation. The strong adsorption of Zn^{2+} ions by nitrogen-rich zincophilic groups in the interface enables the formation of a thin electric double layer on the channel walls. This promotes smooth electrokinetic conduction on the surface and ensures stable deionization within the channel. The synergistic electrokinetic effects facilitate the controlled distribution of Zn^{2+} ions, encouraging uniform electrodeposition on the anode surface. Consequently, symmetric cells based on ZIF-11@Cu-Zn exhibit stable operation for up to 1800 h, nearly 18 times longer than the Cu-Zn-based symmetric cells operating at 0.5 mA cm^{-2}

ZnO, and AZO coated Zn anode k) Zn deposition process on the AZO-coated Zn anode, and l) the cycling stability for the V_2O_5/AZO@Zn and V_2O_5@ bare Zn batteries over 500 cycles. Reproduced with permission.[83] m) Binding energies of the Zn^{2+} with different facets of the TiO_2 and Zn surface, and n) interaction between Zn and different exposed facets of the TiO_2. Reproduced with permission.[84]

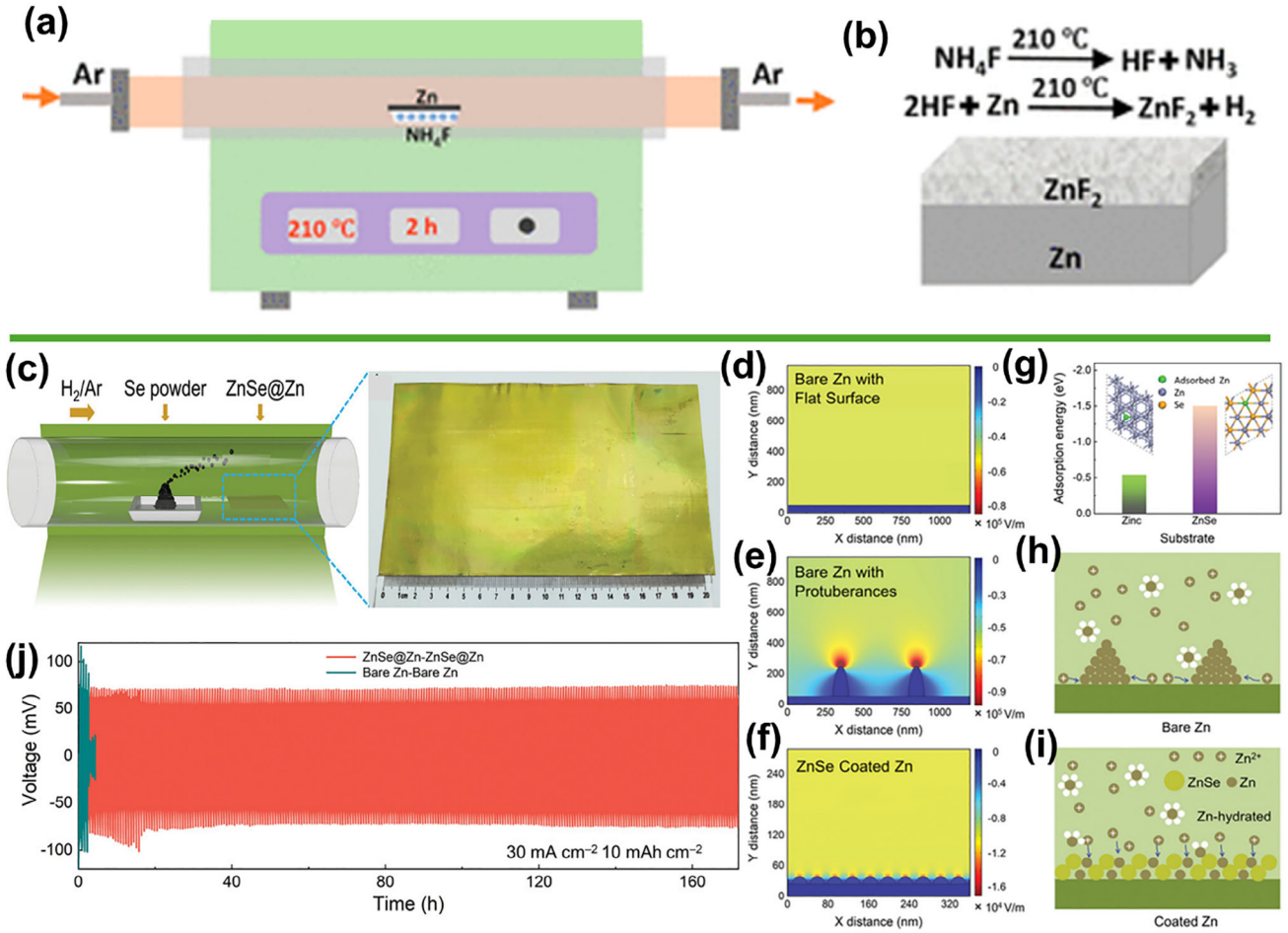

Figure 9. a) Schematic to prepare the ZnF_2 on the surface of the Zn anode with a controlled thickness of 1 µm, b) corresponding chemical reaction to form the ZnF_2 on the Zn anode surface. Reproduced with permission.[85] c) Schematic illustration of the CVD process to prepare ZnSe on the surface of the Zn anode and corresponding optical image for the ZnSe@Zn anode, the Simulated electric field distribution on the Zn anode d) without and e) with protuberances, and f) ZnSe@Zn anode. g) The adsorption energy for the Zn and ZnSe surface for the Zn^{2+}. Schematics of Zn^{2+} diffusion and reduction processes on h) bare Zn and i) ZnSe@Zn electrodes, respectively. Reproduced with permission.[86]

4. Electrolyte Innovations for Stabilizing Zn Anodes

Zn anode surface modification, including coatings with carbon, metal, inorganic, and organic materials, has been widely explored to enhance Zn anode stability by suppressing dendrite growth, minimizing side reactions, and improving Zn plating/stripping efficiency. These modifications create protective layers that regulate Zn deposition and reduce corrosion.[94] However, surface modification approaches have limitations, such as poor long-term adhesion, structural degradation over repeated cycles, and incompatibility with dynamic electrochemical conditions. Additionally, surface treatments often involve complex fabrication processes, increasing costs and limiting scalability.[62] Electrolyte modification offers an alternative and usually more effective solution for stabilizing Zn anodes. By tailoring electrolyte composition, ion solvation structure, and interfacial chemistry, electrolyte engineering can dynamically regulate Zn deposition, form solid electrolyte interphases (SEIs), and suppress unwanted side reactions like H_2 evolution and passivation.[95] Strategies such as highly concentrated electrolytes, water-in-salt electrolytes, and functional additives have demonstrated improved Zn reversibility, enhanced ionic conductivity, and prolonged battery lifespan. Unlike surface modifications, electrolyte modifications are inherently self-adaptive during cycling, ensuring continuous protection without additional processing. Therefore, electrolyte engineering provides a more scalable, cost-effective, and sustainable approach to achieving long-term Zn anode stability in rechargeable batteries.[96]

The electrolyte in ZIB performs a crucial role in battery electrochemistry, with its chemical composition directly influencing the diffusion dynamics and electrochemical reactions of Zn^{2+} ions.[97] The electrolyte can be modified to improve the CE of the Zn anode by suppressing Zn dendrite growth and minimizing side reactions.[97] Zinc salts such as $ZnSO_4$ are extensively employed as electrolyte salts in ZIBs because of their compatibility with electrode materials, long-term stability, cost-effectiveness, and eco-friendly nature, similar to other aqueous electrolytes. However, the solvated structure of Zn ions in aqueous solutions limits the movement and deposition of Zn^{2+} ions.[98] To overcome these challenges, Zn $(CF_3SO_3)_2$ with a wide potential

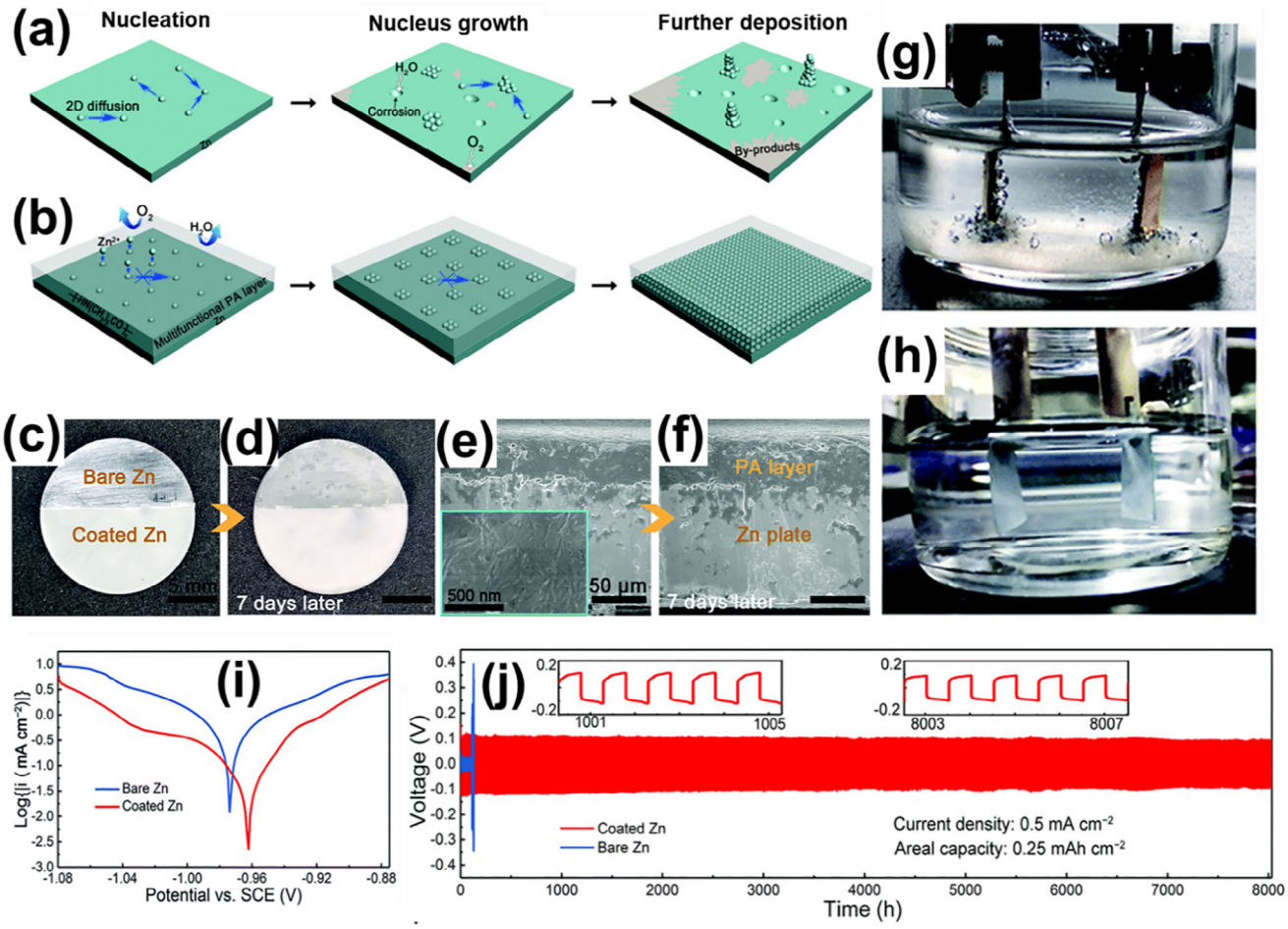

Figure 10. Schematic illustration shows the consequence of the water-based electrolytes on the a) pristine Zn and b) PA-coated Zn anode. c,d) The optical photographs of the Zn anode in water over Zn seven days and corresponding e,f) SEM images. The gas evolution test for the g) pristine Zn and h) PA-coated Zn anode in the symmetric cell at a current density of 0.5 mA cm^{-2}. i) corrosion test for the pristine Zn and PA-coated Zn anode, and j) stability test for the pristine Zn and PA-coated Zn anode in the symmetric cell at 0.5 mA cm^{-2}. Reproduced with permission.[90]

window and high water solubility is used. The presence of $CF_3SO_3^-$ interrupts the strongly bound water around zinc ions, reduces their hydration, and improves their mobility.[99] However, electrolytes such $Zn(CF_3SO_3)_2$ and other, including $Zn(CH_3COO)_2$, $Zn(TFSI)_2$, ZnF_2, $ZnCl_2$, $Zn(ClO_4)_2$, and $Zn(NO_3)_2$, have demonstrated insufficient for aqueous ZIBs.[51] Water-based systems face inherent challenges, including water depletion, lower thermodynamic stability relative to organic electrolytes, and a limited electrochemical window. To overcome these issues, modifying the electrolyte is essential for improving system performance. The most commonly reported electrolyte modification strategies are outlined in **Figure 11** and are discussed in this section.

4.1. Electrolyte Additives for Long-Lasting Zn Anodes

Electrolyte additives provide a simple approach to regulate the electric field distribution on electrode surfaces, facilitating uniform Zn ion diffusion and achieving uniform deposition without modifying the solvation structure.[100] Incorporating additives into the electrolyte improves the reversibility and cycling stability of the Zn electrode in alkaline media.[101] Various electrolyte additives have been introduced to enhance electrochemical performance by addressing challenges such as corrosion, passivation, shape changes, and dendrite formation. The model electrolyte additive must exhibit the resulting combined properties: i) a strong tendency to adsorb onto the zinc metal surface, forming a shielding layer that avoids direct interaction between Zn metal and H_2O molecules. ii) regulate Zn^{2+} flux and nucleation to suppress dendrite-prone crystallographic planes (100) and (110), while promoting the preferential growth of the Zn (002) plane by adjusting the surface morphology and crystallographic orientation. iii) suppression of H_2O activity while modifying the solvation sheath of Zn^{2+} ions and iv) optimization of critical physicochemical characteristics of the electrolyte, such as ionic conductivity, contact angle, and related parameters.[102] Electrolyte additives commonly used in alkaline batteries can be classified into two primary categories based on their chemical composition: organic and inorganic additives.

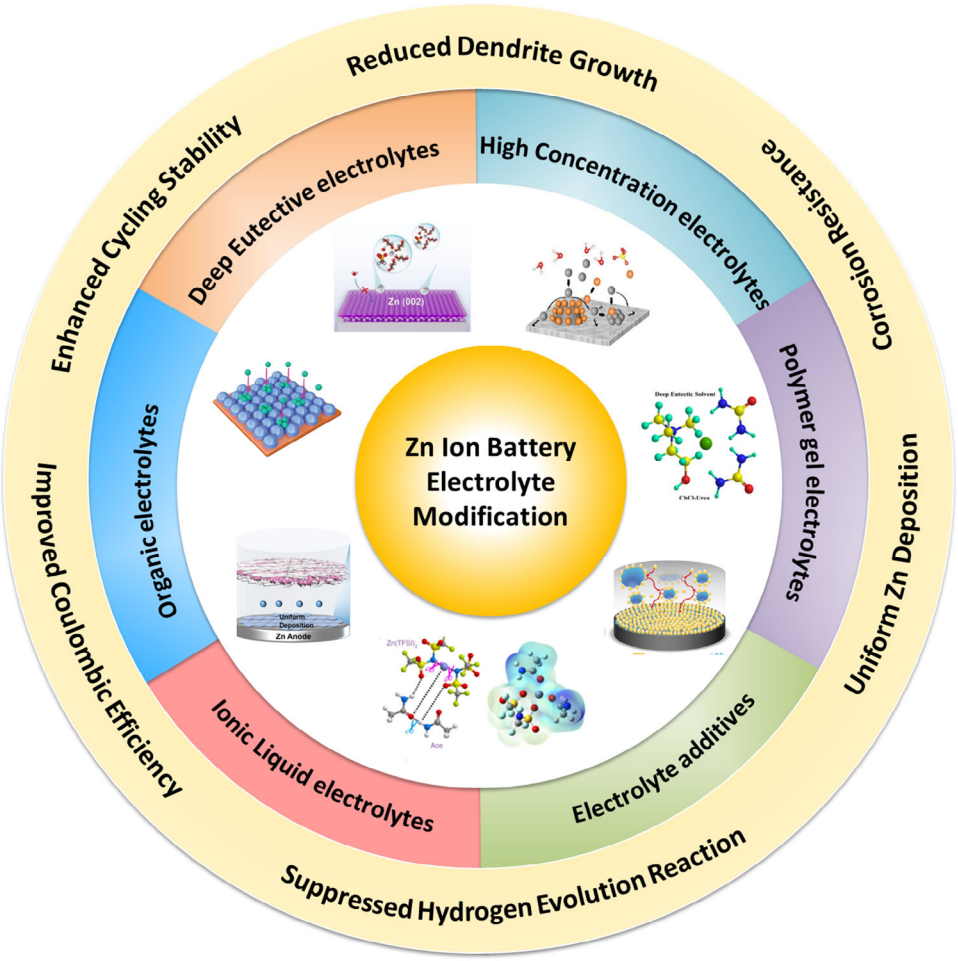

Figure 11. Schematic illustration of the commonly used electrolyte modification strategies.

4.1.1. Organic Additives

Organic electrolyte additives are crucial to overcome the challenges associated with AZIBs, such as zinc dendrite formation, HER, and limited electrochemical stability. These additives enhance ion transport, influence nucleation processes, and improve battery performance by regulating Zn deposition to ensure uniform plating and prevent dendrite growth. For example, formamide (FA) modifies the solvation structure of Zn^{2+} ions by reducing dendrite formation and expanding the electrochemical stability window of the electrolyte, thereby aiding higher voltage operations.[103] Similarly, polyethylene glycol (PEG), a water-soluble polymer, alters the viscosity of the electrolyte, reduces water activity, and facilitates smoother ion diffusion, endorsing even zinc deposition.[104] In addition, organic molecules act as surface-modifying agents that regulate ion transport and zinc deposition processes. Polymer-based coatings, such as chitosan and polymer composites, create a uniform electrolyte environment that minimizes irregularities in ion mobility and provides a protective layer against corrosion.[105] Citric acid, another organic additive, contains polar carboxyl groups that coordinate with Zn^{2+} ions, forming a dynamic interface that reduces side reactions like HER and dendrite formation. This interaction results in smoother, controlled electrodeposits.[106] Triethanolamine (TEA), by adsorbing onto active zinc sites, inhibits zinc ion dissolution and ensures uniform electrodeposition.[107]

Jin and coworkers stated that long-chain polyethylene oxide (PEO) polymer enhances the cycling stability and CE of Zn anode when used as an additive in $ZnSO_4$ electrolyte (**Figure 12a**). The PEO in aqueous electrolytes stabilizes Zn metal anodes through multiple mechanisms. The PEO molecules interact with Zn^{2+} ions via ether groups, regulate ion concentration distribution, and modify electrolyte viscosity, leading to suppressed Zn^{2+} ion transfer kinetics and uniform Zn deposition. In addition to this, PEO molecules are adsorbed on Zn surfaces to enhance anode surface uniformity and electrochemical stability by extenuating H_2 generation during Zn deposition. Adding a minor PEO (0.5%) stabilizes the Zn anode over 3000 h and CE of 99.5%.[108] Similarly, 1-Phenylethylamine hydrochloride (PEA) acts as an effective additive in $ZnSO_4$ electrolytes, which modifies the solvation sheath of Zn^{2+} and develops a protective layer on the surface of the Zn metal anode. ^2H nuclear magnetic resonance (NMR) analysis (Figure 12b) revealed a shift in the ^2H peak of D_2O from 4.780 to 4.835 ppm upon the addition of $ZnSO_4$, indicating coordination between Zn^{2+} and D_2O. As the PEA concentration

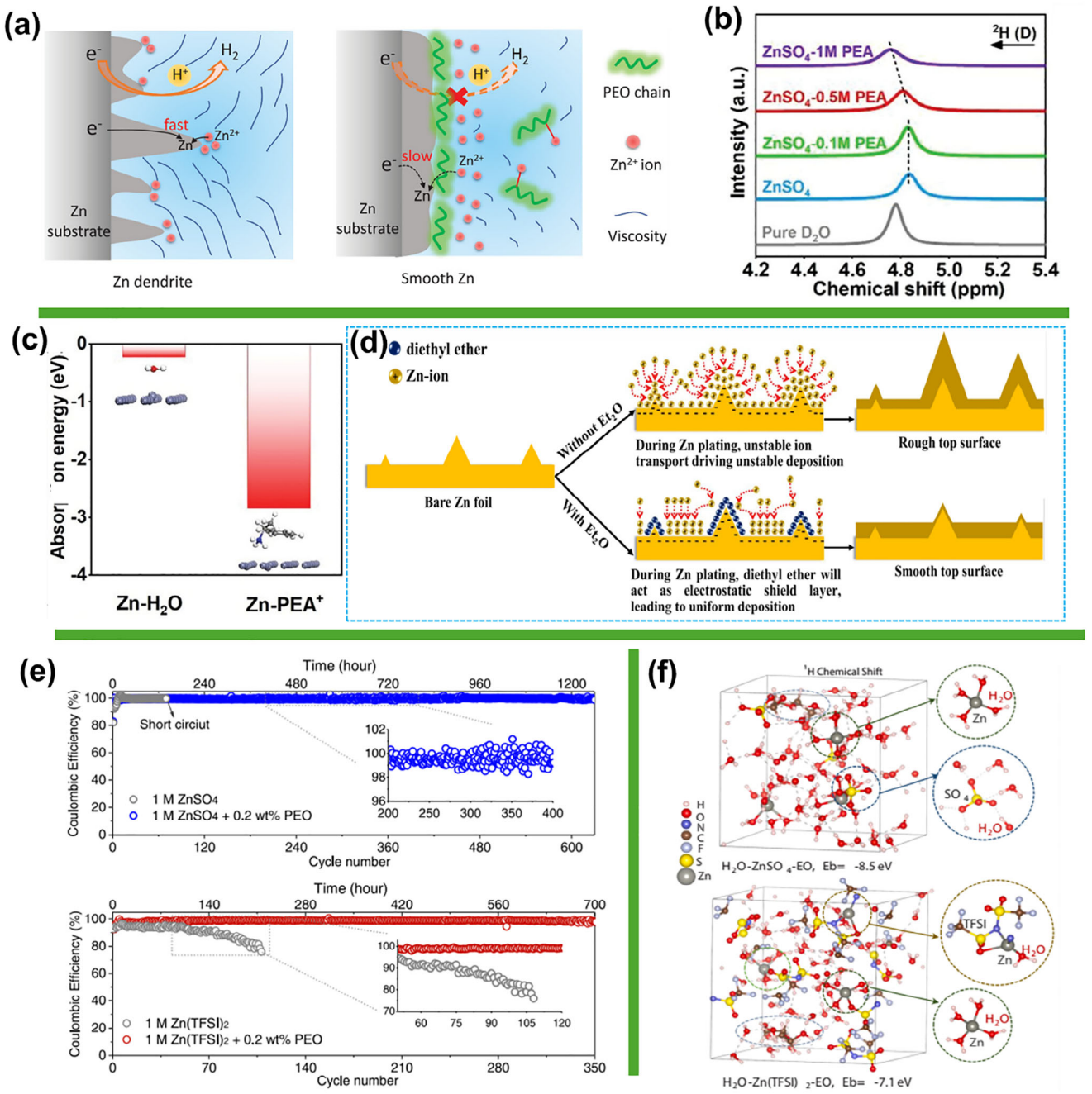

Figure 12. a) Schematic illustration of the PEO polymer molecule in $ZnSO_4$ aqueous electrolytes improving the stability of Zn metals through various mechanisms. Reproduced with permission.[108] b) ^2H NMR spectra of the $ZnSO_4$-PEA electrolytes with different PEA concentrations, c) Absorption energy of H_2O and PEA^+ on the Zn metal surface. Reproduced with permission.[109] d) Schematic illustration of the function with and without diethyl ether electrolyte additive to induce Zn uniform deposition. Reproduced with permission.[102] e) Cycling performance and CE profiles of Zn anodes in $ZnSO_4$-based and $Zn(TFSI)_2$-based electrolytes with and without PEO additive. f) Snapshots of molecular dynamics (MD) simulation for H_2O-$ZnSO_4$-EO and H_2O-$Zn(TFSI)_2$-EO, respectively, illustrating the Zn^{2+} environment in different electrolytes. Reproduced with permission.[110]

increased from 0.1 to 1.0 M, the ^2H peak shifted in the opposite direction, suggesting that some D_2O molecules previously bound in the Zn^{2+} solvation sheath were released. Additionally, the adsorption energy of PEA^+ (2.84 eV) on Zn metal was larger than that of H_2O (0.225 eV) (Figure 12c), implying that PEA^+ cations were strongly adsorbed on the Zn surface, thus reducing water-induced side reactions and improving the corrosion resistance of the Zn metal anode.[109]

In an additional study, Yan et al.[111] used three different organic polymers such as PEO, polyacrylamide (PAM), and poly(sodium 4-styrene sulfonate) (PSS), which modulate the solvation structure of Zn^{2+} and H_2 bonding in aqueous electrolytes.

The interaction of polymer additives with Zn^{2+} or SO_4^{2-} depends on the polarity of the polymer. Polymers with higher polarity exhibit strong interaction with Zn^{2+} ions. The 0.2 wt.% PAM additive in 1 M $ZnSO_4$ electrolyte showed steady cycling over 1300 h with a CE above 99.65%.[111] Other polymers, such as methyl-pyrrolidinium bromide, act as effective electrolyte additives for Zn anodes, which interact with Zn^{2+} ions, regulate ion distribution, and modify viscosity. These actions suppress Zn^{2+} transfer kinetics and promote uniform Zn deposition. Further, polymers, such as poly(tetrafluoroethylene) and poly(ethylene),[112] are added to the electrolyte and act as binders that help to maintain the integrity of the electrode particles and reduce the growth of dendrites. However, the presence of these polymers can lower the electrical conductivity of the electrodes and cause increased polarization, especially when used in high concentrations. Zhao and coworkers reported fluorinated anionic surfactant additives. The adsorption layer of perfluorooctanoic acid, with its strongly electronegative perfluoroalkyl chains, redistributes Zn^{2+} flux near the Zn anode-electrolyte interface and suppresses sulfate anion migration to the Zn anode. This surfactant-like additive lowers surface tension and enhances electrolyte wettability on the Zn electrode. Even a trace amount of perfluorooctanoic acid significantly improves the reversibility of Zn plating, achieving a specific capacity of 153 mAh g^{-1} at 5 A g^{-1} and excellent cycling stability with high CE.[113] Xu and coworkers reported sodium dodecyl benzene sulfonate and diethyl ether (Et_2O) additives, which adsorb onto the Zn surface and form an electrostatic shielding layer (Figure 12d).[102] It was observed that just 2 vol.% of Et_2O is adequate to achieve complete exposure of the initial Zn protrusions, effectively preventing the formation of Zn dendrites. Consequently, the Zn surface remains smooth even after repeated plating/stripping cycles, leading to an extended lifespan for the ZIB. Liu et al.[114] reported that cetyltrimethylammonium bromide (CTAB) as an additive significantly suppresses dendrite formation. The authors showed that adding CTAB to the $ZnSO_4$ electrolyte increased pH from 4.53 to 4.70, 4.82, and 4.92 when 0.1, 0.2, and 0.3 M CTAB were added, respectively. This indicates that CTAB effectively decreases the number of free H^+ ions and prevents anodic corrosion more efficiently than the liquid electrolyte. While a lower pH facilitates zinc anode corrosion, a higher pH hinders the formation of byproducts. The improved stability and reduced side reactions contribute to the high reversibility of the battery, making it more efficient and durable. The assembled Zn-MnO_2 battery demonstrates a remarkable specific capacity of 126.56 mAh g^{-1} at a high current density of 4 A g^{-1} after 1000 cycles. In another study, Yan et al.[110] investigated the impact of incorporating PEO into $ZnSO_4$-based $Zn(TFSI)_2$-based aqueous electrolytes. The study showed the important role of salt anions in shaping the solvation structures and hydrogen bonding networks within the electrolyte. Different anions, such as $TFSI^-$ (trifluoromethanesulfonate) and SO_4^{2-}(sulfate), have distinct impacts on the solvation environment and the reaction kinetics of Zn^{2+}ions. The study demonstrated that adding PEO additive modifies the solvation environment around zinc ions and significantly reduces the overpotential for zinc plating and stripping. This leads to the extended cycle life of the ZIB by seven to ten times (Figure 12e) compared to traditional electrolytes without PEO. The research also revealed that the PEO additive exhibited different effects on two zinc salt solutions, namely $ZnSO_4$ and $Zn(TFSI)_2$ (Figure 12f).

Qiu et al.[115] conducted a fascinating study employing hyaluronic acid (HA) as a polymer additive to enhance the performance of ZIBs. HA, composed of repeating units of d-glucuronic acid and N-acetyl-d-glucosamine, performs an essential role in attaining dendrite-free ZIBs by creating efficient tunnels for smooth Zn^{2+} transport. The −COOH groups reduce cation-anion interactions, while hydrophilic −OH groups modify the hydrogen bond network. SEM images (**Figure 13**a,b) revealed zinc sulfate byproducts on Zn anodes after deposition in pure $ZnSO_4$ electrolyte. Consequently, zinc anodes exhibit a rough surface free from dendrites due to effectively suppressing zinc ion diffusion. In contrast, the $ZnSO_4$–HA electrolyte produced a smoother Zn layer and significantly suppressed byproduct formation. Moreover, Zn/Zn symmetric cells with HA additives demonstrated a cycling life of 2200 h at 1 mA cm^{-2}/1 mAh cm^{-2} and 800 h at 5 mA cm^{-2}/5 mAh cm^{-2}. Further, Liu and coworkers introduced tripropylene glycol (TG) as a dual-function organic electrolyte additive. TG participates in the Zn^{2+} solvation sheath and adsorbs on the Zn anode surface, effectively suppressing side reactions and dendrite growth. Theoretical and experimental studies revealed that TG adsorbs preferentially parallel to the Zn surface (−1.22 164 eV), forming strong chemisorption bonds that prevent uncontrolled 2D diffusion and promote uniform Zn deposition. Additionally, the highest occupied molecular orbital of TG (−6.84 325 eV) compared to water facilitates charge transport on Zn surfaces, as shown in Figure 13c–f. The CE of the Zn/Cu cell was tested in different electrolytes. A cell utilizing a 10% TG electrolyte demonstrated an impressive CE of 99.81% over 1000 cycles, maintaining excellent stability (Figure 13g). SEM images of Zn deposition on a Cu substrate with bare $ZnSO_4$ electrolyte and 10% TG electrolyte (Figure 13h) showed that the Zn anode surface was flat and uniform when 10% TG electrolyte was used.[116] Composite polymer/molecular additives, such as a hydrophobic-zincophilic bifunctional acrylic-polyvinylidene fluoride (PVDF) copolymer layer produced via free radical polymerization, have demonstrated remarkable effectiveness in preventing corrosion and dendrite growth.[117] Moreover, small molecule monomers like alcohols and ethers, known for faster Zn^{2+} transport and lower viscosity, have been explored as zinc electrolyte additives. Alcohols such as ethanol, methanol, and ethylene glycol (EG) enhance Zn^{2+} solvation, affecting its desolvation on the anode by modifying the Zn^{2+} solvation sheath. For instance, ethanol in alkaline electrolytes alters the $Zn(OH)n^{2-}$ complex to form $Zn(OH)_{4-n}(OR)_n^{2-}$, while EG forms $[Zn(EG)_3]^{2+}$ complexes, slowing Zn nucleation.[118] These alcohol additives significantly improve ZIB electrochemical performance at low temperatures. While various organic electrolyte additives have been suggested to resolve issues with the Zn electrode and improve battery performance, it is important to note that, like inorganic additives, organic additives primarily regulate the morphology of deposited Zn but do not provide effective protection against its contact with aqueous electrolytes. Therefore, to optimize ZIB performance and meet market demands, it is promising to employ strategies that can effectively address issues associated with the metallic Zn anode.

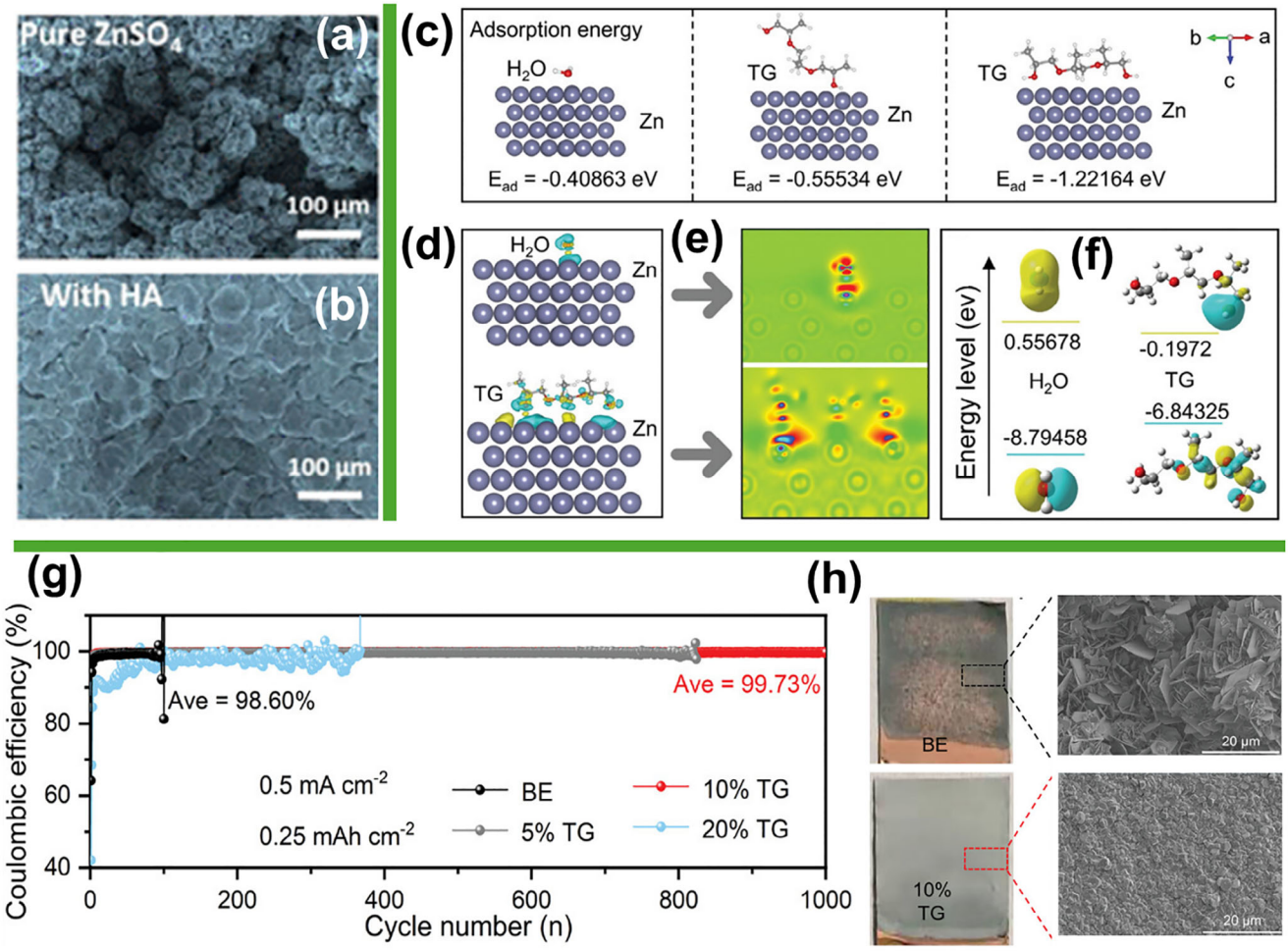

Figure 13. SEM images of the Zn plating layer for 1 h in a) pure $ZnSO_4$ and b) $ZnSO_4$–HA electrolytes. Reproduced with permission.[115] c) Comparison of H_2O and TG molecule adsorption on Zn (002) d) Charge density differences between Zn plates with TG or H_2O and corresponding isosurfaces. e) 2D contour map showing Zn-TG and Zn-H_2O interactions. f) LUMO and HOMO isosurfaces of H_2O and TG. g) CE of ZIB in different electrolytes at 0.5 mA cm^{-2}, 0.25 mAh cm^{-2}, h) Digital photographs and corresponding SEM images for zinc deposition on Cu substrate. Reproduced with permission.[116]

4.1.2. Inorganic Additives

Inorganic additives typically utilize high-redox-potential cations to form an electrostatic shield around Zn ions at dendrite formation sites, promoting uniform Zn deposition. These additives include metal oxides, metal ions, hydroxides, metal nanoparticles, and transition metal compounds.[119] Recently, metal-ion additives have emerged as a promising strategy to enhance the stability of Zn anodes and mitigate dendrite growth by forming protective interfacial layers.[120] In aqueous electrolytes, H^+ ions from solvated H_2O molecules are reduced at the Zn anode, producing H_2 gas that escapes, leaving OH^- ions in the electrolyte. The accumulation of OH^- ions raises the local pH at the anode surface, accelerating uneven side reactions that form protrusions. These protrusions, characterized by strong electric fields at their tips, attract Zn^{2+} ions, intensifying dendrite growth. Metal-ion additives with negative reduction potentials accumulate at the tips of these protrusions, effectively suppressing their growth. Some inorganic additives, such as Bi^{3+}, Sn^{2+}, and Pb^{2+}, prevent zinc metal corrosion due to their high overpotential for H_2 evolution, which suppresses water-induced H_2 evolution. Additionally, additives like Pb^{2+} and Sn^{2+} are reduced before Zn deposition, serving as substrates and preventing dendrite formation.[121] Electrolyte additives containing metal cations with redox potentials lower than Zn^{2+} (−0.76 V vs SHE), such as Na^+ (−2.714 V vs SHE),[122] Mn^{2+} (−1.18 V versus SHE),[123] and Mg^{2+} (−2.372 V versus SHE),[124] can alleviate the tip effect during Zn deposition. For instance, incorporating inorganic additives such as Mg^{2+} into the electrolyte lowers the local pH at the anode surface, preventing zinc dendrites (Figure 14a). Mg^{2+} ions, with their negative reduction potential, accumulate at the tips of protrusions on the Zn anode, suppressing their growth and enhancing battery stability. Furthermore, as explained by Coulomb's law, trivalent cations like Ce^{3+} and La^{3+} have been demonstrated to produce stronger electric fields than divalent cations. These cations can preoccupy active Zn nucleation sites, restricting the surface diffusion of Zn ions and fascinating them from reducing at alternative sites. In^{3+} cations have a slightly higher SHE potential than Zn^{2+}, which

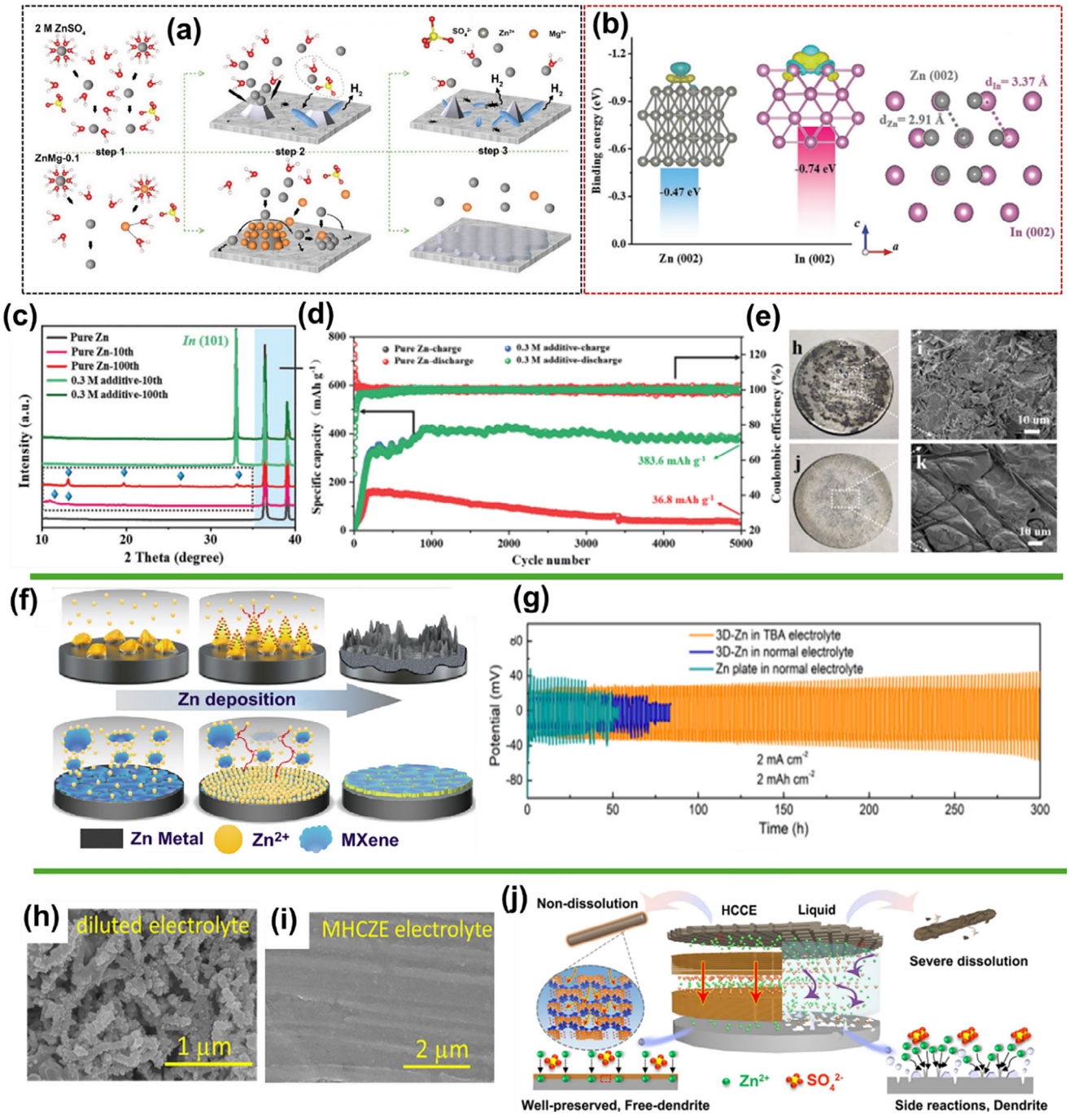

Figure 14. a) Schematics illustration of Zn deposition process in $ZnSO_4$ and ZnMg-0.1 electrolyte. Reproduced with permission.[124] b) The binding energy of Zn on Zn(002) and In(002) planes, along with 3D charge density and atomic arrangements showing lattice mismatch between In(002) and Zn(002). c) XRD patterns for pure Zn and 0.3 m additive modified Zn anodes. d) cycling stability of Zn–V2O5 battery at 5 A g^{-1}. e) FESEM images of electrode surface before and after electrolyte additive modification. Reproduced with permission.[125] f) Schematic of the effect of an MXene additive on the Zn deposition process. Reproduced with permission.[126] g)Cyclingg stability performance of ZIB cells in different electrolytes at 2 mA cm^{-2}. Reproduced with permission.[127] Surface morphology of Zn plate after plating/stripping in (h) $ZnClO_4$ and (i) $NaClO_4$-$ZnClO_4$ electrolyte. Reproduced with permission.[128] j) Schematic illustration of the interface protection effect in HCCE and liquid electrolyte. Reproduced with permission.[129]

form in situ protective indium metal interphase on the anode surface instead of an electrostatic shield. Zhang et al.[125] reported that strong interaction between Zn atoms and In (002) planes, along with the low mismatch between Zn (002) and In (002) planes, promotes zinc growth along Zn (002) and fills transport gaps in the In interphase (Figure 14b,c). This flat, zincophilic interphase lowers the Zn ion gradient, reduces the nucleation barrier, and ensures a smooth anode surface. Zn//V_2O_5 full cells with modified electrolytes exhibit excellent stability, retaining 383.6 mAh g^{-1} at 5 A g^{-1} even after 5000 cycles. (Figure 14d,e).

In a recent report by Sun and coworkers, Ti_3C_2Tx MXene, known for its 2D nature, abundant surface functional groups, excellent metal conductivity, and strong hydrophilicity, was employed as an electrolyte additive to improve the reversibility and kinetics of the Zn plating–stripping process.[126] The electrostatic interaction between Zn^{2+} ions and MXene additives enables their effective adsorption onto the Zn electrode surface, forming a conductive buffer layer. This MXene–Zn^{2+} adsorption layer plays a critical role in regulating the distribution of Zn^{2+} ions on the electrode surface, acting as "seed points" to facilitate homogeneous nucleation. This mechanism ensures uniform Zn deposition while effectively suppressing dendrite formation, as depicted in Figure 14f. Incorporating MXene additives has demonstrated remarkable improvements in the performance of Zn anodes, which achieved outstanding cycling stability of over 1100 cycles at 2 mA cm^{-2} with a CE of nearly 100%. Cationic surfactant-type electrolyte additives like tetrabutylammonium sulfate (TBA_2SO_4) can prevent dendrite formation by creating a TBA^+ protective layer. This layer exhibits remarkable cycling stability due to the unique zincophobic repulsion mechanism and non-redox TBA^+ ions on the Zn anode surface. These ions effectively manage the initial nucleation process and inhibit dendrite growth through a shielding effect, maintaining the Zn anode morphology with minimal change. In symmetric cells, the Zn anode exhibited outstanding cycling stability for over 300 h at a current density of 2 mA cm^{-2} (Figure 14g).[127] In our previous research, adding $NaClO_4$ to $ZnClO_4$ electrolyte proved to be an effective strategy for achieving dendrite-free zinc plating and stripping, ensuring 100% CE.[128] SEM images revealed that the pristine zinc plate had a smooth surface. Following several cycles, the Zn plate in the modified electrolyte maintained a dense and dendrite-free morphology. In contrast, zinc dendrites were significantly formed using a dilute electrolyte (Figure 14h,i). These results show that the concentrated electrolyte prevents dendrite formation and stabilizes capacity during prolonged cycling through the self-passivation effect. Gao et al.[129] proposed a new type of inorganic highly concentrated colloidal electrolyte (HCCE) for ZIBs, which promotes simultaneous robust protection of both cathode and anode and suppresses element dissolution, dendrite growth, and irreversible by-product formation (Figure 14j). The full cell Zn//α-MnO_2 with HCCE electrolytes maintained 100% capacity at 200 mA g^{-1} after 400 cycles (290 mAh g^{-1}) and 89% capacity at 500 mA g^{-1} after 1000 cycles (212 mAh g^{-1}).

In addition to this, certain inorganic additives such as phosphates (K_3PO_4),[130] $Zn_3(PO_4)_2$,[131] and sodium succinate[132] are employed to protect Zn anodes. Incorporating ligand molecules, such as triethylamine hydrochloride, into $ZnCl_2$ and $ZnSO_4$ electrolytes alters the solvation environment of Zn^{2+} ions, suppressing the formation of side products in aqueous systems and promoting a reversible Zn anode.[133] Moreover, graphene and carbon-based inorganic additives have demonstrated substantial potential in enhancing the performance of ZIBs. These additives contribute to the formation of a stable SEI on the Zn anode, effectively preventing dendrite growth and improving cycling stability. For instance, graphene quantum dots (GQDs) have been utilized as electrolyte additives, which enhance Zn^{2+} ion kinetics and resistance to corrosion due to their electrocatalytic properties.[134] Abdulla et al.[135] combined graphene oxide into a $ZnSO_4$ electrolyte, resulting in strong binding energy with Zn^{2+} and achieving uniform field distribution on the Zn anode surface. Typically, the Electrolyte additives can enhance electrode performance but also introduce challenges such as higher fabrication costs, reduced active material content, and lower energy density. Variations in an additive composition may affect functionality, increase impedance, decrease ionic conductivity, and raise polarization. Some additives selectively interact with specific sites, requiring external stimuli for effectiveness. Moreover, focusing solely on electrolyte modifications may limit the potential for more comprehensive solutions, such as interface engineering and structural design. A combined approach that integrates multiple strategies is essential to overcoming these limitations and achieving optimal performance.

4.2. Water-in-Salt (WIS) Electrolytes

Water-in-salt electrolytes (WISs) have emerged as promising solutions for improving the performance of ZIBs by suppressing issues such as zinc dendrite formation, H_2 evolution, and corrosion. The high salt concentration in WISs reduces the activity of free water molecules, enhancing CE and stability during Zn plating/stripping.[136] This concentrated environment alters Zn^{2+} ion solvation and transport behaviors, broadening the electrochemical stability window, reducing polarization, and enabling consistent ion migration. Furthermore, the limited availability of water in high salt-to-water ratio WIS electrolytes disrupts the natural H_2 bonding network, facilitating the incorporation of anions into the Zn^{2+} solvation structure.[137] This partial replacement of water molecules by anions suppresses H_2 evolution during Zn electrodeposition, thereby improving the cycling stability and overall efficiency of ZIBs.[138] Recently, high-concentration colloidal electrolytes derived from palygorskite nano-inorganic materials have been used to substitute traditional liquid electrolytes in aqueous ZIBs. This approach lowers the energy barrier for detaching water molecules from hydrated Zn^{2+} ions on the surface, facilitating a more uniform zinc deposition.[129]

$ZnCl_2$ is one of the most water-soluble inorganic zinc salts, capable of achieving extremely high concentrations of up to 30 M. This high concentration leads to the formation of a $[Zn(OH_2)_2Cl_4]^{2-}$ solvation structure, which significantly improves the CE of asymmetric cells, achieving 95.4% compared to 72.3% at 5 m $ZnCl_2$. When the water-to-$ZnCl_2$ ratio is further reduced to 2.33, a molten hydrate electrolyte is formed, wherein all water molecules are coordinated by Cl^- ions, resulting in a tetrahedral $[ZnCl_4]^{2-}$ solvation structure (**Figure 15a**). This unique solvation environment enables smoother zinc deposition with negligible hydrogen evolution (Figure 15b). This

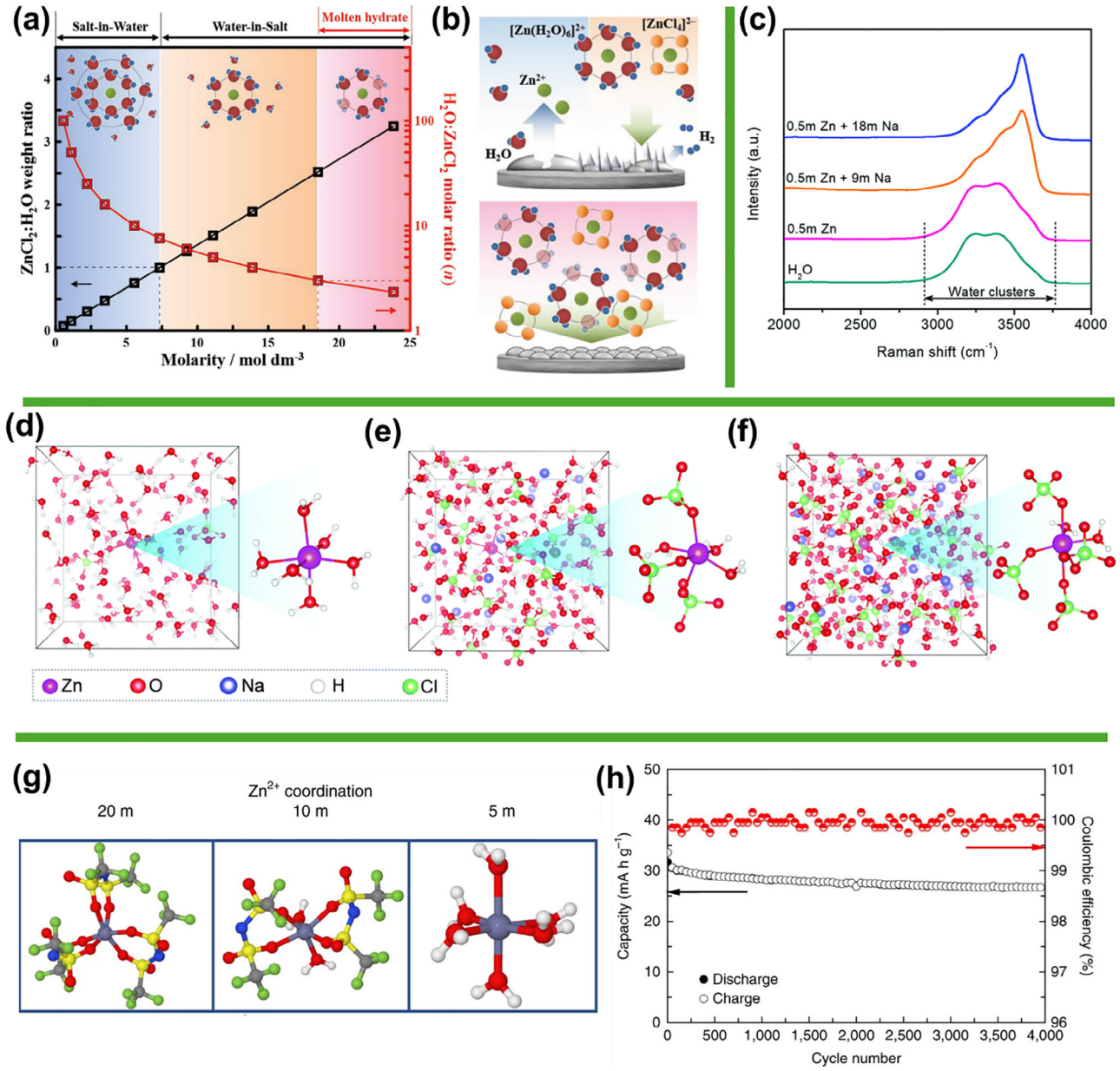

Figure 15. a) The relationship between the molarity of $ZnCl_2.H_2O$ and both the weight ratio of $ZnCl_2/H_2O$ and the molar ratio of $H_2O/ZnCl_2$ b) Schematic illustration depicting zinc deposition in a dilute $ZnCl_2$ electrolyte (top) and a molten hydrate $ZnCl_2$ electrolyte (down). Reproduced with permission.[139] c) Raman spectra of different electrolytes. MD simulations and DFT calculations of the electrolytes. Snapshots of equilibrium trajectories from ab initio MD simulations of d) 0.5 m $Zn(ClO_4)_2$, e) 0.5 m $Zn(ClO_4)_2$ + 9 m $NaClO_4$, and f) 0.5 m $Zn(ClO_4)_2$ + 18 m $NaClO_4$. Reproduced with permission.[144] g) Snapshot of the molecule dynamics simulation cell. h) The cycling stability and CE of the $Zn/LiMn_2O_4$ full cell in HCZE at 4 C. Reproduced with permission.[141]

system demonstrated remarkable durability in Zn/Zn symmetric cells, delivering 4000 cycles over 800 h even at a current density of 10 mA cm^{-2}.[139] Furthermore, it will address the dissolution issues and expand the electrochemical voltage window. Yang et al.[140] designed ZIBs utilizing WIS electrolytes consisting of 20 M $ZnCl_2$ and 1 M HCl. The authors demonstrated that as the concentration of $ZnCl_2$ increases, Zn reduction occurs prior to H_2 evolution due to the high overpotential for H_2 evolution on Zn metal. This widens the voltage gap between Zn reduction and H_2 evolution, reducing parasitic reactions. Besides, the limited solubility of most Zn salts in water combination of WISs with other salts such as lithium bistrifluoromethanesulfonimide (LiTFSI) or potassium acetate (KAc) has been reported. For example $Zn(TFSI)_2$ + 20 M LiTFSI,[141] 1 M $Zn(Ac)_2$ + 31 M KAc,[142] 0.2 M $ZnSO_4$ + 5 M $NaClO_4$[143] and 0.5 N $Zn(ClO_4)_2$ + 18 M $NaClO_4$.[143] This combination results in a low Zn salt content, containing 2–5% of the total electrolyte concentration, which leads to a high overpotential exceeding 0.1 V. A high

density of Zn cations near the electrode interface is crucial to mitigate the poor ionic conductivity in WISs; otherwise, dendrite growth and slow electrode kinetics are intensified.

Alshareef et al.[144] reported the dual-cation high-concentrated electrolyte approach for aqueous ZIBs with a mixture of $Zn(ClO_4)_2$ and $NaClO_4$. The Raman analysis of different electrolytes showed different O–H stretching vibrations, representing various hydrogen-bonding environments in water clusters. As concentration increases, a blue shift and intensity reduction of the O–H peaks at 3250 and 3400 cm^{-1} occur. This suggests a decrease in free water molecules and significant disruption of the hydrogen-bonded water network in concentrated electrolytes (Figure 15c). The detailed solvation structures were studied using ab initio MD simulations on electrolytes at three different concentrations and temperatures (Figure 15d–f). The results showed that Zn^{2+} has a stronger interaction with H_2O and ClO_4^- compared to Na^+, resulting in an extended residence time of ClO_4^- near Zn^{2+}. In a dilute electrolyte (0.5 M $Zn(ClO_4)_2$), Zn^{2+} is primarily coordinated by six water molecules, with limited involvement of ClO_4^-. At intermediate concentrations (0.5 M $Zn(ClO_4)_2$ + 9 M $NaClO_4$), ClO_4^- penetrates the first solvation shell of Zn^{2+}, forming cation-anion aggregates that promote anion reduction while suppressing side reactions on the Zn anode. In the highly concentrated electrolyte (0.5 M $Zn(ClO_4)_2$ + 18 M $NaClO_4$), the solvation structure shows a significant reduction in free water molecules and more robust cationic hydration sheaths, which are essential for electrolyte stabilization. Zinc bis(trifluoromethanesulfonyl)imide ($Zn(TFSI)_2$) is a commonly used electrolyte in ZIBs owing to its electrochemical stability and high ionic conductivity. Wang et al.[141] reported a high-concentration aqueous electrolyte (1 M $Zn(TFSI)_2$ + 20 M LiTFSI) that achieved stable ZIBs performance. In dilute electrolyte (1 M $Zn(TFSI)_2$ + 5 M LiTFSI), Zn^{2+} coordinates primarily with six water molecules. However, as salt concentration increases, $TFSI^-$ anions gradually replace water in the Zn^{2+} solvation shell (Figure 15g). This results in reversible and dendrite-free Zn anode stripping/plating cycles in 1 M $Zn(TFSI)_2$ + 20 M LiTFSI, effectively suppressing HER. The hybrid Zn–Li battery ($Zn/LiMn_2O_4$) exhibits outstanding cycling stability, retaining 85% capacity over 4000 cycles with a CE of 99.9% (Figure 15h). Although WIS (water-in-salt) electrolytes effectively suppress side reactions and address the dendrite issues associated with zinc (Zn) anodes, thus enhancing the stability of zinc-ion batteries (ZIBs), they also have several drawbacks. First, WIS electrolytes often demonstrate low ionic conductivity, high viscosity, and substantial voltage polarization, which can restrict their electrochemical performance. Second, salt precipitation occurs at low temperatures, limiting the operational temperature range of ZIBs. Lastly, the increased costs associated with high-concentration electrolytes reduce the economic benefits of using aqueous electrolytes. These unfavorable factors impede the progress of high-concentration electrolytes for advanced ZIBs.

4.3. Gel Polymer or Solid-State Electrolytes

As mentioned, aqueous electrolytes are advantageous due to their low cost, high ionic conductivity, and environmental friendliness. However, achieving high reversibility and long cycle life for Zn electrodes remains challenging in alkaline electrolytes because of unavoidable Zn corrosion, shape changes, and dendrite growth. To address these issues, developing polymer gel or solid-state electrolytes without liquid solvents presents a promising opportunity.[15a] Polymer gel electrolytes offer a promising solution to challenges such as Zn dendrite growth, HER, and passivation on Zn metal by substantially reducing free water molecules.[145] In addition, polymer gel electrolytes also function as battery separators. However, many solid-state electrolytes face challenges such as low ionic conductivity and high interfacial resistance with Zn electrodes, leading to inadequate reversibility and reduced battery lifespan.[146] To overcome these limitations, Zn-based gel polymer electrolytes have gained attention because they combine the advantages of liquid and solid electrolytes in alkaline systems.[147] Thanks to the adaptability of polymers, gel polymer electrolytes offer excellent flexibility, which makes them well-suited for portable and wearable electronic devices. Moreover, their flexibility and elasticity help accommodate volume changes and suppress dendrite formation on Zn metal during charge and discharge cycles. Polymer gel electrolytes mainly utilize hydrophilic polymers functionalized with monomers, chemical groups, or cations to stabilize water molecules that significantly reduce side reactions and improve ionic conductivity. Commonly used hydrophilic polymers include poly(vinyl alcohol) (PVA),[148] polyacrylamide (PAM),[149] poly(acrylic acid) (PAA),[150] poly(acrylonitrile) (PAN), poly(vinylidene fluoride) (PVDF),[151] and poly(methyl methacrylate) (PMMA)[152] which exhibited excellent ion transport, strong mechanical properties, and close adhesion to the electrodes.

Advanced hydrogel electrolytes, such as $PVA/Zn(CF_3SO_3)_2$, hold self-protecting and self-healing properties. The abundant hydroxyl side groups and hydrogen bonds permit automatic self-repair (**Figure 16a**). This self-healing ability ensures excellent reversibility and long cycling stability (Figure 16b,c).[153] Zwitterionic hydrogel electrolytes have also drawn considerable attention in recent research due to their capacity to enhance Zn^{2+} ion migration via strong electrostatic interactions between Zn^{2+} ions and the negatively charged groups along the polymer support. For instance, a zwitterionic sulfobetaine/cellulose electrolyte containing negatively charged sulfonate groups efficiently directs the transport of Zn^{2+} ions. Simultaneously, the positively charged ammonium nitrogen groups in sulfobetaine enable ion transport while minimizing interruption caused by mixed ion migration. This coordinated mechanism ensures precise and efficient Zn^{2+} transport along the polymer chain during charge and discharge cycles. The polyzwitterionic hydrogel electrolyte (PZHE) incorporates negatively charged sulfonic acid groups and positively charged amide groups to manage Zn^{2+} ion transport.[154] The sulfonic acid groups provide a pathway for Zn^{2+} ions, controlling their movement in a regulated manner along the polymer structure (Figure 16d). Furthermore, numerous hydrogen bonds and other static interactions within the hydrogel have outstanding self-healing properties. These features, including regulated Zn^{2+} diffusion and self-healing properties, contribute significantly to the long-lasting performance and stability of ZIBs. Li et al.[149] demonstrated a solid-state ZIB utilizing a hierarchical polymer electrolyte composed of gelatin and PAM. The polymer electrolyte was synthesized by grafting polyacrylamide (PAM) onto gelatin chains, which were integrated into a PAN

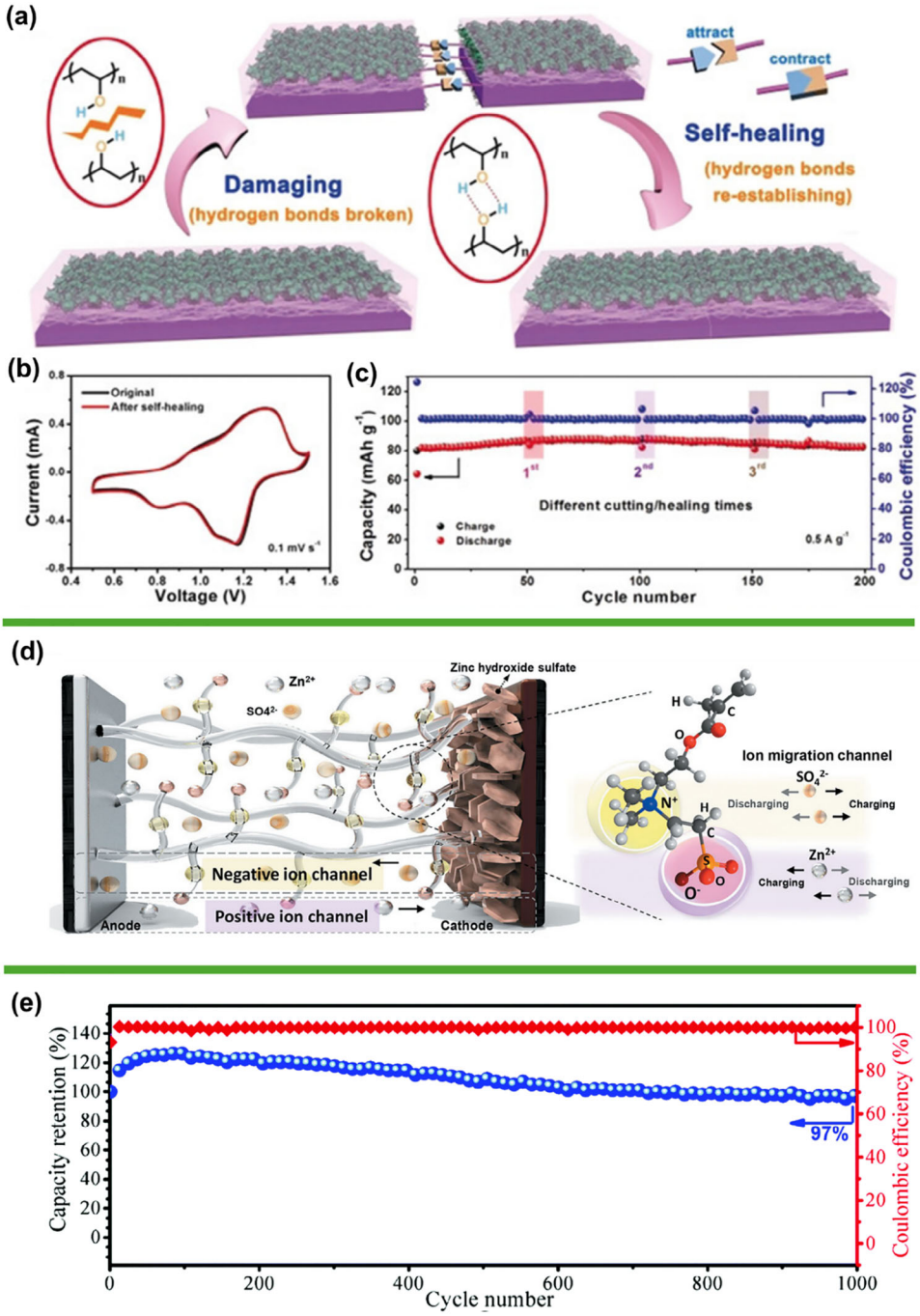

Figure 16. a) Schematic representation of the self-repair mechanism in integrated ZIBs. b) Cyclic voltammetry profiles of aqueous ZIBs recorded before and after self-repair at 0.1 mV s^{-1}. c) Extended cycling performance of self-repairing aqueous ZIBs in their initial state and following repeated cutting and healing cycles. Reproduced with permission: Copyright 2018, Wiley.[153] d) A schematic of the ion migration pathways in the ZSC-gel electrolyte and the mechanism of the ion channel. Reproduced with permission.[154] Copyright 2020, Wiley-VCH. e) Long-term cycling performance and the corresponding CE at 2772 mA g^{-1}. Reproduced with permission.[149]

electrospun fiber membrane network. This flexible solid-state ZIB, featuring an α-MnO_2/CNT cathode, achieved an impressive areal energy density of 6.18 mW h cm^{-2} and an areal power density of 148.2 mW cm^{-2}, along with remarkable cycling stability, retaining 97% capacity after 1000 cycles (Figure 16e). The influence of gel electrolytes on Zn electrodes has been explored in Zn–air batteries. In one study, a gel electrolyte was prepared by combining a hydroponics gel with a 6 M KOH aqueous solution. During discharge, the Zn metal surface developed a rough texture due to the formation of white ZnO. Still, the circular Zn plate maintained its shape, indicating that the gel electrolyte did not alter the physical structure of the Zn electrode.[155] Moreover, studies

reported durable sulfate-tolerant gum bio-electrolytes by blending xanthan with aqueous $ZnSO_4$ and $MnSO_4$ solutions. These electrolytes demonstrate enhanced mechanical stability and are capable of enduring bending and twisting, which efficiently defeats the formation of zinc dendrites.[156] Nevertheless, gel electrolytes face substantial challenges due to water evaporation, which seriously affects ion migration and comprises complex fabrication processes. Additionally, the strong electrostatic bonding properties of divalent Zn^{2+} ions result in slow diffusion kinetics and low ionic conductivity, making the use of all-solid-state electrolytes in ZIBs uncommon.[157]

4.4. Deep Eutectic Electrolytes

Deep eutectic solvents (DESs) are a class of materials formed by eutectic mixtures of anionic acids and cationic bases. They were introduced first by Abbott et al. in 2003.[158] DESs have gained attention in electrochemical energy storage for their straightforward synthesis and eco-friendliness.[159] Comprising binary or ternary systems with hydrogen bond donors and acceptors, DESs are characterized by freezing points significantly lower than their individual components. When used as battery electrolytes, they are known as eutectic electrolytes and share features with ionic liquids, such as low vapor pressure, nonflammability, and environmental friendliness.[160] Unlike conventional electrolytes, which consist of solvated ions formed by simple dissolution, eutectic electrolytes contain complex ions resulting from strong interactions between components.[114,161] For instance, a 2.0 M $ZnCl_2$ aqueous electrolyte contains solvated Zn^{2+} and Cl^- ions, whereas an $AlCl_3$/acetamide eutectic electrolyte comprises $AlCl_4^-$, $Al_2Cl_7^-$ anions, and $[AlCl_2(AcA)_2]^+$ cations.[162] Eutectic electrolytes offer distinct advantages over traditional electrolytes, including structural adaptability, excellent thermal and chemical stability, low vapor pressure, and broad electrochemical windows, making them highly promising for advanced battery applications.

Acetamide, with its high dielectric constant (41 at 20 °C), is an ideal DES solvent for electrolytes, but its coordination with Zn salts is limited due to the high lattice energy of Zn^{2+}. $ZnCl_2$-based DESs show potential in electrochemistry, and incorporating small, polar, low-viscosity cosolvents can help modify DES properties. With its high solubility for acetamide and $ZnCl_2$ and a large dielectric constant (78 at 25 °C), water is an excellent cosolvent choice. Shi et al.[163] recently reported an aqueous DES electrolyte for ZIBs, composed of acetamide, $ZnCl_2$, and water in a molar ratio of 1:3:1 (ZES-1). In this system, Zn^{2+} forms a $[ZnCl(acetamide)_2(H_2O)]^+$ complex, where water enables faster desolvation and lower dissociation energy compared to acetamide, ensuring uniform Zn nucleation. The ZES-1 electrolyte demonstrated excellent compatibility with the Zn anode, achieving stable Zn plating/stripping for over 1000 cycles with 98% CE and maintaining long-term stability for 1400 h in symmetric cells (**Figure 17a**). SEM images of the Zn surface after 10 electrochemical cycles in ZES-1, ZES-6, and ZES-20 electrolytes are shown in Figure 17b.

Geng et al.[164] introduced a DES electrolyte based on ethylene glycol (EG) and $ZnCl_2$, enabling a dendrite-free Zn anode and extending the lifespan of ZIBs. By optimizing the $ZnCl_2$/EG molar ratio, the intermolecular interactions are enhanced, promoting coordination between EG and Zn^{2+} to form $[ZnCl(EG)]^+$ and $[ZnCl(EG)_2]^+$ cations. As illustrated in Figure 17c, these interactions involve (I) EG molecules donating two −OH groups to chelate with Zn^{2+}, forming $[ZnCl(EG)]^+$ and $[ZnCl(EG)_2]^+$, and (II) Cl^- ions forming hydrogen bonds with the −OH groups of EG, as seen in Figure 17c. The electrostatic potential maps of $[ZnCl(EG)]^+$ and $[ZnCl(EG)_2]^+$ in DESs indicate that $[ZnCl(EG)_2]^+$ can well shield the repulsion between Zn^{2+} cations. Chen et al.[165] developed a hydrated DES (HDES) electrolyte composed of ethylene glycol (EG), zinc trifluoromethanesulfonate (ZnOTf), and water for aqueous ZIBs. This innovative electrolyte effectively reduces water-induced side reactions and enhances Zn^{2+} mass transfer kinetics, enabling highly reversible Zn anodes. Theoretical and spectroscopic analyses revealed that HDES exhibits a higher oxygen evolution overpotential and a lower hydrogen evolution overpotential, providing an expanded electrochemical stability window exceeding 2 V (versus Zn/Zn^{2+}). XRD analysis (Figure 17e) showed prominent peaks for $ZnxOTFy(OH)_{2x-y}{\cdot}nH_2O$ byproducts on zinc anodes cycled in aqueous electrolytes, while no significant byproducts were observed after ten cycles in HDES, indicating suppressed side reactions. Additionally, the Zn/Cu half-cell demonstrated a high CE of 99.6% over 1000 cycles (Figure 17f).

Qiu et al.[166] introduced a novel $Zn(TFSI)_2$-based eutectic solvent (ZES) to prepare an in situ Zn anode-compatible SEI layer by modifying the ionic coordination environment (**Figure 18a**). Regulating the solvation structure has proven to be a practical approach for altering the reductive potentials of electrolyte components. However, because Zn^{2+} possesses a high charge density, Zn salts exhibit limited dissociation in common solvents across a broad concentration range, which restricts control over their coordination behavior. Typically, Zn^{2+} with a higher redox potential (−0.76 V vs NHE, free $TFSI^-$: −0.87 V vs Zn/Zn^{2+}) reacts preferentially on the Zn anode. However, combined experimental and modeling studies revealed that Zn-$TFSI^-$ complexes (0.37 V vs Zn/Zn^{2+}) are more easily reduced in deep eutectic electrolytes. As a result, Zn^{2+}-$TFSI^-$ complexes decomposed preferentially, forming a uniform and dense SEI layer primarily composed of ZnF_2 on the Zn anode surface (Figure 18b,c). The DFT geometry optimization structures revealed that Zn^{2+} preferentially coordinates with the C=O group of Ace and both oxygen atoms of $TFSI^-$. The $[ZnTFSI(Ace)_2]^+$ complex presents $TFSI^-$ in bidentate coordination, representing the most uniform electrostatic potential surface and low binding energy. The SEI-coated Zn anode demonstrated stable electrochemical performance in ZES electrolytes, enabling dendrite-free Zn plating/stripping with nearly 100% CE over extended cycling (>2000 cycles) (Figure 18d). As illustrated in Figure 18e, the 1 m $Zn(TFSI)_2$ electrolyte led to the uncontrolled formation of loose Zn dendrites. In contrast, the ZES electrolytes achieved smooth, dendrite-free Zn deposits, even at a higher capacity of 2.5 mAh cm^{-2}. After deposition, the Zn anode was found to be covered by a thin surface layer, signifying surface modification. This indicates that the additional Zn-electrolyte interphase likely plays a critical role in regulating the reversible Zn/Zn^{2+} redox process, facilitating efficient Zn^{2+} transport and deposition.

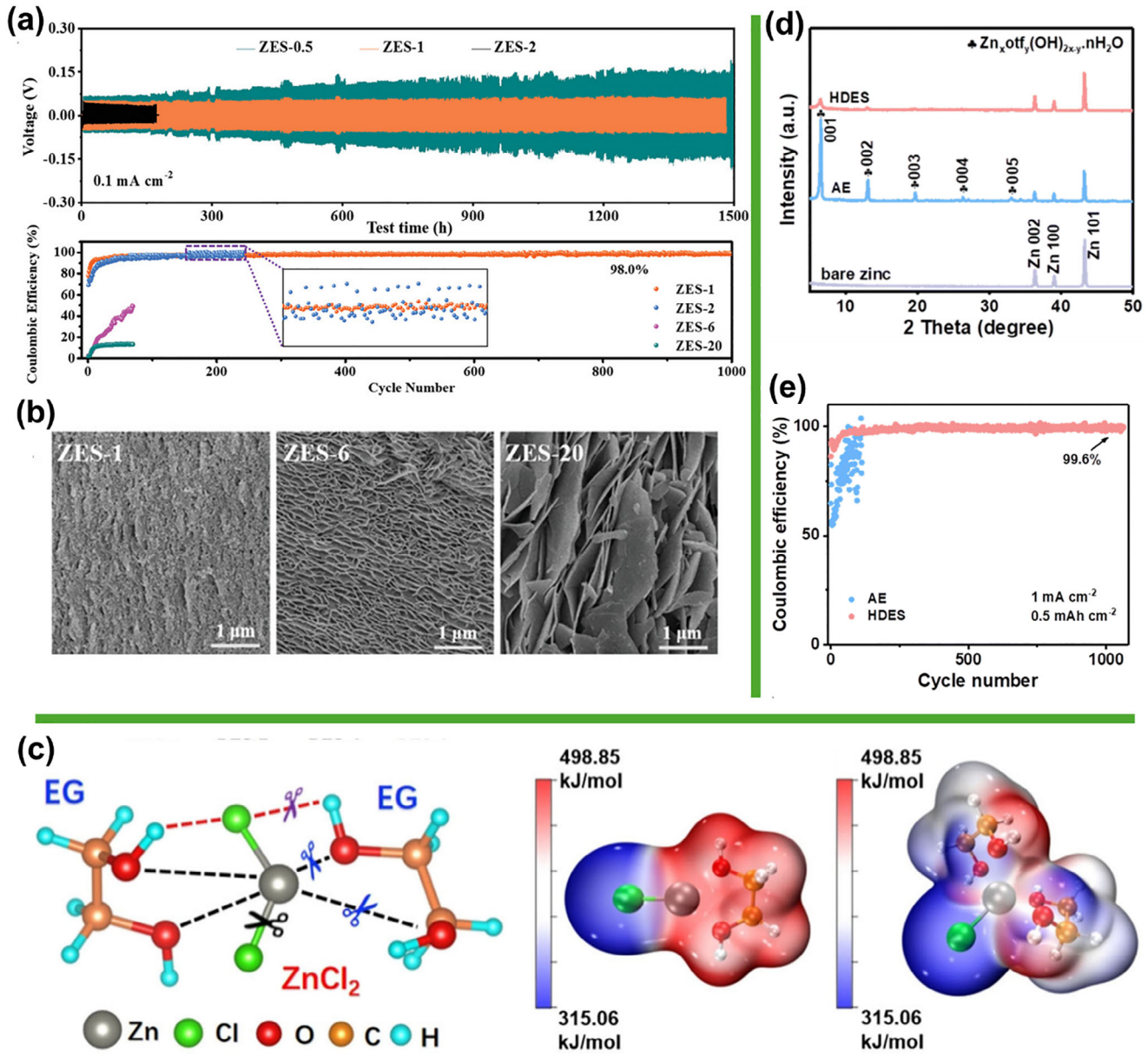

Figure 17. a) Performance of Zn plating/stripping ZIBs in different electrolytes. b) SEM images of Zn surface after 10 electrochemical cycles in ZES-1, ZES-6, and ZES-20 electrolytes. Reproduced with permission.[163] c) schematic diagram showing the interactions between $ZnCl_2$ and EG with electrostatic potential maps of $[ZnCl(EG)]^+$ and g) $[ZnCl(EG)_2]^+$ in DES. Reproduced with permission.[164] d) XRD pattern of Zn anode in aqueous electrolyte and HDES. e) comparison of CE of Zn//Zn symmetric cells in aqueous electrolyte and HDES. Reproduced with permission.[165]

5. Separator Modifications for Dendrite-Free Zn Anodes

In addition to Zn anode surface and electrolyte modifications, separator modifications have recently been proposed to enhance the long-term stability of Zn anodes. While surface and electrolyte modifications offer significant advantages, researchers are now exploring advanced separator engineering to determine whether this approach can provide greater efficiency than conventional methods. In ZIBs, the separator, often referred to as the proximate of the Zn anode, plays an essential role in facilitating ion transport, blocking electrons, and preventing direct contact between the cathode and anode.[167] It significantly influences the deposition behavior of Zn ions. Glass fiber (GF) is commonly employed as a separator in aqueous ZIBs due to its low electrical conductivity, suitable porosity, and compatibility with aqueous electrolytes.[168] However, previous studies have revealed that the large and irregular pore structure of GF separators results in slow and uneven ion transport, which accelerates dendrite growth.[169] These dendrites can penetrate the fragile separator, leading to short circuits and reduced battery lifespan. Therefore, optimizing the material and design of the separator is crucial for improving the performance and durability of the Zn anode by ensuring uniform ion distribution and mitigating dendrite formation.[170]

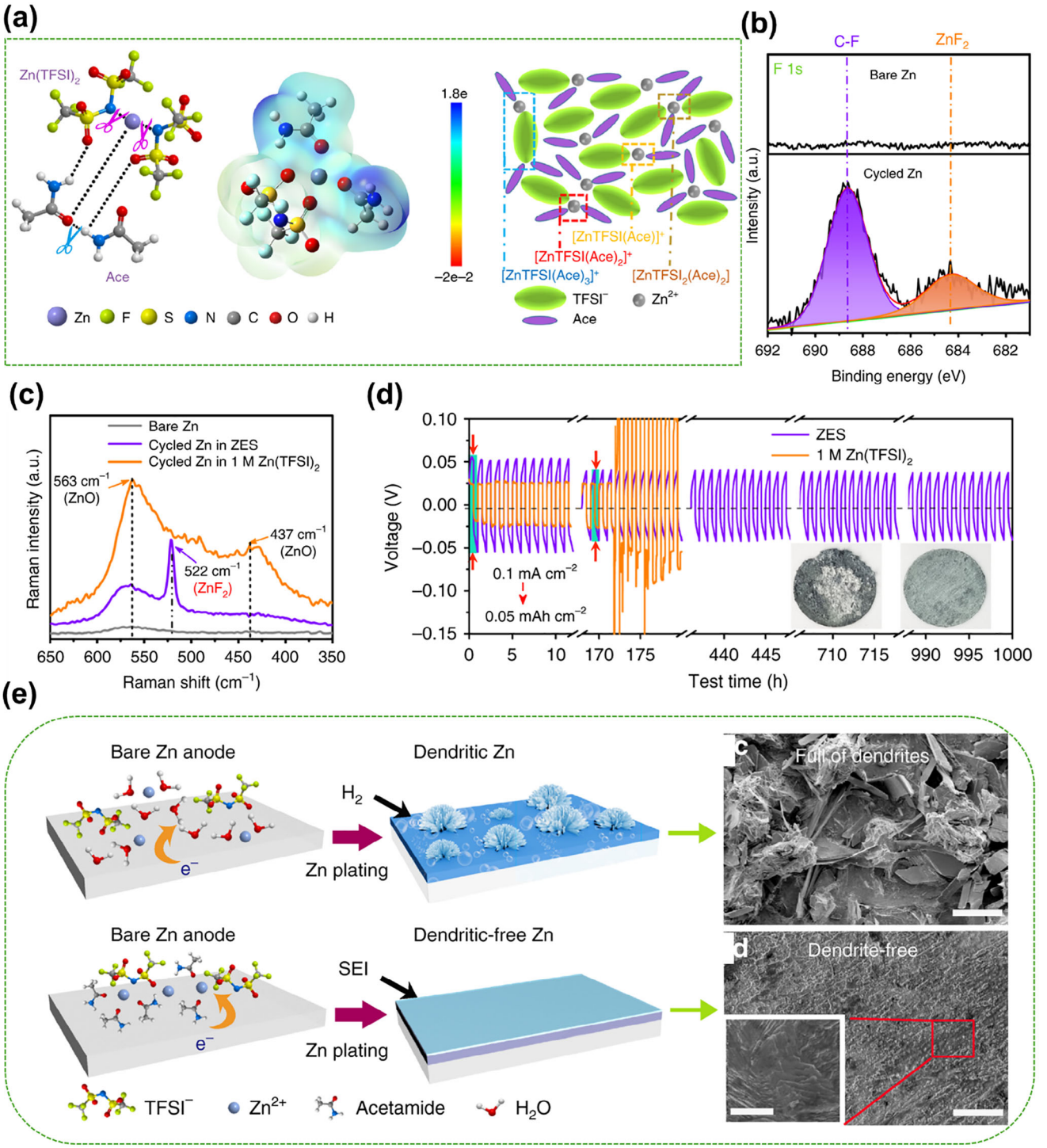

Figure 18. a) Schematics of the typical environment surrounding active Zn species within the ZES. b) XPS spectra and c) Raman spectra of the cycled Zn anode in ZES and 1 M $Zn(TFSI)_2$. d) Voltage responses of Zn/Zn symmetric cells in ZES and 1 M $Zn(TFSI)_2$ electrolytes at 0.1 mA cm^{-2} (0.05 mAh cm^{-2} for each half cycle. e) Morphologies of Zn anode in 1 M $Zn(TFSI)_2$ and ZES electrolytes at 1 mA cm^{-2}. Reproduced with permission.[166]

Separator developments are typically categorized into two main approaches: surface modification of commercial separators and the development of novel separators.[171] Surface modification of commercial separators is a relatively straightforward strategy and has been extensively reported in the literature. Materials commonly used for Zn anode surface coatings, such as carbon materials and MXene, can also be effectively utilized for separator modification. For instance, Li et al.[172] employed a CVD technique to directly grow a graphene interface on the surface of the GF separator, forming a functionalized separator decorated with

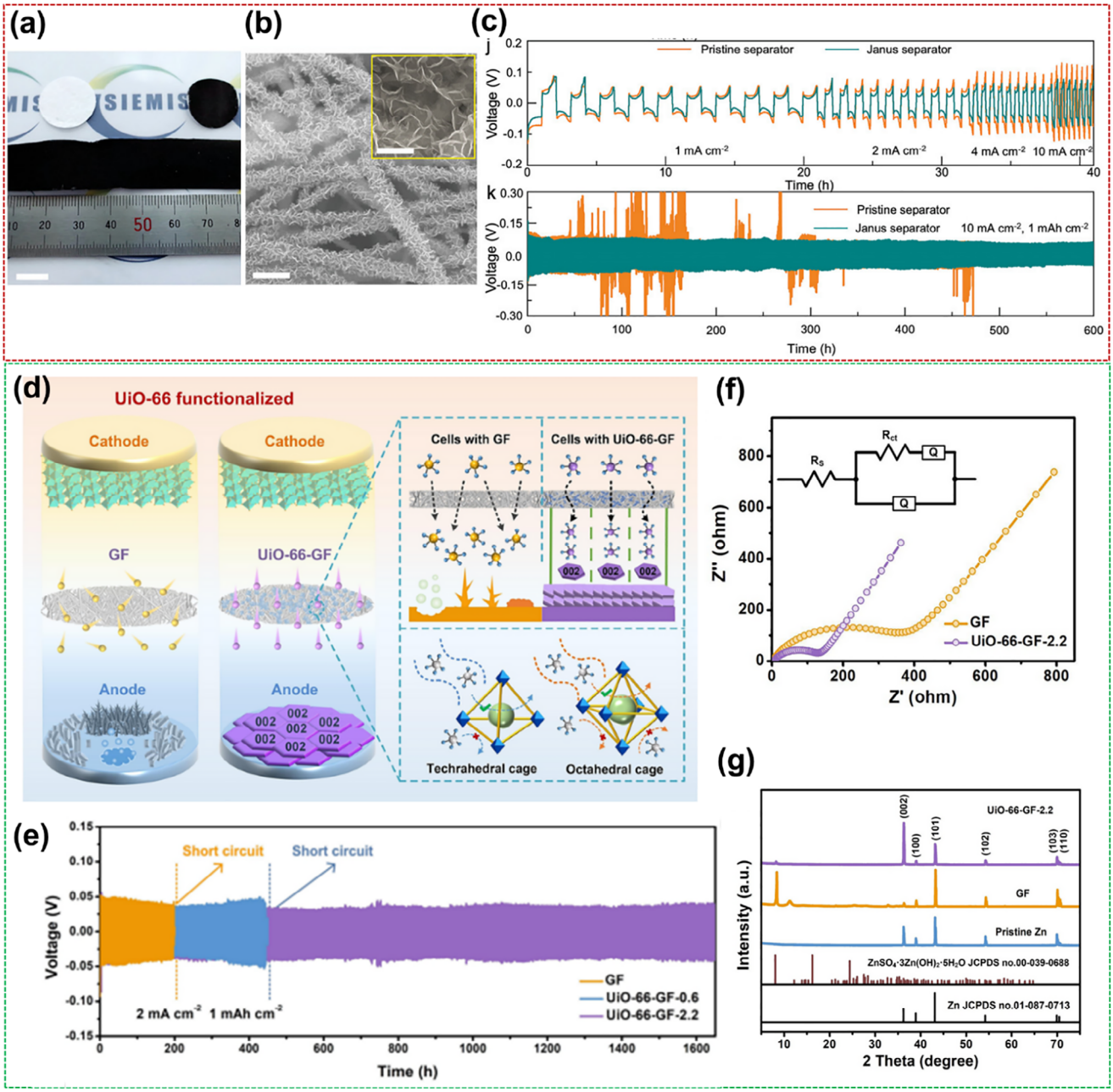

Figure 19. a) Digital photograph, b) top-view SEM image, and c) galvanostatic cycling performance of a Zn/Zn symmetric cell featuring a 3D graphene/glass fiber functionalized separator. Reproduced with permission.[172] d) Schematic illustration of the UiO-66-GF separator-based ZIBs. e) Stability performance of ZIB cells fabricated with GF and UiO-66-GF separators. f) EIS spectra and corresponding equivalent circuit diagram for the full cell, where the pristine and UiO modified separator are used with MnO_2 as a cathode. g) XRD pattern of Zn anode after cycling. Reproduced with permission.[170a]

vertically oriented 3D graphene structures (3D VG) (**Figure 19a,b**). The separator is then treated with air plasma to introduce oxygen and nitrogen heteroatoms. The resulting 3D VG scaffold can reduce the local current density at the anode/electrolyte interface while the heteroatoms help to promote a uniform flux of Zn^{2+}. The Zn/Zn symmetric cells exhibited an exceptional cycle life of 600 h at a current density of 10 mA cm^{-2} and an areal capacity of 1 mA h cm^{-2}, as illustrated in Figure 19c. This remarkable performance is attributed to the uniform electric field distribution and the reduction in local current density on the Zn anode surface. This design promotes uniform Zn ion flux and avoids dendrite formation, which leads to an excellent energy density of 182 Wh kg^{-1} for the V_2O_5//Zn cell.

Song et al.[170] developed a UiO-66 MOF-functionalized glass fiber separator to enhance charge carrier transport and ensure uniform electric field distribution on the Zn anode surface. The

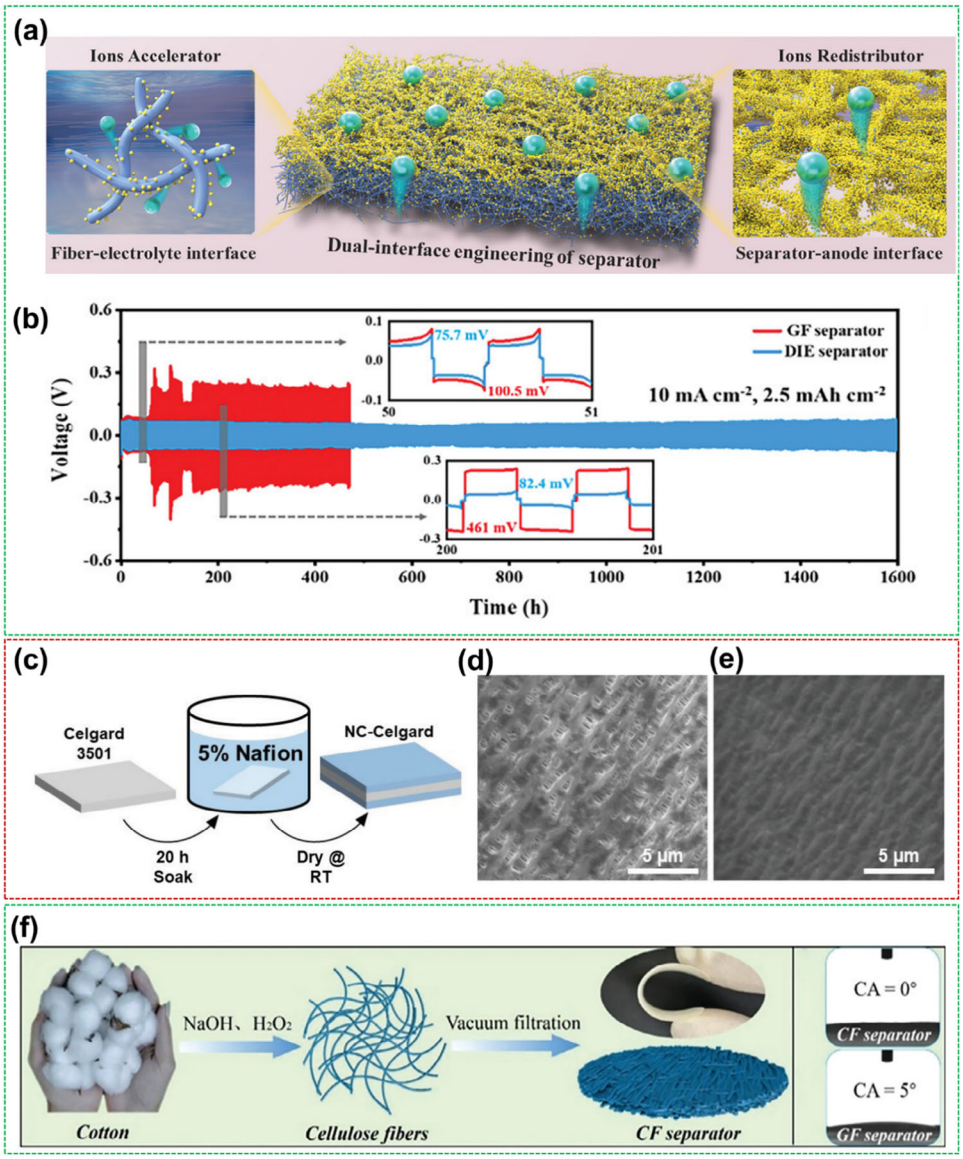

Figure 20. a) Schematic illustration of a dual-interface engineering separator. b) Cycling performance of Zn/Zn symmetric cells. Reproduced with permission.[173] c) Synthesis and d–e) SEM images of the polyolefin separator before and after Nafion modification. Reproduced with permission.[114] f) Schematic illustration of CF separator fabrication and contact angle comparison. Reproduced with permission.[174]

Zn anode exhibits a preferential (002) plane orientation when regulated by UiO-66-GF separator, advantageous for corrosion resistance and dendrite-free zinc deposition (Figure 19d). Interestingly, the Zn/Zn cell with UiO-66-GF-2.2 separator demonstrates more than 1650 h of stable reversible plating/stripping with a high CE at 2.0 mA cm^{-2} (Figure 19e). The Zn//MnO_2 full cell with modified UiO-66-GF-2.2 separator demonstrated a notably low resistance, indicating rapid electrochemical kinetics (Figure 19f). Furthermore, to know the role of UiO-66-GF separator in suppressing Zn dendrites, XRD patterns of Zn anodes before and after cycling were examined (Figure 19g). In the case of the full cell ZIBs with the GF separator, the (101) diffraction intensity increases, indicating vertical Zn ion deposition. However, in the case of the modified UiO-66-GF-2.2 separator-based ZIB, a higher (002) orientation and an increased (002)/(101) intensity ratio suggest horizontal Zn-ion deposition after cycling.

While the carbon modification layer can enhance the functionality of the separator, if the carbon material detaches during cycling, it can easily pass through the separator and lead to a short circuit, particularly with large pore sizes. In this context, non-carbon materials may be more appropriate. Liang et al.[173] introduced a dual-interface engineering (DIE) approach to design a separator that acts as an efficient ion transport modulator. They modified GF separators by decorating them with $BaTiO_3$ (BTO) (**Figure 20a**). BTO exhibits strong zincophilic properties and a spontaneous polarization effect, which allows it to be effectively coated onto the GF surface, filling the interstitial spaces and improving both interfaces. The DIE-modified GF separator

efficiently captured and accelerated Zn^{2+} transport at the fiber-electrolyte interface. At the separator–anode interface, it facilitated the redistribution and uniform ion flow. As a result, Zn//Cu asymmetric cells demonstrated significant improvements in plating/stripping stability and CE. The Zn/Zn symmetric cells operated stably for up to 1600 cycles, even at a high current density of 10 mA cm^{-2}, with a considerable reduction in overpotential (Figure 20b).

Furthermore, self-assembled separators are fabricated as molecules, fibers, and compounds that spontaneously organize into robust, free-standing films through strong (chemical bonds) or weak interactions (hydrogen bonds, electrostatic, or coordination). This simple strategy is widely used for making functionalized separators and presents precise control over thickness and composition. Using this idea, Arnot et al.[114] reported a self-assembled Nafion-coated Celgard 3501 (NC-Celgard) separator (Figure 20c–e) that significantly improves the cycle life of Zn anodes at high depth-of-discharge (DOD). The NC-Celgard separator effectively blocked zincate ions ($[Zn(OH)_4]_2^-$) but allowed hydroxide ion transport in alkaline electrolytes. Zn//Ni cells tested at 50% DOD demonstrated over 100 cycles before failure, delivering an average energy density of 180 Wh L^{-1} per cycle throughout their operational life, significantly surpassing the performance of cells using standard separators.

Biomass materials are well known for their abundance, eco-friendliness, degradability, and low cost. Among them, cellulose, as one of the representative biomass materials, stands out with its high surface area and mechanical strength, making it a widely studied functional separator for ZIBs. Zhou et al.[174] prepared a cotton-derived cellulose separator (CF) using vacuum filtration (Figure 20f). This cellulose-based separator, with numerous hydroxyl groups, exhibited stronger hydrophilicity, a more uniform pore size distribution, and higher ionic conductivity compared to the GF separator. These characteristics improved Zn^{2+} transfer, reduced the desolvation barrier and Zn nucleation overpotential, and effectively inhibited dendrites and side reactions. Zn/Zn symmetric cells with CF separators demonstrated excellent long-term cycling performance, while Zn//MnO_2 batteries also showed improved rate and cycling performance compared to those with other separators. Thus, biomass-based separators can also improve the Zn anode corrosion resistance in aqueous ZIBs, contributing to better cycling stability of the Zn anode. Additionally, combining biomass cellulose with other materials allows the functionalized separators for ZIBs to achieve improved performance. For instance, Cao et al.[175] developed a composite separator made of cellulose and graphene oxide (GO), combining both materials advantages to create a highly stable, dendrite-free anode. This separator has a negatively charged surface with abundant zincophilic oxygen containing functional groups, which promote strong interaction with Zn species. Additionally, the minimal mismatch between the GO (002) and Zn (002) planes encourages a preferential horizontal deposition of Zn, facilitating the reversible growth of Zn along this plane and promoting dendrite-free deposition. Biomass-cellulose composite-based separators are highly effective for constructing cost-efficient, durable, environmentally friendly, high-performance ZIBs. Research on separators for ZIBs has gained significant interest, leading to notable progress. However, compared to artificial surface coatings and electrolyte engineering, advanced separators remain a relatively untapped area with great potential. Further innovation is needed to develop cost-effective separators that enhance performance while ensuring economic viability for large-scale production. Achieving a better cost-performance ratio than traditional GF separators will be key to the future success and adoption of advanced ZIB systems.

6. Conclusion and Future Perspectives

ZIBs have gained significant attention as a promising alternative to LIBs due to the abundance and low cost of Zn, along with their inherent safety during operation. However, the long-term performance and stability of ZIBs largely depend on the behavior of the Zn metal anode. Despite its advantages, Zn anodes face critical challenges, including dendrite formation, corrosion, H_2 evolution, and passivation layer development. These issues can lead to severe capacity degradation, internal short-circuiting, and poor cycle life, limiting the practicality of ZIBs. To address these challenges, extensive research efforts have focused on stabilizing Zn anodes through various modification strategies. Key approaches include Zn anode surface engineering, electrolyte optimization, separator modifications, and interfacial regulation, all of which aim to improve Zn deposition behavior, suppress side reactions, and enhance electrochemical stability. In this review, we systematically summarize the latest advancements in Zn anode modification strategies, highlighting their impact on the electrochemical performance of ZIBs.

One widely explored strategy is Zn anode surface modification through the coating of different materials, such as carbon-based, metal-based, inorganic, and organic compounds. Carbon coatings improve conductivity and regulate Zn deposition, effectively reducing dendrite formation. Metal-based coatings, such as gold or other zincophilic metals, promote uniform Zn plating and mitigate unwanted side reactions. Inorganic coatings, including metal oxides, sulfides, and MXenes, serve as protective layers to prevent corrosion and H_2 evolution. Additionally, organic coatings, such as polymer-based films, offer flexibility, and chemical stability, further suppressing side reactions. These surface modification strategies collectively improve Zn anode reversibility, extend cycle life, and enhance the overall electrochemical performance of ZIBs. Beyond surface modifications, electrolyte engineering has been extensively explored to optimize Zn anode behavior and improve ZIB stability. Strategies such as water-in-salt electrolytes, eutectic electrolytes, and functional additives (organic and inorganic) help to regulate Zn deposition, suppress dendrite growth, and minimize side reactions like H_2 evolution and corrosion. Additives, like inorganic and organic molecules facilitate the formation of a stable SEI, improving Zn reversibility. Additionally, polymer gel and solid-state electrolytes enhance ion transport while reducing water activity, further stabilizing cycling performance. These electrolyte modifications significantly extend the lifespan and efficiency of ZIBs. Another effective approach for Zn anode stabilization is separator modification, which plays a crucial role in regulating ion transport and preventing dendrite formation. Functionalized separators, incorporating materials such as metal oxides, polymers, or carbon-based coatings, help achieve uniform Zn deposition and reduce side reactions. Advanced separators with selective ion channels enhance Zn^{2+} diffusion while blocking unwanted species,

leading to improved cycling stability. These advancements in separator engineering contribute to the long-term performance, safety, and commercial viability of ZIBs. Despite significant advancements in Zn anode modification to stabilize the ZIB technology for sustainable applications over the past decade, further development is needed for practical applications. Many research studies overlook real-world challenges, raising concerns about the feasibility of laboratory breakthroughs. We present key challenges, perspectives, and future directions for advancing ZIBs toward commercialization to address this.

i. Various materials, including carbon-based, metal-based, inorganic, and organic materials, have been used to coat the Zn anode. Despite significant advancements in these coatings, challenges remain in optimizing their properties to achieve a balance between enhancing electrochemical performance and ensuring scalability, cost-effectiveness, and environmental sustainability. For example, many of the coatings mentioned require further improvements to reduce the risks of delamination, cracking, and degradation during cycling, as these factors can compromise battery stability over time. Additionally, the scalability of the coating processes needs to be addressed since methods that work at the laboratory scale often encounter substantial difficulties when adapted for large-scale manufacturing. Moreover, a deeper exploration of the complex interactions between various coatings and the electrochemical behavior of the Zn anode is necessary. Understanding how different materials can synergistically interact will be crucial for optimizing performance over extended cycling periods and for commercializing ZIBs as competitive energy storage solutions. Research into hybrid coatings, which combine carbon, metal, inorganic, and organic materials, may present new opportunities to enhance the electrochemical behavior of Zn anodes. These hybrid coatings have the potential to leverage the best attributes of each material class, such as the high conductivity of carbon, the structural stability of metals, the corrosion resistance of inorganic materials, and the tunability of organic compounds. Additionally, incorporating nanostructures into these coatings could improve ionic and electron transport pathways, further enhancing the electrochemical performance of Zn anodes.
ii. In aqueous electrolytes, Zn^{2+} ions primarily exist in a solvated form, migrating through the bulk electrolyte. Understanding electrolyte properties and developing optimization strategies is crucial to address issues related to the Zn anode. Various approaches have been explored, including adjusting Zn salt types and concentrations, adding additives, using eutectic electrolytes, water-in-salt electrolytes, and employing polymer gel-based electrolytes. While significant progress has been made in electrolyte engineering, challenges remain, particularly regarding the performance of both the Zn anode and the cathode in ZIB cells, leaving ample room for further advancements. Future research should focus on the following key areas. The long-term cycling stability of ZIBs depends mainly on the durability of Zn anodes. Advanced electrolyte strategies are needed to improve discharge depth and enhance CE for reversible plating/stripping processes. Eutectic and gel electrolytes, which reduce free water content, show promise in stabilizing Zn anodes by minimizing side reactions, expanding the electrochemical stability window, and improving temperature tolerance. However, challenges such as lower ionic conductivity remain. While additives can mitigate side reactions at the Zn anode, organic additives in aqueous Zn-based electrolytes compromise the safety and cost-effectiveness of ZIBs.
iii. Traditionally, the stability of Zn anodes in water-based electrolytes has been assessed through plating/stripping tests, often conducted over extended periods ranging from 1000 to more than 2000 h at different current densities and capacities. While these tests are crucial for evaluating the performance of Zn anodes, they are time-consuming and costly. As a result, they contribute to significant delays in commercializing ZIBs despite their considerable potential. The need for more efficient and cost-effective methods has become evident, as relying on such long-duration testing slows down the development process. To address these challenges and accelerate the commercialization of ZIBs, it is imperative to integrate advanced tools like machine learning (ML), artificial intelligence (AI), and other predictive modeling techniques. These technologies can help simulate and predict the stability and performance of Zn anodes in various engineering conditions, significantly reducing the time and cost associated with experimental testing. By using data-driven approaches, researchers can quickly identify promising materials, optimize electrolyte compositions, and predict the long-term behavior of the anode, thereby minimizing the need for prolonged experimental cycles. This shift toward advanced predictive tools helps streamline the development process and enables researchers to make more informed decisions, accelerating the timeline for scaling up ZIBs for commercial use. Ultimately, these innovations can play a pivotal role in overcoming the current bottlenecks in ZIB commercialization, leading to faster and more cost-efficient advancements in this promising energy storage technology.
iv. Besides the above, the ML-driven predictive models can enhance Zn^{2+} deposition efficiency, minimize dendrite formation, and improve coulombic efficiency. While solid-state electrolytes mitigate issues like dendrite growth and side reactions, they do not entirely eliminate Zn anode instability due to interfacial resistance and mechanical degradation. Hence, integrating interfacial self-healing materials offers a promising avenue by dynamically repairing cracks, suppressing dendrites, and prolonging the Zn anode lifespan. Future advancements in ML-guided electrolyte design and self-healing interfaces could revolutionize Zn-based batteries, enabling safer and more durable energy storage solutions.
v. A promising direction for future research involves utilizing advanced characterization techniques and computational modeling to gain insights into the fundamental mechanisms governing Zn deposition and dissolution at the anode surface. In particular, in situ optical and electrochemical analysis can provide real-time visualization of Zn plating/stripping dynamics, enabling a deeper understanding of dendrite formation, interfacial stability, and side reactions. These techniques, such as in situ optical microscopy, electrochemical quartz crystal microbalance (EQCM), and in situ Raman spectroscopy, allow researchers to monitor morpho-

logical and electrochemical changes during cycling, offering critical data for optimizing coatings and interfaces. This understanding will facilitate the design of more efficient protective layers that mitigate the challenges posed by side reactions and instability. Furthermore, integrating machine learning tools and data-driven approaches could accelerate the discovery of new coating materials and help develop predictive models that optimize battery performance based on real-time experimental feedback. Another critical area for future development is the exploration of sustainable, low-cost, and environmentally friendly coating materials. With the increasing global demand for energy storage systems, there is a pressing need to create coatings that are not only effective but also adhere to the principles of green chemistry. Biodegradable, abundant, and eco-friendly materials could help minimize the environmental impact of ZIB production while reducing costs, making them more appealing for large-scale applications.

vi. Scalability remains a significant challenge that must be addressed in future research. While the results from laboratory-scale studies are encouraging, the processes used for coating Zn anodes need to be adapted into commercially viable techniques that can be seamlessly integrated into mass production. Adaptable deposition techniques, including atomic layer deposition (ALD), chemical vapor deposition (CVD), and solution-based processing, should be further explored and optimized to fabricate large quantities of coated anodes.

vii. The performance of ZIBs, including capacity, cycle stability, and energy density, is crucial for practical applications. Hence, equal importance should be given to both half and full cells when addressing Zn anode stabilization. Further, to achieve optimal energy storage and stability in ZIBs, it is crucial to select an appropriate cathode material while also considering factors like the efficient use of the Zn anode and the average discharge voltage to meet desired energy density requirements. Much of the current research on ZIBs does not reflect real-world conditions for commercial use, such as low cathode mass loading, excessive Zn-anode mass, and overly abundant electrolytes. To accelerate the path to commercialization, it is essential to report electrochemical parameters that more accurately simulate industrial conditions. These include ensuring a balanced charge and mass distribution across both electrodes, maintaining realistic cathode mass loadings (10-15 mg cm^{-2}), using limited electrolyte volumes (≈100 µL for 1 cm^2 electrodes), calculating energy density based on the total mass and volume of the ZIB, analyzing cycling stability at C-rates below 2C, and confirming reproducibility through average results from at least three cells. The energy density of most ZIBs with stabilized Zn anodes typically falls within the range of 200–500 Wh kg^{-1}, comparable to LIBs. Moreover, many ZIBs exhibit outstanding reversibility, maintaining stability over 1000 cycles. These outstanding features highlight the immense potential of ZIBs with stabilized anodes for future applications. Implementing this approach will align future ZIB research with practical needs, bridging the gap between academic insights and industrial scalability.

Acknowledgements

This work was supported by the Japan Society for the Promotion of Science (JSPS) KAKENHI Grant Number JP22F22368, JP20H00392, and JP23H05459. N.R.C. and E.A. appreciate the financial support from the Khalifa University of Science and Technology (KUST) under Award No. 8474000620.

Conflict of Interest

The authors declare no conflict of interest.

Keywords

anode modifications, aqueous electrolyte, electrolytes engineering, Zn anode, Zn ion battery

Received: December 9, 2024
Revised: March 14, 2025
Published online: August 19, 2025

[1] B. Dunn, H. Kamath, J.-M. Tarascon, *Science* **2011**, *334*, 928.
[2] a) H. Imahori, *Bull. Chem. Soc. Jpn.* **2023**, *96*, 339; b) T. Nakamura, Y. Kondo, N. Ohashi, C. Sakamoto, A. Hasegawa, S. Hu, M. A. Truong, R. Murdey, Y. Kanemitsu, A. Wakamiya, *Bull. Chem. Soc. Jpn.* **2024**, 97; c) K. Ariga, S. Akakabe, R. Sekiguchi, M. L. Thomas, Y. Takeoka, M. Rikukawa, M. Yoshizawa-Fujita, *ACS Omega* **2024**, *9*, 22203; d) P. A. Shinde, V. Mahamiya, M. Safarkhani, N. R. Chodankar, M. Ishii, R. Ma, A. A. Ghaferi, L. K. Shrestha, K. Ariga, *Adv. Funct. Mater.* **2024**, *34*, 2406333; e) G. Chen, M. Isegawa, T. Koide, Y. Yoshida, K. Harano, K. Hayashida, S. Fujita, K. Takeyasu, K. Ariga, J. Nakamura, *Angew. Chem., Int. Ed.* **2024**, *63*, 202410747.
[3] a) X. Guan, Z. Li, X. Geng, Z. Lei, A. Karakoti, T. Wu, P. Kumar, J. Yi, A. Vinu, *Small* **2023**, *19*, 2207181; b) K. Ariga, *Bull. Chem. Soc. Jpn.* **2023**, 97; c) K. Ariga, J. Song, K. Kawakami, *Chem. Commun.* **2024**, *60*, 2152; d) K. Dong, Z. Sun, G. Jing, J. Wang, B. Tang, N. Zhao, L. Kong, F. Guo, *J. Energy Storage* **2024**, *85*, 111048; e) S. Chahal, R. Bhushan, P. Kumari, X. Guan, J. M. Lee, S. J. Ray, A. K. Thakur, A. Vinu, P. Kumar, *Matter* **2024**, *7*, 237.
[4] a) F. M. N. U. Khan, M. G. Rasul, A. S. M. Sayem, N. K. Mandal, *J. Energy Storage* **2023**, *71*, 108033; b) M. Ishii, Y. Yamashita, S. Watanabe, K. Ariga, J. Takeya, *Nature* **2023**, *622*, 285; c) S. d. Kalyana Sundaram, M. M. Hossain, M. Rezki, K. Ariga, S. Tsujimura, *Biosensors* **2023**, *13*, 1018; d) T. Fukushima, M. Higashi, M. Yamauchi, *Bull. Chem. Soc. Jpn.* **2023**, *96*, 1209; e) M. Li, M. Liu, F. Qi, F. R. Lin, A. K. Y. Jen, *Chem. Rev.* **2024**, *124*, 2138; f) P. A. Shinde, L. K. Shrestha, K. Ariga, *Green Energy Environ.* **2025**; g) K. Ariga, *Small* **2024**, *20*, 2305636.
[5] S. Saifi, X. Xiao, S. Cheng, H. Guo, J. Zhang, P. Müller-Buschbaum, G. Zhou, X. Xu, H.-M. Cheng, *Nat. Commun.* **2024**, *15*, 6546.
[6] a) F. Creutzig, P. Agoston, J. C. Goldschmidt, G. Luderer, G. Nemet, R. C. Pietzcker, *Nat. Energy* **2017**, *2*, 17140; b) D. A. Elalfy, E. Gouda, M. F. Kotb, V. Bureš, B. E. Sedhom, *Energy Strat. Rev.* **2024**, *54*, 101482; c) N. R. Chodankar, S. J. Patil, S. K. Hwang, S. V. Karekar, K. Jayaramulu, W. Zhang, D. P. Dubal, Y. S. Huh, Y.-K. Han, *J. Mater. Chem. A* **2021**, *9*, 26603.
[7] a) F. Degen, M. Winter, D. Bendig, J. Tübke, *Nat. Energy* **2023**, *8*, 1284; b) K. Wang, K. Jiang, B. Chung, T. Ouchi, P. J. Burke, D. A. Boysen, D. J. Bradwell, H. Kim, U. Muecke, D. R. Sadoway, *Nature* **2014**, *514*, 348.
[8] O. Schmidt, A. Hawkes, A. Gambhir, I. Staffell, *Nat. Energy* **2017**, *2*, 17110.

[9] R. Zhang, C. Wang, P. Zou, R. Lin, L. Ma, T. Li, I.-h. Hwang, W. Xu, C. Sun, S. Trask, *Nat. Energy* **2023**, *8*, 695.
[10] Y. Song, L. Wang, L. Sheng, D. Ren, H. Liang, Y. Li, A. Wang, H. Zhang, H. Xu, X. He, *Energy Environ. Sci.* **2023**, *16*, 1943.
[11] A. G. Olabi, Q. Abbas, P. A. Shinde, M. A. Abdelkareem, *Energy* **2023**, *266*, 126408.
[12] a) R. Thirupathi, V. Kumari, S. Chakrabarty, S. Omar, *Prog. Mater. Sci.* **2023**, *137*, 101128; b) J. Hu, Y. Hong, M. Guo, Y. Hu, W. Tang, S. Xu, S. Jia, B. Wei, S. Liu, C. Fan, *Energy Storage Mater.* **2023**, *56*, 267; c) C. Wei, J. Song, Y. Wang, X. Tang, X. Liu, *Adv. Funct. Mater.* **2023**, *33*, 2304223; d) Z. Ju, T. Zheng, B. Zhang, G. Yu, *Chem. Soc. Rev.* **2024, 53, 8980**.
[13] a) R. Stephanie, C. Y. Park, P. A. Shinde, E. Alhajri, N. R. Chodankar, T. J. Park, *Energy Storage Mater.* **2024**, *68*, 103336; b) N. R. Chodankar, P. A. Shinde, S. J. Patil, G. S. Rama Raju, S.-K. Hwang, S. J. Marje, H. B. Tyagaraj, E. Al Hajri, A. Al Ghaferi, Y. S. Huh, Y.-K. Han, *ChemSusChem* **2023**, *16*, 202300730; c) H. Tang, L. Duan, J. Liao, X. Sheng, J. Xu, X. Zhou, *Energy Storage Mater.* **2023**, *62*, 102935; d) R. Li, J. Yu, F. Chen, Y. Su, K. C. Chan, Z. L. Xu, *Adv. Funct. Mater.* **2023**, *33*, 2214304.
[14] a) X. Li, L. Wang, Y. Fu, H. Dang, D. Wang, F. Ran, *Nano Energy* **2023**, *116*, 108858; b) S. W. Gourley, R. Brown, B. D. Adams, D. Higgins, *Joule* **2023**, *7*, 1415.
[15] a) D. Li, Y. Tang, S. Liang, B. Lu, G. Chen, J. Zhou, *Energy Environ. Sci.* **2023**, *16*, 3381; b) H. Lu, J. Hu, X. Wei, K. Zhang, X. Xiao, J. Zhao, Q. Hu, J. Yu, G. Zhou, B. Xu, *Nat. Commun.* **2023**, *14*, 4435.
[16] X. Zhang, Z. Deng, C. Xu, Y. Deng, Y. Jia, H. Luo, H. Wu, W. Cai, Y. Zhang, *Adv. Energy Mater.* **2023**, *13*, 2302749.
[17] H. Xu, W. Yang, M. Li, H. Liu, S. Gong, F. Zhao, C. Li, J. Qi, H. Wang, W. Peng, *Small* **2024**, *20*, 2310972.
[18] Y.-P. Deng, R. Liang, G. Jiang, Y. Jiang, A. Yu, Z. Chen, *ACS Energy Lett.* **2020**, *5*, 1665.
[19] a) L. E. Blanc, D. Kundu, L. F. Nazar, *Joule* **2020**, *4*, 771; b) Y. Liang, H. Dong, D. Aurbach, Y. Yao, *Nat. Energy* **2020**, *5*, 646.
[20] Y. Zhu, G. Liang, X. Cui, X. Liu, H. Zhong, C. Zhi, Y. Yang, *Energy Environ. Sci.* **2024**, *17*, 369.
[21] G. Li, L. Sun, S. Zhang, C. Zhang, H. Jin, K. Davey, G. Liang, S. Liu, J. Mao, Z. Guo, *Adv. Funct. Mater.* **2024**, *34*, 2301291.
[22] B. Li, X. Zhang, T. Wang, Z. He, B. Lu, S. Liang, J. Zhou, *Nanomicro Lett.* **2021**, *14*, 6.
[23] J. Hao, X. Li, X. Zeng, D. Li, J. Mao, Z. Guo, *Energy Environ. Sci.* **2020**, *13*, 3917.
[24] L. Wang, K.-W. Huang, J. Chen, J. Zheng, *Sci. Adv.* **2019**, *5*, aax4279.
[25] G. Fang, J. Zhou, A. Pan, S. Liang, *ACS Energy Lett.* **2018**, *3*, 2480.
[26] P. Yu, Y. Zeng, H. Zhang, M. Yu, Y. Tong, X. Lu, *Small* **2019**, *15*, 1804760.
[27] Q.-H. Yang, L.-F. Wang, X.-Y. Wang, M.-M. Zhen, *Rare Met.* **2024**, *43*, 2940.
[28] X. Chen, W. Li, D. Reed, X. Li, X. Liu, *Electrochem. Energy Rev.* **2023**, *6*, 33.
[29] T. Wang, S. Tang, Y. Xiao, W. Xiang, J. S. Yu, *Energy Environ. Sci.* **2025**, *18*, 545.
[30] B. Tang, L. Shan, S. Liang, J. Zhou, *Energy Environ. Sci.* **2019**, *12*, 3288.
[31] Z. Cao, P. Zhuang, X. Zhang, M. Ye, J. Shen, P. M. Ajayan, *Adv. Energy Mater.* **2020**, *10*, 2001599.
[32] a) Z. Hou, B. Zhang, *EcoMat* **2022**, *4*, 12265; b) N. Zhang, X. Chen, M. Yu, Z. Niu, F. Cheng, J. Chen, *Chem. Soc. Rev.* **2020**, *49*, 4203.
[33] M. Song, H. Tan, D. Chao, H. J. Fan, *Adv. Funct. Mater.* **2018**, *28*, 1802564.
[34] a) W. Du, E. H. Ang, Y. Yang, Y. Zhang, M. Ye, C. C. Li, *Energy Environ. Sci.* **2020**, *13*, 3330; b) Z. Yi, G. Chen, F. Hou, L. Wang, J. Liang, *Adv. Energy Mater.* **2021**, *11*, 2003065.
[35] Y. Zuo, K. Wang, P. Pei, M. Wei, X. Liu, Y. Xiao, P. Zhang, *Mater. Today Energy* **2021**, *20*, 100692.
[36] V. Yufit, F. Tariq, D. S. Eastwood, M. Biton, B. Wu, P. D. Lee, N. P. Brandon, *Joule* **2019**, *3*, 485.
[37] Q. Yang, Q. Li, Z. Liu, D. Wang, Y. Guo, X. Li, Y. Tang, H. Li, B. Dong, C. Zhi, *Adv. Mater.* **2020**, *32*, 2001854.
[38] Q. Yang, G. Liang, Y. Guo, Z. Liu, B. Yan, D. Wang, Z. Huang, X. Li, J. Fan, C. Zhi, *Adv. Mater.* **2019**, *31*, 1903778.
[39] Z. Yang, C. Lv, W. Li, T. Wu, Q. Zhang, Y. Tang, M. Shao, H. Wang, *Small* **2022**, *18*, 2104148.
[40] Q. Liu, R. Chen, L. Xu, Y. Liu, Y. Dai, M. Huang, L. Mai, *ACS Energy Lett.* **2022**, *7*, 2825.
[41] X. Jia, C. Liu, Z. G. Neale, J. Yang, G. Cao, *Chem. Rev.* **2020**, *120*, 7795.
[42] K. Wippermann, J. Schultze, R. Kessel, J. Penninger, *Corros. Sci.* **1991**, *32*, 205.
[43] L. Ma, Q. Li, Y. Ying, F. Ma, S. Chen, Y. Li, H. Huang, C. Zhi, *Adv. Mater.* **2021**, *33*, 2007406.
[44] a) M. Fleischmann, H. Thirsk, *Electrochim. Acta* **1960**, *2*, 22; b) E. Budevski, G. Staikov, W. Lorenz, *Electrochim. Acta* **2000**, *45*, 2559.
[45] Y. Lee, B. Ma, P. Bai, *Energy Environ. Sci.* **2020**, *13*, 3504.
[46] C. Li, X. Xie, S. Liang, J. Zhou, *Energy Env. Mater.* **2020**, *3*, 146.
[47] H. Jia, Z. Wang, B. Tawiah, Y. Wang, C.-Y. Chan, B. Fei, F. Pan, *Nano Energy* **2020**, *70*, 104523.
[48] S.-B. Wang, Q. Ran, R.-Q. Yao, H. Shi, Z. Wen, M. Zhao, X.-Y. Lang, Q. Jiang, *Nat. Commun.* **2020**, *11*, 1634.
[49] D. Chao, W. Zhou, C. Ye, Q. Zhang, Y. Chen, L. Gu, K. Davey, S. Z. Qiao, *Angew. Chem.* **2019**, *131*, 7905.
[50] C. Xie, Y. Li, Q. Wang, D. Sun, Y. Tang, H. Wang, *Carbon Energy* **2020**, *2*, 540.
[51] C. Li, S. Jin, L. A. Archer, L. F. Nazar, *Joule* **2022**, *6*, 1733.
[52] J. Shin, J. Lee, Y. Park, J. W. Choi, *Chem. Sci.* **2020**, *11*, 2028.
[53] D. Strmcnik, P. P. Lopes, B. Genorio, V. R. Stamenkovic, N. M. Markovic, *Nano Energy* **2016**, *29*, 29.
[54] a) J. Chen, W. Zhao, J. Jiang, X. Zhao, S. Zheng, Z. Pan, X. Yang, *Energy Storage Mater.* **2023**, *59*, 102767; b) C.-C. Kao, C. Ye, J. Hao, J. Shan, H. Li, S.-Z. Qiao, *ACS Nano* **2023**, *17*, 3948.
[55] L. Ma, S. Chen, N. Li, Z. Liu, Z. Tang, J. A. Zapien, S. Chen, J. Fan, C. Zhi, *Adv. Mater.* **2020**, *32*, 1908121.
[56] A. Bayaguud, Y. Fu, C. Zhu, *J. Energy Chem.* **2022**, *64*, 246.
[57] L. Lei, Y. Sun, X. Wang, Y. Jiang, J. Li, *Frontiers Mater.* **2020**, *7*, 96.
[58] a) Y. Liu, H. He, A. Gao, J. Ling, F. Yi, J. Hao, Q. Li, D. Shu, *Chem. Eng. J.* **2022**, *446*, 137021; b) A. Yu, W. Zhang, N. Joshi, Y. Yang, *Energy Storage Mater.* **2024**, *64*, 103075.
[59] Y. Liang, M. Qiu, P. Sun, W. Mai, *Adv. Funct. Mater.* **2023**, *33*, 2304878.
[60] L. Yuan, J. Hao, C.-C. Kao, C. Wu, H.-K. Liu, S.-X. Dou, S.-Z. Qiao, *Energy Environ. Sci.* **2021**, *14*, 5669.
[61] F. Tao, Y. Liu, X. Ren, J. Wang, Y. Zhou, Y. Miao, F. Ren, S. Wei, J. Ma, *J. Energy Chem.* **2022**, *66*, 397.
[62] Y. Gong, B. Wang, H. Ren, D. Li, D. Wang, H. Liu, S. Dou, *Nano-Micro Lett.* **2023**, *15*, 208.
[63] a) C. Han, J. Zhu, C. Zhi, H. Li, *J. Mater. Chem. A* **2020**, *8*, 15479; b) N. R. Chodankar, S. J. Patil, S.-K. Hwang, P. A. Shinde, S. V. Karekar, G. S. R. Raju, K. S. Ranjith, A. G. Olabi, D. P. Dubal, Y. S. Huh, *Energy Storage Mater.* **2022**, *49*, 564.
[64] N. R. Chodankar, A. K. Nanjundan, D. Losic, D. P. Dubal, J. B. Baek, *Mater. Today Adv.* **2020**, *6*, 100053.
[65] N. R. Chodankar, H. D. Pham, A. K. Nanjundan, J. F. S. Fernando, K. Jayaramulu, D. Golberg, Y.-K. Han, D. P. Dubal, *Small* **2020**, *16*, 2002806.
[66] Y. Du, C. Liu, Y. Liu, Q. Han, X. Chi, Y. Liu, *Electrochim. Acta* **2020**, *339*, 135867.

[67] Z. Li, L. Wu, S. Dong, T. Xu, S. Li, Y. An, J. Jiang, X. Zhang, *Adv. Funct. Mater.* **2021**, *31*, 2006495.
[68] H. Zhao, H. Zuo, J. Wang, S. Jiao, *J. Energy Storage* **2024**, *98*, 113125.
[69] a) M. Yu, F. Guo, L. Xu, Y. Zhang, W. Ni, J. Wang, Y. Wei, X. Chen, J. Yang, H. Li, *Adv. Funct. Mater.* **2025**, *35*, 2411935; b) W. Liu, K. Rui, X. Ye, X. Zheng, Y. Zhang, M. Wang, X. Lin, B. Liu, L. Han, Y. Sun, *Adv. Energy Sust. Res.* **2024**, *5*, 2400001.
[70] J. Zhou, M. Xie, F. Wu, Y. Mei, Y. Hao, R. Huang, G. Wei, A. Liu, L. Li, R. Chen, *Adv. Mater.* **2021**, *33*, 2101649.
[71] a) M. Bai, K. Xie, K. Yuan, K. Zhang, N. Li, C. Shen, Y. Lai, R. Vajtai, P. Ajayan, B. Wei, *Adv. Mater.* **2018**, *30*, 1801213; b) A. Xia, X. Pu, Y. Tao, H. Liu, Y. Wang, *Appl. Surf. Sci.* **2019**, *481*, 852.
[72] M. Cui, Y. Xiao, L. Kang, W. Du, Y. Gao, X. Sun, Y. Zhou, X. Li, H. Li, F. Jiang, C. Zhi, *ACS Appl. Energy Mater.* **2019**, *2*, 6490.
[73] Q. Lu, C. Liu, Y. Du, X. Wang, L. Ding, A. Omar, D. Mikhailova, *ACS Appl. Mater. Interfaces* **2021**, *13*, 16869.
[74] L. Hong, L.-Y. Wang, Y. Wang, X. Wu, W. Huang, Y. Zhou, K.-X. Wang, J.-S. Chen, *Adv. Sci.* **2022**, *9*, 2104866.
[75] Z. Cai, Y. Ou, B. Zhang, J. Wang, L. Fu, M. Wan, G. Li, W. Wang, L. Wang, J. Jiang, Z. W. Seh, E. Hu, X.-Q. Yang, Y. Cui, Y. Sun, *J. Am. Chem. Soc.* **2021**, *143*, 3143.
[76] S. Xie, Y. Li, X. Li, Y. Zhou, Z. Dang, J. Rong, L. Dong, *Nano-Micro Lett.* **2021**, *14*, 39.
[77] Y. Zhang, G. Wang, F. Yu, G. Xu, Z. Li, M. Zhu, Z. Yue, M. Wu, H.-K. Liu, S.-X. Dou, C. Wu, *Chem. Eng. J.* **2021**, *416*, 128062.
[78] L.-L. Zhao, S. Zhao, N. Zhang, P.-F. Wang, Z.-L. Liu, Y. Xie, J. Shu, T.-F. Yi, *Energy Storage Mater.* **2024**, *71*, 103628.
[79] a) P. Liang, J. Yi, X. Liu, K. Wu, Z. Wang, J. Cui, Y. Liu, Y. Wang, Y. Xia, J. Zhang, *Adv. Funct. Mater.* **2020**, *30*, 1908528; b) J. Cao, D. Zhang, C. Gu, X. Zhang, M. Okhawilai, S. Wang, J. Han, J. Qin, Y. Huang, *Nano Energy* **2021**, *89*, 106322.
[80] M. Zhou, S. Guo, G. Fang, H. Sun, X. Cao, J. Zhou, A. Pan, S. Liang, *J. Energy Chem.* **2021**, *55*, 549.
[81] a) A. Pfau, K. D. Schierbaum, W. Göpel, *Surf. Sci.* **1995**, *331–333*, 1479; b) Y. Guo, J. Robertson, *Appl. Phys. Lett.* **2014**, *105*, 222110; c) A. Subrahmanyam, A. Karuppasamy, *Sol. Energy Mater. Sol. Cells* **2007**, *91*, 266; d) H. B. Michaelson, *J. Appl. Phys.* **1950**, *21*, 536; e) K. Hiehata, A. Sasahara, H. Onishi, *Nanotechnology* **2007**, *18*, 084007.
[82] H. Liu, J.-G. Wang, W. Hua, H. Sun, Y. Huyan, S. Tian, Z. Hou, J. Yang, C. Wei, F. Kang, *Adv. Sci.* **2021**, *8*, 2102612.
[83] H. Jin, S. Dai, K. Xie, Y. Luo, K. Liu, Z. Zhu, L. Huang, L. Huang, J. Zhou, *Small* **2022**, *18*, 2106441.
[84] Q. Zhang, J. Luan, X. Huang, Q. Wang, D. Sun, Y. Tang, X. Ji, H. Wang, *Nat. Commun.* **2020**, *11*, 3961.
[85] J. Han, H. Euchner, M. Kuenzel, S. M. Hosseini, A. Groß, A. Varzi, S. Passerini, *ACS Energy Lett.* **2021**, *6*, 3063.
[86] X. Yang, C. Li, Z. Sun, S. Yang, Z. Shi, R. Huang, B. Liu, S. Li, Y. Wu, M. Wang, Y. Su, S. Dou, J. Sun, *Adv. Mater.* **2021**, *33*, 2105951.
[87] a) J. Hao, B. Li, X. Li, X. Zeng, S. Zhang, F. Yang, S. Liu, D. Li, C. Wu, Z. Guo, *Adv. Mater.* **2020**, *32*, 2003021; b) S. Bhoyate, S. Mhin, J.-e. Jeon, K. Park, J. Kim, W. Choi, *ACS Appl. Mater. Interfaces* **2020**, *12*, 27249; c) H. Jia, M. Qiu, C. Lan, H. Liu, M. Dirican, S. Fu, X. Zhang, *Adv. Sci.* **2022**, *9*, 2103952; d) J. Zheng, Z. Cao, F. Ming, H. Liang, Z. Qi, W. Liu, C. Xia, C. Chen, L. Cavallo, Z. Wang, H. N. Alshareef, *ACS Energy Lett.* **2022**, *7*, 197; e) G. Liang, J. Zhu, B. Yan, Q. Li, A. Chen, Z. Chen, X. Wang, B. Xiong, J. Fan, J. Xu, C. Zhi, *Energy Environ. Sci.* **2022**, *15*, 1086; f) P. Cao, X. Zhou, A. Wei, Q. Meng, H. Ye, W. Liu, J. Tang, J. Yang, *Adv. Funct. Mater.* **2021**, *31*, 2100398; g) H. Peng, C. Liu, N. Wang, C. Wang, D. Wang, Y. Li, B. Chen, J. Yang, Y. Qian, *Energy Environ. Sci.* **2022**, *15*, 1682.
[88] Y. Yang, C. Liu, Z. Lv, H. Yang, X. Cheng, S. Zhang, M. Ye, Y. Zhang, L. Chen, J. Zhao, C. C. Li, *Energy Storage Mater.* **2021**, *41*, 230.
[89] N. Zhang, S. Huang, Z. Yuan, J. Zhu, Z. Zhao, Z. Niu, *Angew. Chem., Int. Ed.* **2021**, *60*, 2861.
[90] Z. Zhao, J. Zhao, Z. Hu, J. Li, J. Li, Y. Zhang, C. Wang, G. Cui, *Energy Environ. Sci.* **2019**, *12*, 1938.
[91] Y. Wang, T. Guo, J. Yin, Z. Tian, Y. Ma, Z. Liu, Y. Zhu, H. N. Alshareef, *Adv. Mater.* **2022**, *34*, 2106937.
[92] M. Liu, L. Yang, H. Liu, A. Amine, Q. Zhao, Y. Song, J. Yang, K. Wang, F. Pan, *ACS Appl. Mater. Interfaces* **2019**, *11*, 32046.
[93] M. He, C. Shu, A. Hu, R. Zheng, M. Li, Z. Ran, J. Long, *Energy Storage Mater.* **2022**, *44*, 452.
[94] B. Li, X. Zhang, T. Wang, Z. He, B. Lu, S. Liang, J. Zhou, *Nano-Micro Lett.* **2022**, *14*, 1.
[95] Y. Li, H. Yao, X. Liu, X. Yang, D. Yuan, *Nano Res.* **2023**, *16*, 9179.
[96] L. Miao, Z. Guo, L. Jiao, *Energy Mater.* **2023**, *3*, 300014.
[97] Y. Du, Y. Li, B. B. Xu, T. X. Liu, X. Liu, F. Ma, X. Gu, C. Lai, *Small* **2022**, *18*, 2104640.
[98] L. Li, S. Jia, Y. Shi, C. Wang, H. Qiu, Y. Ji, M. Cao, D. Zhang, *Inorg. Chem. Front.* **2024**, *11*, 4485.
[99] S. Chen, D. Ji, Q. Chen, J. Ma, S. Hou, J. Zhang, *Nat. Commun.* **2023**, *14*, 3526.
[100] a) Y. Wang, Z. Wang, F. Yang, S. Liu, S. Zhang, J. Mao, Z. Guo, *Small* **2022**, *18*, 2107033; b) J. Hao, L. Yuan, Y. Zhu, M. Jaroniec, S. Z. Qiao, *Adv. Mater.* **2022**, *34*, 2206963.
[101] J. Wan, R. Wang, Z. Liu, L. Zhang, F. Liang, T. Zhou, S. Zhang, L. Zhang, Q. Lu, C. Zhang, *ACS Nano* **2023**, *17*, 1610.
[102] M. Song, S. Li, Y. Zhu, H. Wan, X. Xu, L. Li, L. Sun, L. Tian, Y. Xu, *Dalton Trans.* **2024**, *53*, 2714.
[103] Y. Hou, S. Liu, S. Wang, W. Zhang, S. Li, J. Qiu, *ACS Appl. Mater. Interfaces* **2024**, *16*, 67821.
[104] Z. Song, C. Yang, N. Kiatwisarnkij, A. Lu, N. Tunghathaithip, K. Lolupiman, T. Bovornratanaraks, X. Zhang, G. He, J. Qin, *ACS Appl. Mater. Interfaces* **2024**, *16*, 64834.
[105] N. Almenara, R. Gueret, A. J. Huertas-Alonso, U. T. Veettil, M. H. Sipponen, E. Lizundia, *ACS Sustainable Chem. Eng.* **2023**, *11*, 2283.
[106] J. Cao, F. Zhao, W. Guan, X. Yang, Q. Zhao, L. Gao, X. Ren, G. Wu, A. Liu, *Small* **2024**, *20*, 2400221.
[107] C. Wang, H. Huang, X. Sun, X. Deng, Y. Lei, W. Hao, Y. Liu, X. Chen, W. Zhao, *ACS Omega* **2023**, *8*, 8092.
[108] Y. Jin, K. S. Han, Y. Shao, M. L. Sushko, J. Xiao, H. Pan, J. Liu, *Adv. Funct. Mater.* **2020**, *30*, 2003932.
[109] M. Wang, Y. Cheng, H. Zhao, J. Gao, J. Li, Y. Wang, J. Qiu, H. Zhang, X. Chen, Y. Wei, *Small* **2023**, *19*, 2302105.
[110] M. Yan, C. Xu, Y. Sun, H. Pan, H. Li, *Nano Energy* **2021**, *82*, 105739.
[111] M. Yan, N. Dong, X. Zhao, Y. Sun, H. Pan, *ACS Energy Lett.* **2021**, *6*, 3236.
[112] H. Li, C. Xu, C. Han, Y. Chen, C. Wei, B. Li, F. Kang, *J. Electrochem. Soc.* **2015**, *162*, A1439.
[113] F. Zhao, Z. Jing, X. Guo, J. Li, H. Dong, Y. Tan, L. Liu, Y. Zhou, R. Owen, P. R. Shearing, D. J. L. Brett, G. He, I. P. Parkin, *Energy Storage Mater.* **2022**, *53*, 638.
[114] Z. Liu, R. Wang, Y. Gao, S. Zhang, J. Wan, J. Mao, L. Zhang, H. Li, J. Hao, G. Li, L. Zhang, C. Zhang, *Adv. Funct. Mater.* **2023**, *33*, 2308463.
[115] M. Qiu, P. Sun, G. Cui, W. Mai, *ACS Appl. Mater. Interfaces* **2022**, *14*, 40951.
[116] Z. Liu, R. Wang, Q. Ma, J. Wan, S. Zhang, L. Zhang, H. Li, Q. Luo, J. Wu, T. Zhou, J. Mao, L. Zhang, C. Zhang, Z. Guo, *Adv. Funct. Mater.* **2024**, *34*, 2214538.
[117] X. Zhou, R. Chen, E. Cui, Q. Liu, H. Zhang, J. Deng, N. Zhang, C. Xie, L. Xu, L. Mai, *Energy Storage Mater.* **2023**, *55*, 538.
[118] J. Lee, B. Hwang, M.-S. Park, K. Kim, *Electrochim. Acta* **2016**, *199*, 164.
[119] Y. Zhou, X. Ni, B. Hao, X. Zhou, C. Yan, J. Zhou, T. Qian, *Energy Storage Mater.* **2024**, *66*, 103227.
[120] a) C. Yuan, J. Xiao, C. Liu, X. Zhan, *J. Mater. Chem. A* **2024**, *12*, 19060; b) M. Qiu, L. Ma, P. Sun, Z. Wang, G. Cui, W. Mai, *Nano-Micro Lett.* **2021**, *14*, 31.

[121] X. Nie, L. Miao, W. Yuan, G. Ma, S. Di, Y. Wang, S. Shen, N. Zhang, *Adv. Funct. Mater.* **2022**, *32*, 2203905.
[122] Y. Xu, J. Zhu, J. Feng, Y. Wang, X. Wu, P. Ma, X. Zhang, G. Wang, X. Yan, *Energy Storage Mater.* **2021**, *38*, 299.
[123] B. W. Olbasa, F. W. Fenta, S.-F. Chiu, M.-C. Tsai, C.-J. Huang, B. A. Jote, T. T. Beyene, Y.-F. Liao, C.-H. Wang, W.-N. Su, *ACS Appl. Energy Mater.* **2020**, *3*, 4499.
[124] P. Wang, X. Xie, Z. Xing, X. Chen, G. Fang, B. Lu, J. Zhou, S. Liang, H. J. Fan, *Adv. Energy Mater.* **2021**, *11*, 2101158.
[125] K. Ouyang, D. Ma, N. Zhao, Y. Wang, M. Yang, H. Mi, L. Sun, C. He, P. Zhang, *Adv. Funct. Mater.* **2022**, *32*, 2109749.
[126] C. Sun, C. Wu, X. Gu, C. Wang, Q. Wang, *Nano-Micro Lett.* **2021**, *13*, 89.
[127] A. Bayaguud, X. Luo, Y. Fu, C. Zhu, *ACS Energy Lett.* **2020**, *5*, 3012.
[128] S. J. Patil, N. R. Chodankar, S.-K. Hwang, P. A. Shinde, G. S. Rama Raju, K. S. Ranjith, S. V. Karekar, Y.-S. Huh, Y.-K. Han, *J. Mater. Chem. A* **2023**, *11*, 5112.
[129] J. Gao, X. Xie, S. Liang, B. Lu, J. Zhou, *Nano-Micro Lett.* **2021**, *13*, 69.
[130] C. Han, W. Li, H. K. Liu, S. Dou, J. Wang, *Nano Energy* **2020**, *74*, 104880.
[131] M. J. Park, H. Yaghoobnejad Asl, S. Therese, A. Manthiram, *J. Mater. Chem. A* **2019**, *7*, 7159.
[132] J. Cui, Y. Chen, Y. Dong, H. Zhang, D. G. Ivey, *J. Mater. Chem. A* **2024**, *12*, 28475.
[133] L. Qian, W. Yao, R. Yao, Y. Sui, H. Zhu, F. Wang, J. Zhao, C. Zhi, C. Yang, *Adv. Funct. Mater.* **2021**, *31*, 2105736.
[134] B. Ramasubramanian, S. Ramakrishna, *Mater. Circ. Econ.* **2023**, *5*, 3.
[135] J. Abdulla, J. Cao, D. Zhang, X. Zhang, C. Sriprachuabwong, S. Kheawhom, P. Wangyao, J. Qin, *ACS Appl. Energy Mater.* **2021**, *4*, 4602.
[136] S. Tagliaferri, G. Nagaraju, M. Sokolikova, R. Quintin-Baxendale, C. Mattevi, *Nanoscale Horiz.* **2024**, *9*, 742.
[137] a) X. Gao, H. Dong, C. J. Carmalt, G. He, *ChemElectroChem* **2023**, *10*, 202300200; b) C. Zhou, Z. Xu, M. Chen, Q. Nan, J. Zhang, Y. Gao, Z. Zhao, Z. Xing, J. Li, P. Rao, *EES Batteries* **2025**, *1*, 161.
[138] F. W. Fenta, R. Bouchal, *J. Mater. Chem. A* **2024**, *12*, 25035.
[139] C.-Y. Chen, K. Matsumoto, K. Kubota, R. Hagiwara, Q. Xu, *Adv. Energy Mater.* **2019**, *9*, 1900196.
[140] B. Yang, T. Qin, Y. Du, Y. Zhang, J. Wang, T. Chen, M. Ge, D. Bin, C. Ge, H. Lu, *Chem. Commun.* **2022**, *58*, 1550.
[141] F. Wang, O. Borodin, T. Gao, X. Fan, W. Sun, F. Han, A. Faraone, J. A. Dura, K. Xu, C. Wang, *Nat. Mater.* **2018**, *17*, 543.
[142] S. Chen, R. Lan, J. Humphreys, S. Tao, *Energy Storage Mater.* **2020**, *28*, 205.
[143] N. R. Chodankar, S. J. Patil, S. Lee, J. Lee, S.-K. Hwang, P. A. Shinde, I. V. Bagal, S. V. Karekar, G. Seeta Rama Raju, K. Shanmugam Ranjith, D. P. Dubal, Y.-S. Huh, Y.-K. Han, *InfoMat* **2022**, *4*, 12344.
[144] Y. Zhu, J. Yin, X. Zheng, A.-H. Emwas, Y. Lei, O. F. Mohammed, Y. Cui, H. N. Alshareef, *Energy Environ. Sci.* **2021**, *14*, 4463.
[145] A. Sumboja, M. Lübke, Y. Wang, T. An, Y. Zong, Z. Liu, *Adv. Energy Mater.* **2017**, *7*, 1700927.
[146] S. Clark, A. R. Mainar, E. Iruin, L. C. Colmenares, J. A. Blázquez, J. R. Tolchard, A. Latz, B. Horstmann, *J. Mater. Chem. A* **2019**, *7*, 11387.
[147] J. Liu, C. Guan, C. Zhou, Z. Fan, Q. Ke, G. Zhang, C. Liu, J. Wang, *Adv. Mater.* **2016**, *28*, 8732.
[148] M. Yao, Z. Yuan, S. Li, T. He, R. Wang, M. Yuan, Z. Niu, *Adv. Mater.* **2021**, *33*, 2008140.
[149] H. Li, C. Han, Y. Huang, Y. Huang, M. Zhu, Z. Pei, Q. Xue, Z. Wang, Z. Liu, Z. Tang, Y. Wang, F. Kang, B. Li, C. Zhi, *Energy Environ. Sci.* **2018**, *11*, 941.
[150] T. N. T. Tran, H.-J. Chung, D. G. Ivey, *Electrochim. Acta* **2019**, *327*, 135021.
[151] J. J. Xu, H. Ye, J. Huang, *Electrochem. Commun.* **2005**, *7*, 1309.
[152] J. J. Xu, H. Ye, *Electrochem. Commun.* **2005**, *7*, 829.
[153] S. Huang, F. Wan, S. Bi, J. Zhu, Z. Niu, J. Chen, *Angew. Chem., Int. Ed.* **2019**, *58*, 4313.
[154] F. Mo, Z. Chen, G. Liang, D. Wang, Y. Zhao, H. Li, B. Dong, C. Zhi, *Adv. Energy Mater.* **2020**, *10*, 2000035.
[155] A. A. Mohamad, *J. Power Sources* **2006**, *159*, 752.
[156] S. Zhang, N. Yu, S. Zeng, S. Zhou, M. Chen, J. Di, Q. Li, *J. Mater. Chem. A* **2018**, *6*, 12237.
[157] C. Zhao, X. Wang, C. Shao, G. Li, J. Wang, D. Liu, X. Dong, *Sustainable Energy Fuels* **2021**, *5*, 332.
[158] A. P. Abbott, G. Capper, D. L. Davies, R. K. Rasheed, V. Tambyrajah, *Chem. Commun.* **2003**, 70.
[159] J. Wu, Q. Liang, X. Yu, Q. F. Lü, L. Ma, X. Qin, G. Chen, B. Li, *Adv. Funct. Mater.* **2021**, *31*, 2011102.
[160] a) E. L. Smith, A. P. Abbott, K. S. Ryder, *Chem. Rev.* **2014**, *114*, 11060; b) B. B. Hansen, S. Spittle, B. Chen, D. Poe, Y. Zhang, J. M. Klein, A. Horton, L. Adhikari, T. Zelovich, B. W. Doherty, *Chem. Rev.* **2020**, *121*, 1232; c) A. P. Abbott, J. C. Barron, K. S. Ryder, D. Wilson, *Chem.–Eur. J.* **2007**, *13*, 6495; d) L. Geng, X. Wang, K. Han, P. Hu, L. Zhou, Y. Zhao, W. Luo, L. Mai, *ACS Energy Lett.* **2021**, *7*, 247.
[161] X. Lu, E. J. Hansen, G. He, J. Liu, *Small* **2022**, *18*, 2200550.
[162] W. Chu, X. Zhang, J. Wang, S. Zhao, S. Liu, H. Yu, *Energy Storage Mater.* **2019**, *22*, 418.
[163] J. Shi, T. Sun, J. Bao, S. Zheng, H. Du, L. Li, X. Yuan, T. Ma, Z. Tao, *Adv. Funct. Mater.* **2021**, *31*, 2102035.
[164] L. Geng, J. Meng, X. Wang, C. Han, K. Han, Z. Xiao, M. Huang, P. Xu, L. Zhang, L. Zhou, L. Mai, *Angew. Chem., Int. Ed.* **2022**, *61*, 202206717.
[165] R. Chen, C. Zhang, J. Li, Z. Du, F. Guo, W. Zhang, Y. Dai, W. Zong, X. Gao, J. Zhu, Y. Zhao, X. Wang, G. He, *Energy Environ. Sci.* **2023**, *16*, 2540.
[166] H. Qiu, X. Du, J. Zhao, Y. Wang, J. Ju, Z. Chen, Z. Hu, D. Yan, X. Zhou, G. Cui, *Nat. Commun.* **2019**, *10*, 5374.
[167] a) L. Li, S. Jia, Z. Cheng, C. Zhang, *ChemSusChem* **2023**, *16*, 202202330; b) Y. Fang, X. Xie, B. Zhang, Y. Chai, B. Lu, M. Liu, J. Zhou, S. Liang, *Adv. Funct. Mater.* **2022**, *32*, 2109671.
[168] B. Li, Y. Zeng, W. Zhang, B. Lu, Q. Yang, J. Zhou, Z. He, *Sci. Bull.* **2024**, *15*, 688.
[169] H. Du, Z. Yi, H. Li, W. Lv, N. Hu, X. Zhang, W. Chen, Z. Wei, F. Shen, H. He, *Chem.–Eur. J.* **2024**, *30*, 202303461.
[170] a) Y. Song, P. Ruan, C. Mao, Y. Chang, L. Wang, L. Dai, P. Zhou, B. Lu, J. Zhou, Z. He, *Nano-Micro Lett.* **2022**, *14*, 218; b) L. Yang, M. Zhou, Y. Xie, X. Shen, S. Liang, G. Fang, *Energy Storage Mater.* **2024**, *67*, 103271.
[171] D. J. Arnot, M. B. Lim, N. S. Bell, N. B. Schorr, R. C. Hill, A. Meyer, Y. T. Cheng, T. N. Lambert, *Adv. Energy Mater.* **2021**, *11*, 2101594.
[172] C. Li, Z. Sun, T. Yang, L. Yu, N. Wei, Z. Tian, J. Cai, J. Lv, Y. Shao, M. H. Rümmeli, J. Sun, Z. Liu, *Adv. Mater.* **2020**, *32*, 2003425.
[173] Y. Liang, D. Ma, N. Zhao, Y. Wang, M. Yang, J. Ruan, G. Yang, H. Mi, C. He, P. Zhang, *Adv. Funct. Mater.* **2022**, *32*, 2112936.
[174] W. Zhou, M. Chen, Q. Tian, J. Chen, X. Xu, C.-P. Wong, *Energy Storage Mater.* **2022**, *44*, 57.
[175] J. Cao, D. Zhang, C. Gu, X. Wang, S. Wang, X. Zhang, J. Qin, Z. S. Wu, *Adv. Energy Mater.* **2021**, *11*, 2101299.

Pragati A. Shinde is a Japan Society for the Promotion of Science (JSPS) Fellow at the Center for Materials Nanoarchitectonics (MANA), National Institute for Materials Science (NIMS), Japan. She earned her Ph.D. in Physics from Shivaji University, India, in 2018. Following her doctoral studies, she gained extensive research experience as a Brain Korea-21 (BK-21) Postdoctoral Fellow at Yonsei University, South Korea, and as a Postdoctoral Research Associate at the University of Sharjah, UAE. Her research focuses on the design and synthesis of advanced functional nanomaterials, with a particular emphasis on 2D materials and carbon-based systems for electrochemical energy storage. Her work integrates innovative material architectures to address critical challenges in sustainable energy storage technologies. She has published 60 peer-reviewed journal articles and holds three US patents.

Nilesh R. Chodankar is currently a Scientist in the Department of Mechanical Engineering at Khalifa University, Abu Dhabi, United Arab Emirates. He earned his Ph.D. in Materials Science from Shivaji University, Kolhapur, India, in 2016. Following his doctoral studies, he pursued postdoctoral research at Chonnam National University, South Korea. He later joined Dongguk University in Seoul as an Assistant Professor in the Department of Energy and Materials Engineering. Dr. Chodankar also serves as an Associate Editor for the Journal of Energy Storage and Carbon Letters. His research focuses on the design and development of atomically thin 2D nanomaterials for advanced energy storage systems, including supercapacitors and post–lithium-ion battery chemistries. He has authored over 115 research articles in internationally reputed journals and holds four patents (two from Korea and two from the United States) related to aqueous energy storage technologies.

Katsuhiko Ariga received his Ph.D. degree from the Tokyo Institute of Technology in 1990. He joined the National Institute for Materials Science (NIMS) in 2004 and is currently the leader of the Supermolecules Group and senior scientist with special missions of the Research Centre for Materials Nanoarchitectonics (MANA), NIMS. He is also appointed as a professor at the University of Tokyo.